Field dependent spin - lattice relaxation

G. L. Sturgess

FIELD DEPENDENT SPIN - LATTICE RELAXATION

G.L.Sturgess B.Sc.

A thesis presented in canditature for the degree of Doctor of Philosophy at the University of Durham

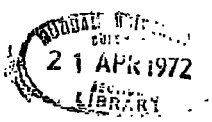

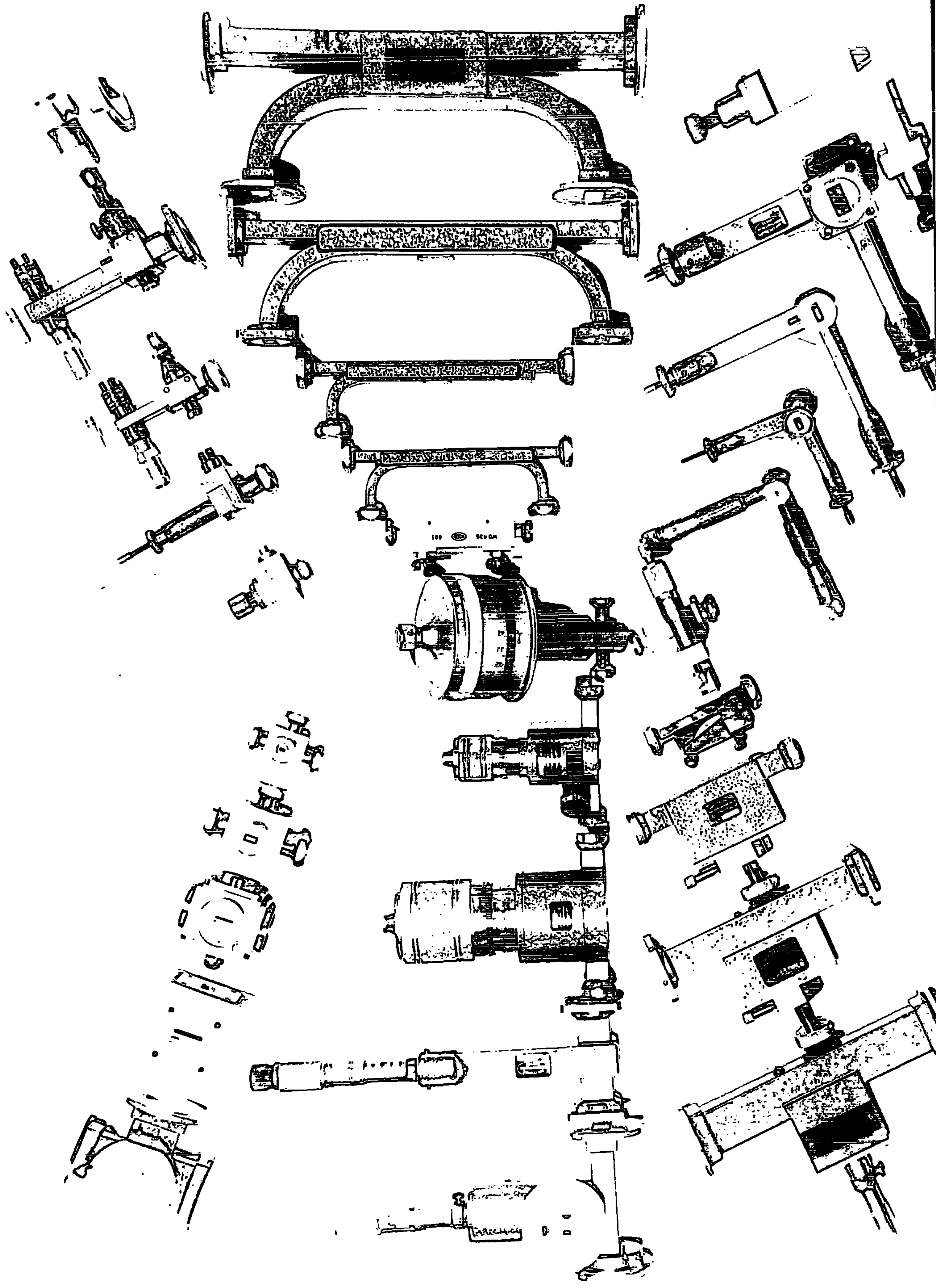

The British R.C.S.C. standard waveguide sizes used in the work described in this thesis are as follows :

WG 16	.900" x .400"	8.20 - 12.4 GHz
WG 18	.622" x .311"	12.4 - 18.0 GHz
WG 20	.420" x .170"	18.0 - 26.5 GHz
WG 22	.280" x .140"	26.5 - 40.0 GHz
WG 26	.122" x .061"	60.0 - 90.0 GHz

('Specification for Tubing, Waveguide,' R.C.S.C., DEF 5351, HMSO 1959)

ABSTRACT

The spin-lattice relaxation times, T_1, of Cr^{3+} ions in a range of samples of artificial ruby have been measured at $4.2^{\circ}K$, in the direct (one phonon) relaxation process regime, at frequencies of 9.3, 16, 22, 35.5, and 71 GHz, corresponding to magnetic fields, H, up to 25 kG.

These results have been compared with the predictions of the Van Vleck theory of paramagnetic relaxation, that T_1 should be proportional to H^{-2} for a non-Kramer's ion and H^{-4} for an isolated Kramer's doublet. The observed dependencies, between -0.3 and -1, at low magnetic fields are not in agreement with theory, but at high fields (between fields corresponding to 35.5 and 71 GHz) the average dependency for $\Delta M=1$ transitions at polar angle 90° is $T_1 \propto H^{-2.55}$, indicating that the energy levels are tending to behave as isolated Kramer's doublets, due to their increasing separation in energy and the decreasing degree of mixing of pure spin states. At low fields the high degree of mixing of states and the masking effect of the zero field splitting on the field dependent energy separation of the energy levels appear to cause the low degree of dependence of T_1 on H.

In contrast to other published collations of T_1 measurements performed on different samples at various frequencies, all of these results have been obtained under the same experimental

conditions from the same samples, frequency of observation (magnetic field) being the only variable.

In addition to the variation of T_1 with H, a linear variation of T_1 with mean lattice strain, ε, derived from observations of the linewidth broadening in the samples used, has been observed. The design and construction of the spectrometers used for these measurements is described in detail

ACKNOWLEDGEMENTS

'No man is an Island, entire of it self' is nowhere more true than in the field of scientific research and I should like to record my grateful thanks to those who have supported me in this work.

To Dr. J.S. Thorp, my supervisor, for his instigation and support of this project and his cheerful encouragement and advice at all times.

To Professor D.A. Wright for the use of the Research facilities of the Department.

To the Staff of the Departmental Workshops, headed by Mr. Frank Spence, for their expert advice and skilful, rapid execution of my requests for equipment; especially Mr. Ron Waite and Mr. Paul Wilson, who had to bear with me more than most.

To the Science Research Council, for their award of a State Studentship.

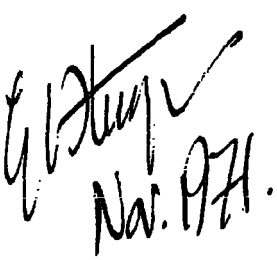

CONTENTS

Chapter 1

INTRODUCTION

1.1 MICROWAVE SPECTROSCOPY

Microwave spectroscopy consists of the observation of the interaction with atomic systems of electromagnetic radiation in the microwave region of the spectrum, this broadly being from 1GHz. to 300GHz., the high frequency limit between microwaves and the far infrared being rather ill defined.

The nature of the interaction is essentially magnetic, and takes placé, at these frequencies, between the magnetic component of the electromagentic wave, and the magnetic dipoles of the electrons of the atoms or ions being observed. In the case of paramagnetism, certain ions possess unpaired electrons in unfilled orbital shells, and it is these electrons which give rise to a residual magnetic dipole moment. In the case of solids, if paramagnetic ions are distributed in a diamagentic host lattice, the magnetic properties of the material will be dominated by those of the paramagnetic ions, although these will be modified by the influence of the crystalline electric field of the host lattice at the paramagnetic ion site.

The first experimental observation of the interaction of microwaves with matter was that performed by Cleeton & Williams (1934), who observed the absorption spectrum of ammonia at frequencies between 7 and 30GHz., although severely hampered by the lack of any commercial microwave equipment available at that

time. The rapid acceleration of research into microwave apparatus, caused by the requirements of radar during the last war, made the ready availability of microwave generators and circuit elements an inducement to continue research in the subject, and resonant magnetic absorption was first reported by Zavoisky (1945), and Cummerow & Halliday (1946).

1.2 THE PARAMAGNETIC ION IN A CRYSTALLINE ENVIRONMENT

A free ion has associated quantum numbers J, L and S, corresponding to the total, orbital and spin angular momenta respectively; J being the vector sum of L and S, and a result of quantum theory is that the ground state of such an ion has degeneracy (2J+1) in the absence of any applied magentic field.

The strong electric fields present in a crystal lattice can modify this quantum state in several ways. The first is the breaking of the coupling between L and S, resulting in the orbital ground state degeneracy being due to S alone, and therefore (2S+1) in value, the higher orbital states being usually far removed in energy from the ground state: this condition is known as 'quenching'. The second effect can be a partial lifting of the degeneracy of the ground state, subject to the limitation of Kramers' Theorem (Kramers 1930) which states that an ion with an odd number of unpaired electrons must retain twofold degeneracy of those levels. The energy splitting caused by this lifting of the ground state degeneracy is called the zero field splitting, and frequently corresponds to quanta of microwave radiation.

This situation applies in the case of ions of the iron group of transition elements, only the lowest orbital energy level normally being populated, and the energy splitting of the higher orbital states corresponding to quanta of energy of optical frequencies.

In a crystalline environment, if the spin-orbit coupling is incompletely quenched, the degeneracy of the ground state may not correspond to the true spin quantum number of the free ion, S, and therefore an effective spin, S', is assigned to the ion, such that the observed degeneracy is (2S'+1). In the case of complete quenching S' is equal to S.

The application of a magnetic field, H, causes further lifting of the degeneracy of the ground state, splitting the levels into discrete spin energy states, with an energy separation E, where

$$E = g\beta H M \qquad 1.01$$

where β is the Bohr magneton, the unit of magnetic moment, g is the spectroscopic splitting factor, equal to 2.002 for a free electron spin, and otherwise giving an indication of the degree of orbital quenching, and analagous to the Lande g-factor for a free ion; M is the magnetic quantum number, having values in the range +S' to -S'. A quantum mechanical selection rule dictates that transitions may only be observed between spin states for which $\Delta M = 1$. This only applies however for pure spin states, and a

further effect of the crystalline field is to cause mixing of the pure spin states. Thus, in an ion having $S' = 3/2$ (e.g. Cr^{3+}), an energy level $|i\rangle$ may be described, using the notation of Dirac (1947), by,

$$|i\rangle = a_i|3/2\rangle + b_i|1/2\rangle + c_i|-1/2\rangle + d_i|-3/2\rangle \qquad 1.02$$

the eigenvectors $a_i, \ldots$ being normalised by,

$$|a_i|^2 + |b_i|^2 + |c_i|^2 + |d_i|^2 = 1 \qquad 1.03$$

The consequence of this is that the selection rule $\Delta M = 1$ breaks down, and the so called 'forbidden' transitions may be observed. Using Cr^{3+} in Al_2O_3 (ruby) as an example, when H is parallel to the trigonal axis of ruby (described in this thesis as the c-axis, or by polar angle $\theta = 0^o$) the energy levels are pure spin states, $|3/2\rangle$, $|1/2\rangle$ etc., but as θ is changed, so the degree of mixing (the values of a_i, b_i etc.) varies, and so transitions which could be described by $\Delta M = 2$ and $\Delta M = 3$, become observable, the relative intensities of the allowed and forbidden transitions being determined by the values of the eigenvectors.

Figure 1.1 shows the energy level diagram for the ground state of Cr^{3+} in ruby, showing the effects of the various fields which lift the degeneracy of this orbital level.

The spin Hamiltonian (Abragam & Pryce, 1951) is a convenient description of the ground state levels of an ion. The precise form is a function of the particular symmetry of the host lattice, but generally it can be expressed as:

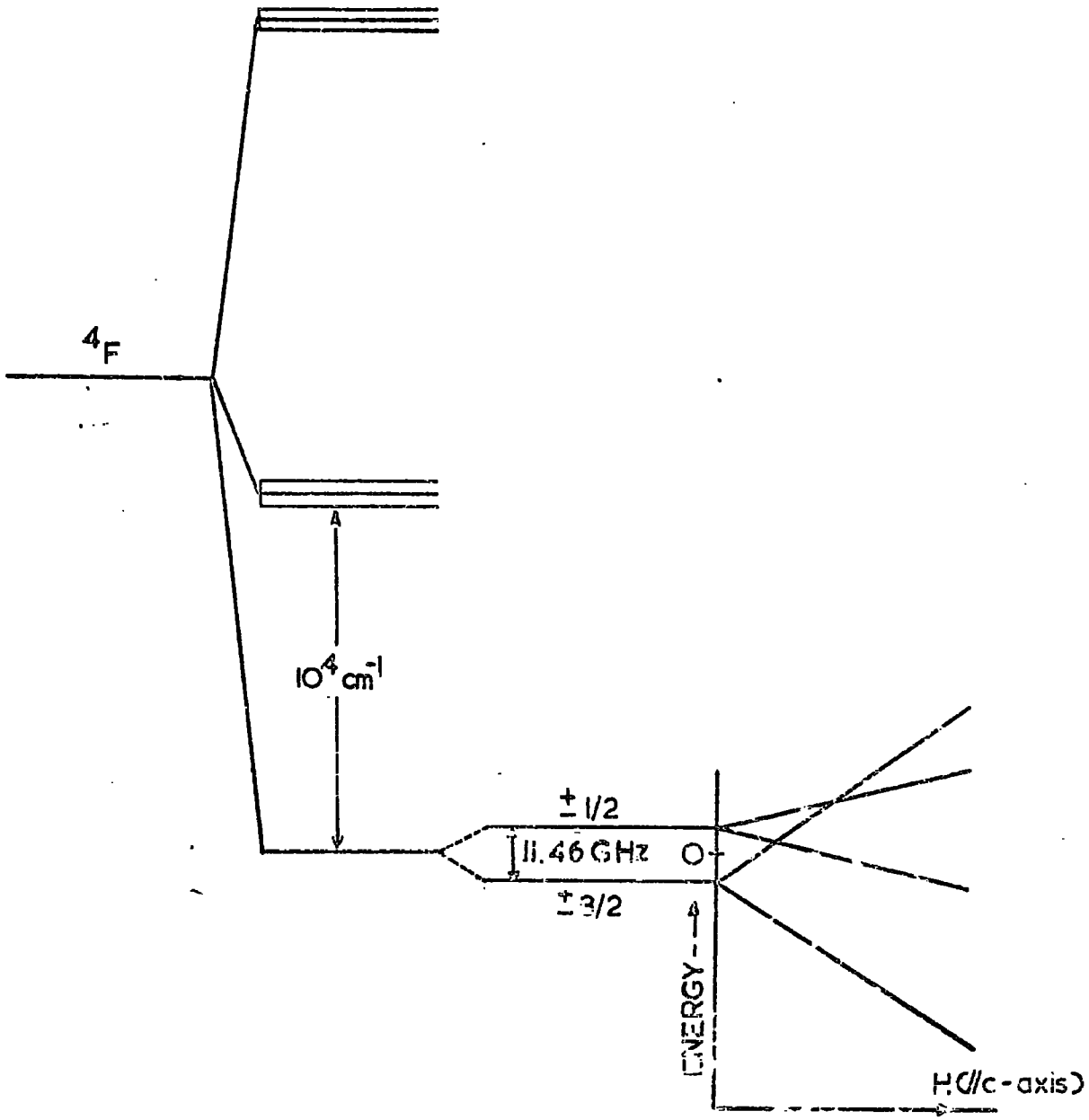

FIGURE 1.1 GROUND STATE ENERGY LEVELS OF Cr^{3+} IN ALUMINA, SUBJECT TO STARK AND ZEEMAN SPLITTINGS BY CRYSTALLINE ELECTRIC AND APPLIED MAGNETIC FIELDS

(not to scale)

$$\mathcal{H}_s = g\beta \underline{H}.\underline{S}' + D(S_z'^2 + S'(S'+1)) + E(S_x'^2 + S_y'^2) + \text{HFS terms} \quad 1.04$$

The first term represents the energy of the spin magnetic moment due to its orientation with respect to the applied magnetic field. The second term possesses axial symmetry, and is proportional to the transverse component of S', and may be interpreted as a quadrupole interaction between ion and lattice. The third term is a non-axially symmetric anistropy in the x - y plane due to an electric moment of high order. The energy separation of the ground state levels in zero magnetic field is due to the D & E terms in the Hamiltonian; in an axially symmetric system, such as ruby, with S' = 3/2 the term E is approximately zero, and hence the zero field splitting is 2D.

If the nucleus of the ion has a nuclear magnetic moment, then additional hyperfine splitting (HFS) terms must be added to $\mathcal{H}_s$, but in the case of ruby this is not necessary. The values of the constants in $\mathcal{H}_s$ for ruby as measured by Geusic (1956) are:

$g_\parallel = 1.9844$ $g_\perp = 1.9867$ $2D = -0.3831$ cm^{-1} = 11.48 GHz.

Using the spin Hamiltonian, the solutions of

$$\mathcal{H}_s |i\rangle = E_i |i\rangle \quad 1.05$$

are derived in terms of E_i, the eigenvalues (energies) of the states $|i\rangle$.

Figure 1.2 is a diagram of the energy levels of the chromium ion in ruby at polar angles of 0° and 90°, showing the various

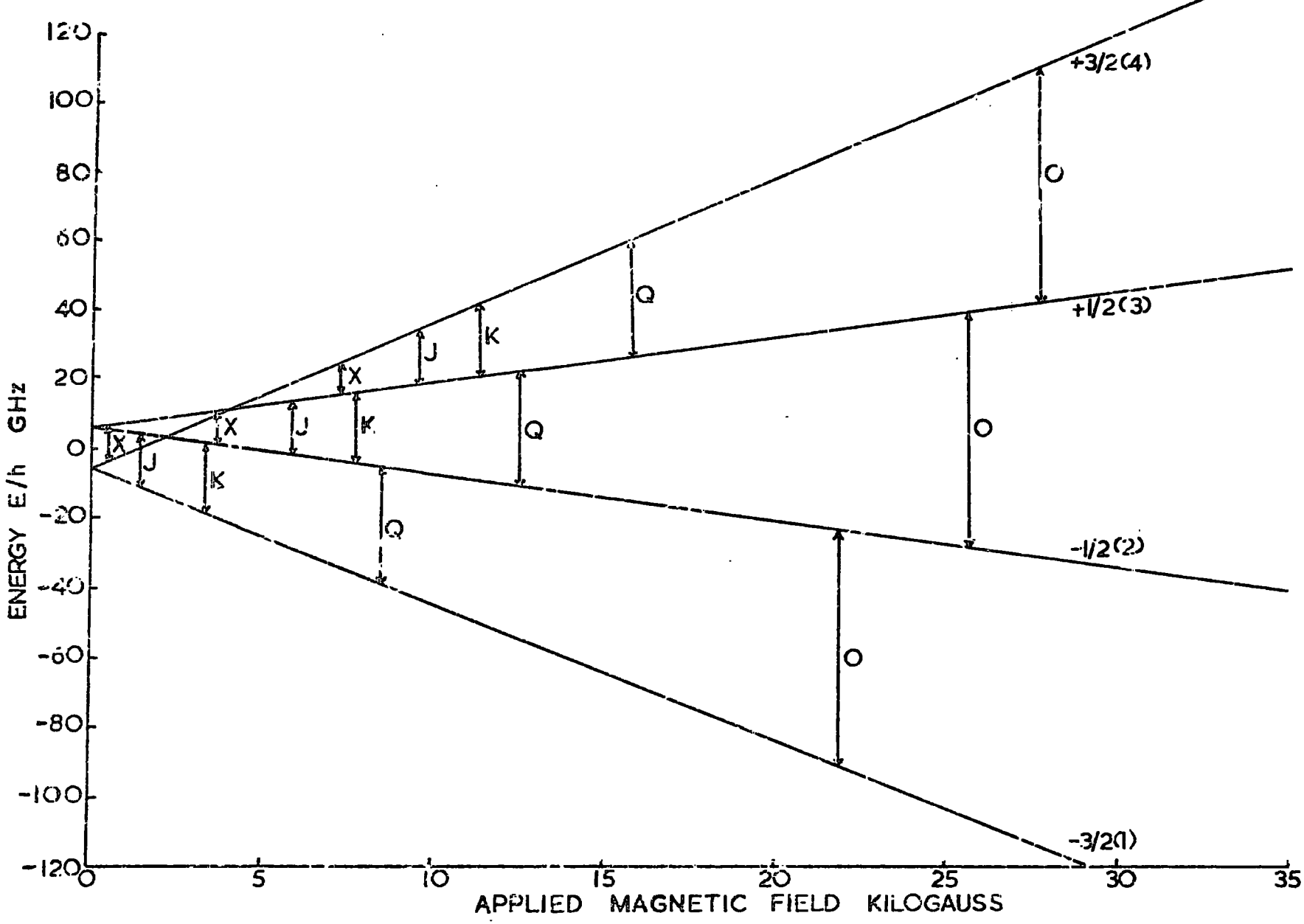

FIGURE 1.2c ENERGY LEVELS OF Cr^{3+} IN ALUMINA : POLAR ANGLE 0°

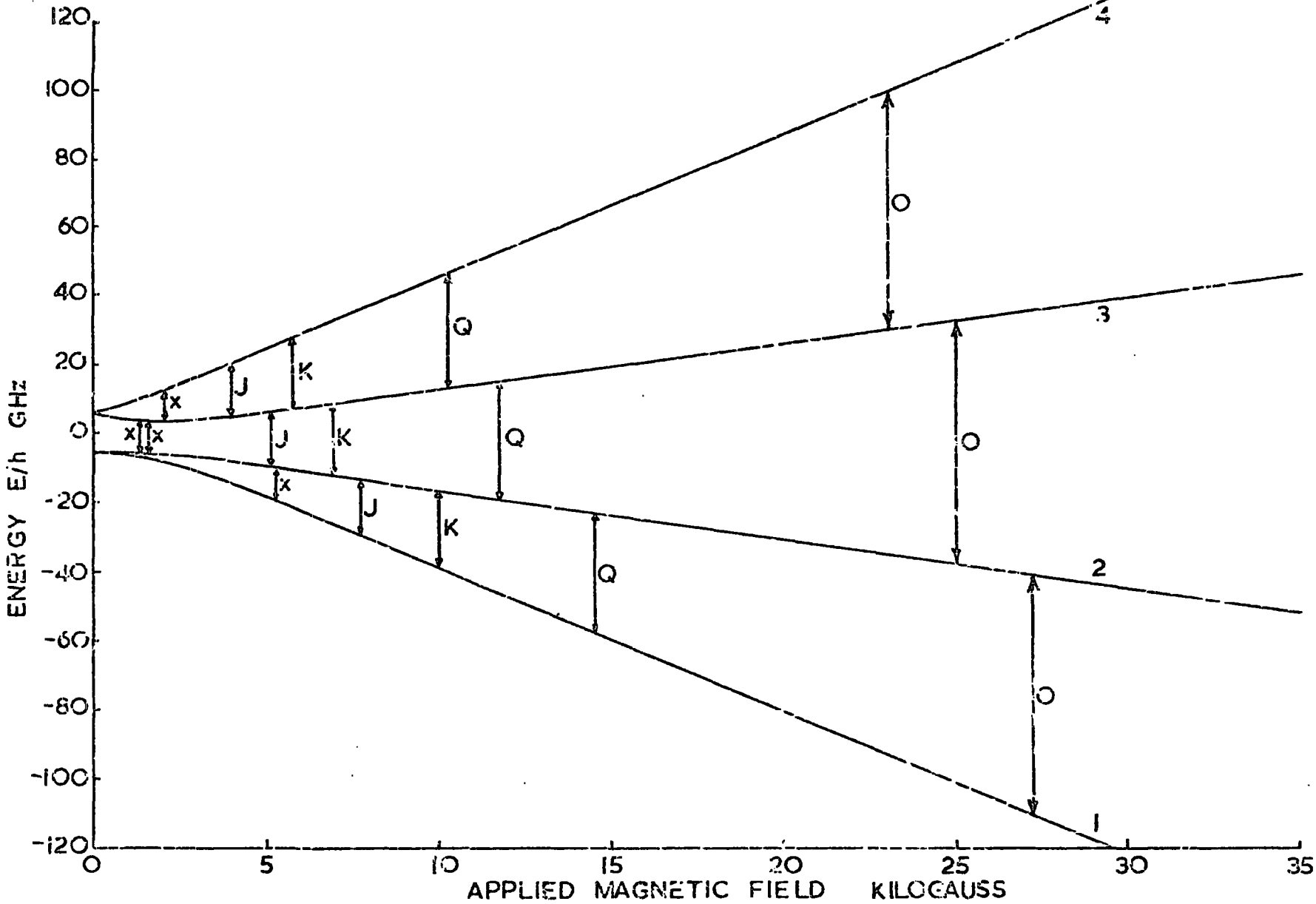

FIGURE 1.2 b ENERGY LEVELS OF Cr^{3+} IN ALUMINA : POLAR ANGLE 90°

allowed transitions at the frequencies with which this thesis is concerned. The notation used is that of Schulz-du Bois (1959), assigning quantum numbers from 3/2 to -3/2 to each energy level, in order of decreasing energy, although these numbers only designate the corresponding pure spin state at a polar angle of 0^{o}.

1.3 ELECTRON SPIN RESONANCE

This is one of the titles given to the technique of investigating the energy levels described by the observation of the absorption of radio frequency (r.f.) power in a spin system in a magnetic field; the quanta of r.f. energy exciting resonant transitions between the Zeeman energy levels of the ground state.

The macroscopic influence of an r.f. magnetic field on a spin system was described phenomenologically by Bloch (1946) in terms of a dynamic complex susceptibility, χ, having real and imaginary parts χ' and χ''. The real part of the susceptibility represents a reactive effect, zero at resonance, which will alter the phase of the r.f. field, or, if in a cavity, will alter the frequency of the cavity. The imaginary part is responsible for the absorption of power by the spin system according to

$$P_{abs} = -\tfrac{1}{2}\omega\mu_{o}\chi''H_{rf}^{2} \qquad 1.06$$

where the r.f. magnetic field is of magnitude H_{rf}, and angular frequency ω. χ' and χ'' are both frequency dependent in the region of ω_{o}, the resonance frequency, as shown in Figure 1.3.

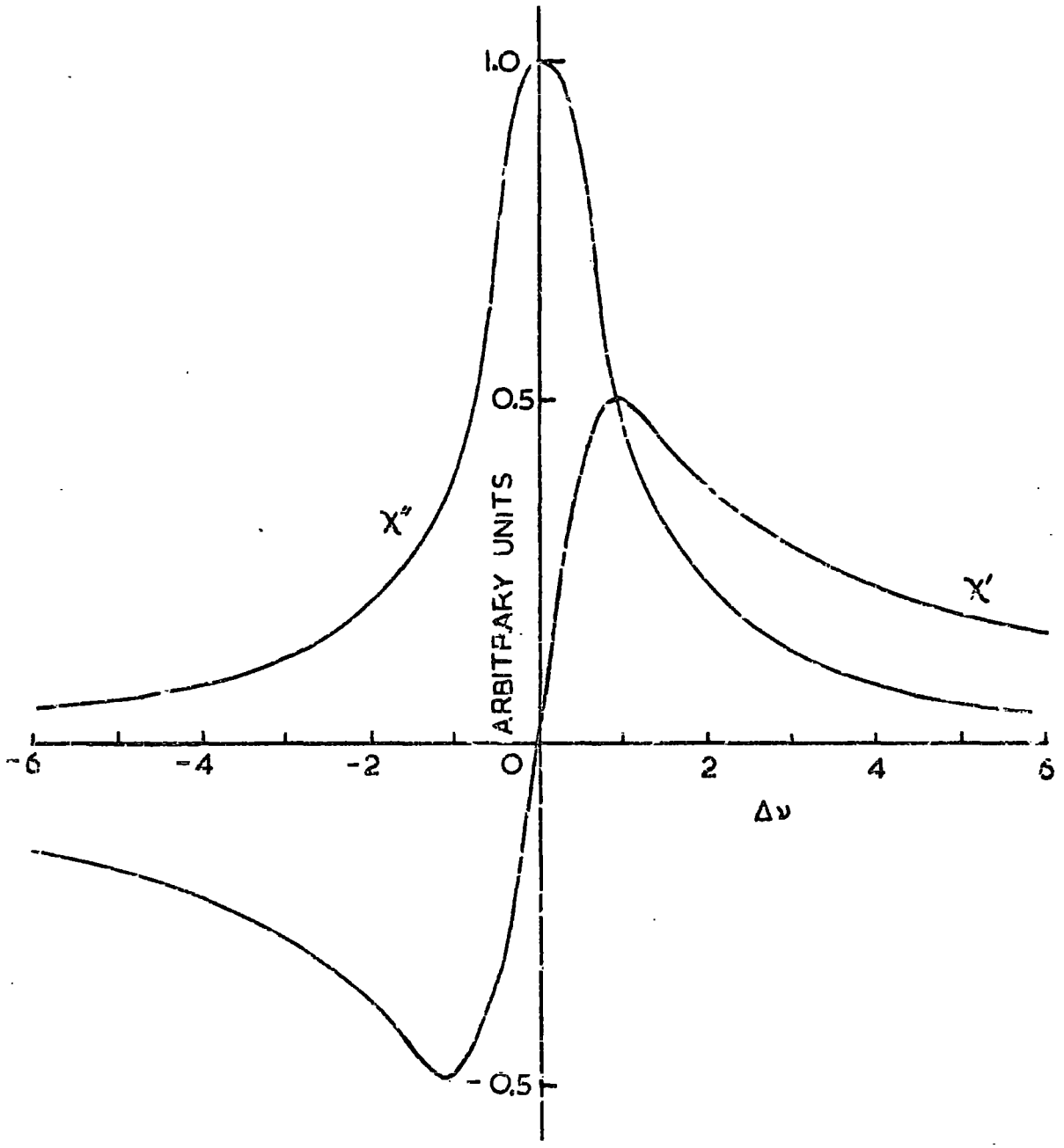

FIGURE 1.3

χ' AND χ'' AS FUNCTIONS OF FREQUENCY FOR A LORENTZIAN LINESHAPE

In microscopic terms, the power absorption may be dealt with by first order perturbation theory, whence it may be shown that, for a simple two level system, the transition probability, W_{12}, of a stimulated absorptive transition is

$$W_{12} = \left(\frac{g\beta H_{rf}}{\hbar}\right)^2 . g(\nu) \qquad 1.07$$

where $g(\nu)$ describes the resonance lineshape in terms of frequency. The associated power absorption is simply the product of transition probability, population difference between the two levels and the energy of a single quantum of r.f. power involved in the transition

$$P_{abs} = \left(\frac{g\beta H_{rf}}{\hbar}\right)^2 g(\nu) . (n_1 - n_2) . h\nu \qquad 1.08$$

$g(\nu)$ is a normalised function, so that $\int_0^\infty g(\nu)\,d\nu = 1$; the form of $g(\nu)$ close to the resonance frequency ω_o is commonly Lorentzian, although other symmetrical and non-symmetrical lineshapes are found. Far from resonance the value of $g(\nu)$ is approximately zero. For values of ω_o lying in the microwave region, the resonance condition, that the r.f. quantum energy should equal the splitting of the paramagentic energy levels (eq. 1.01) :-

$$E = g\beta H_o = h\nu_o \qquad 1.09$$

is met by magnetic fields of several kilogauss.

1.4 THE SOLID STATE MASER

In 1917 Einstein postulated that in a multilevel system of discrete energy states, the effect of incident rediation of the correct frequency would be to stimulate both upward (absorptive) and downward (emissive) transitions within the system; that the stimulated emission would be coherent with the incident radiation, and that the probabilities of stimulated emission and absorption would be equal.

Normally the population n_1 of a lower level, of energy E_1, is higher than the population n_2 of a higher level, E_2, the relative populations being determined by the Bolzmann statistics as

$$\frac{n_1}{n_2} = \exp\left((E_2 - E_1)/kT\right) \qquad 1.10$$

T being the absolute temperature of the system, and k Boltzmann's constant. Therefore, in a system in thermal equilibrium, power, P, will normally be absorbed from incident radiation of frequency ν, where $h\nu = (E_1 - E_2)$, since the transition probabilities for absorbtion, W_{12}, and emission, W_{21}, are equal, but $n_1 > n_2$ (eq. 1.08)

$$P_{abs} = h\nu W_{12}n_1 - h\nu W_{21}n_2 = h\nu W_{12}(n_1 - n_2) \qquad 1.11$$

There is also a probability of spontaneous emission from level 2 to level 1, but this is so small that it may usually be ignored.

About 1951 Townes, and separately Weber (1953), proposed a device in which the populations of the energy levels were inverted so that $n_1 < n_2$, which would result in stimulated emission in a suitable radiation field, and this was put forward as an amplifying system for microwaves. In 1954 Gordon, Zieger & Townes achieved coherent radiation at 23.9 GHz. by electrostatically separating the excited molecules from a beam of ammonia, and directing these into a microwave resonant cavity, and coined the name MASER for this device (Microwave Amplification by Stimulated Emission of Radiation). The use of a three level system, involving an additional source of r.f. power to achieve inversion, or partial inversion, of two energy levels, and emission from a transition to an intermediate level was proposed by Basov & Prokhorov (1955), and extended independently by Bloembergen (1956) to include the use of the paramagnetic energy levels in a solid as a c.w. three level maser. The first demonstration of a Bloembergen type maser was by Scovil, Feher & Seidel (1957), using the Gd^{3+} ions in lanthanum ethyl sulphate, and the first use of ruby as a maser material was by Makhov et.al. (1958). Figure 1.4 is a diagram of the energy levels involved in the operation of a three level maser.

The operation of a three level solid state maser imposes several stringent conditions on the spin system to be used.

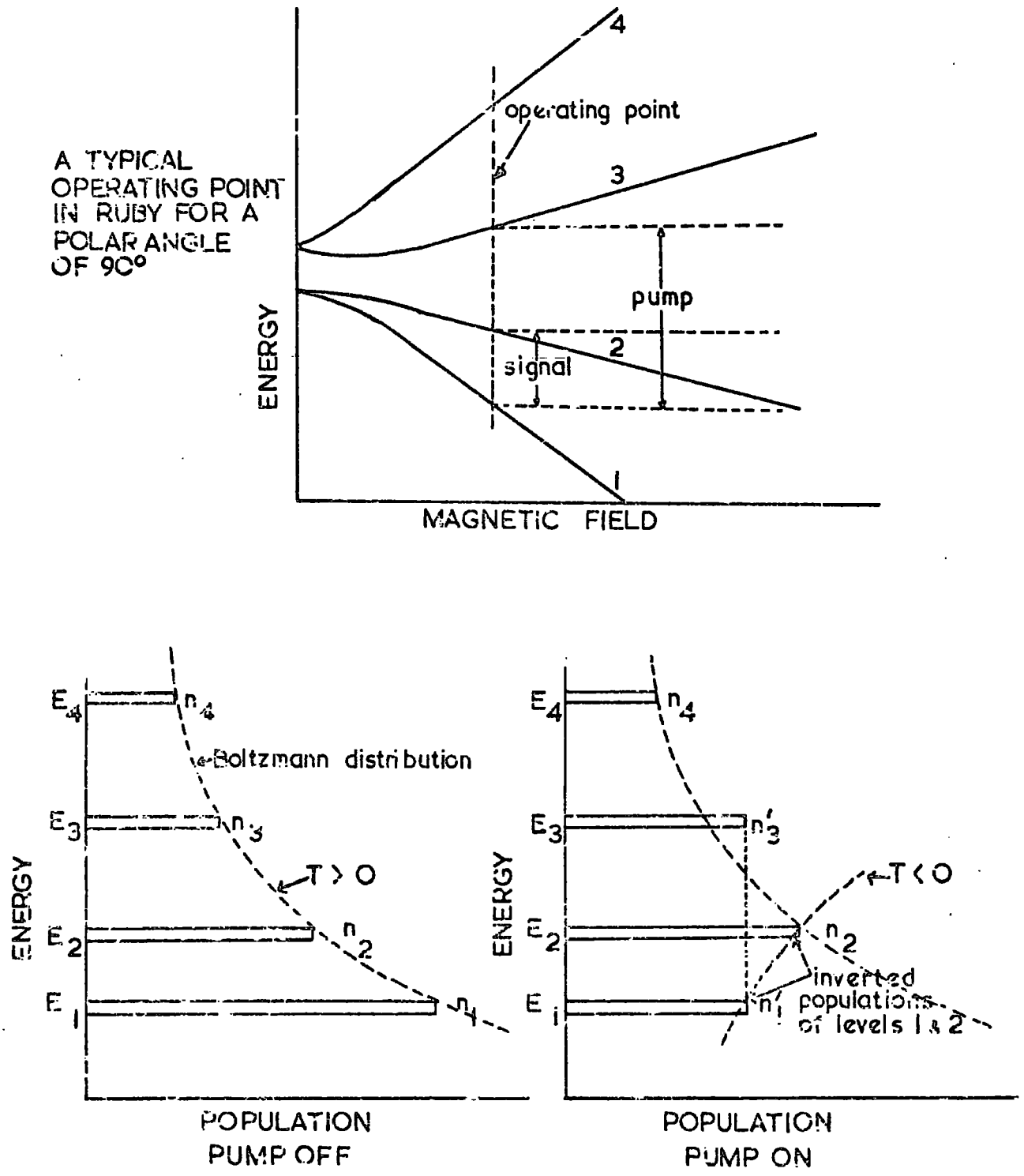

FIGURE 1.4 THE ENERGY LEVELS AND THEIR POPULATION DIFFERENCES INVOLVED IN THE OPERATION OF A THREE LEVEL MASER

Firstly, there must be three suitable paramagnetic energy levels, whose splittings can be brought into the microwave region by the application of a magnetic field, and are such that sufficient pump power is available at ν_{13} from a microwave generator, and the signal frequency, ν_{23} or ν_{12}, is one at which there is a requirement for low noise amplification of low level signals. The paramagnetic and host lattice ions should preferably have no nuclear magnetic moment in order to eliminate hyperfine splitting of the levels, and the crystalline field at the active ion should be such that the mixing of pure spin states (eq. 1.02) causes a large matrix element between levels 1 and 3 (the pump transition), giving a high transition probability W_{13}, and allowing this forbidden $\Delta M = 2$ transition to be used at a reasonable pump power level.

The concentration of paramagnetic ions must be high enough to overcome losses in the maser cavity and circuitry, and to give a useable power output, but must be low enough to reduce spin-spin interactions to the minimum, which implies a narrow linewidth, to allow saturation of the pump transition (this is equalisation of the populations n_1 and n_3). The values of the spin-lattice relaxation times for the three transitions is also of the utmost importance, as they determine the inversion ratio, I, defined as the ratio of the population differences between the signal levels in the inverted and thermal equilibrium cases;

attainment of a high value of I is one of the chief criteria for optimum maser performance.

In addition to these electronic properties, a maser material should have certain physical properties, viz: it must be chemically stable and durable, but fairly easily machineable to shape for practical applications, and also, in view of the fact that all masers are operated at low, usually helium, temperatures, it must be capable of withstanding thermal shock, and also have good thermal conductivity at these temperatures to avoid heating of the material due to the absorption of pump power. The host material must also not be lossy at the frequencies and temperatures involved. The material must also be capable of being grown into single crystals, of at least centimetre dimensions for most applications, and of a high degree of crystalline perfection, without voids, strain, misorientation of axes etc., and with homogeneous distribution of the active ions.

The fulfilment of all these requirements has eliminated many materials which otherwise may have satisfied some requirements only, and the material which has achieved foremost utilisation in practical masers is the system of Cr^{3+} in aluminium oxide, ruby, which is the material examined in this thesis.

A limitation to the c.w. operation of multilevel masers at very high microwave frequencies has been the shortening of

relaxation times, and consequent degredation of the inversion ratio, at millimetric frequencies. These frequencies are becoming an important part of the microwave spectrum, due to the very large potential bandwidths available, but the lack of very low noise amplifiers operating in this region has inhibited its exploitation for communications purposes.

1.5 PARAMAGNETIC RELAXATION

In order to describe the mechanism whereby a spin system achieves thermal equilibrium within itself and with its surroundings three processes must be considered. These are spin-spin relaxation, cross relaxation and spin-lattice relaxation, which is the main concern of this thesis. Spin-spin relaxation is the process by means of which the spin system achieves thermal equilibrium within itself, cross relaxation is the attainment of equilibrium between spins of different species, while spin-lattice relaxation describes the way in which the spin system transfers energy to the lattice.

Dipolar interactions within a spin system have the effect of broadening the Zeeman levels of the system (this is a contribution to the homogeneous broadening of the resonance line), and they also effect the transitions between the broadened levels by means of which excited spins transfer their energy to non-excited spins and hence establish equilibrium within the system. Waller (1936) performed the first calculation of the

spin-spin relaxation time, T_2, considering a simple $S = \frac{1}{2}$ system in low magnetic field, such that the Zeeman energy was less than the internal field due to the surrounding nearest neighbour ions, and obtained the result

$$T_2 \propto \frac{6g^2\beta^2 N^{\frac{1}{2}}}{hr^3} \qquad 1.13$$

N being the number of nearest neighbour ions at distance r from the centre being considered. For pure paramagnetic salts with typical interatomic spacings of a few angstroms this results in $T_2 \cong 10^{-9}$ secs., and even in magnetically dilute systems, T_2 is very short in comparison with the spin lattice relaxation time.

Kronig & Bouwkamp (1938) considered the case, usual under E.S.R. conditions, of the Zeeman energy being much greater than the dipolar energy,

$$g\beta H \gg \frac{g^2\beta^2}{r^3} \qquad 1.14$$

and in this situation found that

$$T_2 = \frac{6g^2\beta^2 N^{\frac{1}{2}}}{hr^3} \exp(H/H_i)^2 \qquad 1.15$$

where H_i is the average internal field due to the other spins acting at the spin in question. In order of magnitude $1/T_2$ is equal to half the homogenous resonance linewidth, and since it does not involve the lattice energy, it is essentially temperature independent.

For more complicated spin systems, either with $S > \frac{1}{2}$ or containing more than one type of spin centre, the process of cross-relaxation, discussed by Bloembergen et. al. (1959), and further by Grant (1964), must be considered. Where the levels of a single multilevel spin system are exactly, or to a close approximation, equispaced, or where the energy spacings of the levels are in simple whole number ratios (harmonically spaced, Chang (1960)), or where these relationships apertain between the energy levels of two different spin systems in the same sample, then spin energy may be transferred by the transition of one or more excited ions to their ground state, with the simultaneous trnasition of a non-excited ion to an excited state, the total spin energy being conserved.

If the energy spacings of the levels involved, say $h\nu_a$ and $h\nu_b$, are not exactly equal, so that, say,

$$2h\nu_a \cong h\nu_b \qquad 1.16$$

implying that the simultaneous downward transition of two 'a' spin results in the upward transition of one 'b' spin, then the dipole - dipole coupling will take up or supply the energy difference necessary for energy conversion. Measurements of cross-relaxation times (Pershan (1960), Mims & McGee (1960)), and harmonic cross relaxation (Kopvillem (1960)) are in fairly good agreement with the theories of Bloembergen and Grant.

The time that it takes for a spin system to return from

an initial perturbed state to a state in thermal equilibrium with its surroundings (the lattice in the case of a solid) is known as the spin-lattice relaxation time, T_1. Considering a simple two level system, with energy levels E_1 and E_2, $E_1 < E_2$, and respective spin populations n_1 and n_2 ($n_1 + n_2 = N$ the total spin population), the rates at which relaxation transitions occur between the levels may be defined by relaxation transition probabilities, w_{12} and w_{21} for upward and downward transitions respectively, (these are not the same as the stimulated transition probabilities W_{12} etc.). It is the calculation of these transition probabilities from consideration of the properties of the paramagentic ions and the host lattice, and external experimental conditions, that theories of relaxation have attempted.

Relaxation rate equations may be written describing the rate of change with time of the populations, n_1 and n_2;

$$dn_1/dt = w_{21}n_2 - w_{12}n_1 \qquad 1.17a$$

$$dn_2/dt = w_{12}n_1 - w_{21}n_2 \qquad 1.17b$$

Since N is usually very large ($\sim 10^{20}$) it is permissible to treat n_1 and n_2 as continuous variables, even though the transitions do cause discrete changes of the populations. In thermal equilibrium, the populations are constant, and so, denoting the thermal equilibrium populations as n_{1o} and n_{2o},

$dn_{1o}/dt = dn_{2o}/dt = 0$, and this will be the case (c.f. eq. 1.10) if,

$$w_{21}/w_{12} = n_{1o}/n_{2o} = \exp((E_2 - E_1)/kT) \qquad 1.18$$

A single rate equation may be derived from 1.17 by subtraction;

$$dn_1/dt - dn_2/dt = d\Delta n/dt = (w_{21} - w_{12})N - (w_{12} + w_{21})\Delta n \qquad 1.19$$

Δn being the population difference, $n_1 - n_2$, and Δn_o the thermal equilibrium value. If the system is disturbed so as to produce a population difference Δn^* at time t =0, then the solution of 1.19 for the time varying value of Δn is;

$$\Delta n(t) = \Delta n_o + (\Delta n^* - \Delta n_o) \exp -(w_{12} + w_{21}).t \qquad 1.20$$

The time constant describing the relaxation of Δn back to equilibrium is the spin lattice relaxation time, T_1, which can therefore be written

$$T_1 = (w_{12} + w_{21})^{-1} \qquad 1.21$$

In the case, which usually applies at microwave frequencies, that the exponent of eq. 1.18 obeys the condition $(E_2 - E_1)/kT \ll 1$, then the approximation $w_{21} = w_{12}$ may be made in which case

$$T_1 = \tfrac{1}{2}w_{12} \qquad 1.22$$

In the general case of a multilevel spin system containing p levels, relaxation will be a complex process involving all the levels, and the general rate equation for the i th level will be, (c.f. eq. 1.17)

$$dn_i/dt = \sum_{\substack{j=1 \\ j\neq i}}^{p} (w_{ji}n_j - w_{ij}n_i) \qquad 1.23$$

as before, the transition probabilities between any two levels will be in the Boltzmann ratio of the populations of those two levels, (c.f. eq. 1.18)

$$w_{ij}/w_{ji} = \exp((E_j - E_i)/kT) \qquad 1.24$$

Since the populations are all interrelated by the rate equations it is not possible to perform a subtraction of the type which results in eq. 1.19 in the two level case, but the relaxation behaviour of the system will be controlled by (p - 1) relaxation times, T_{ij}, where

$$T_{ij} = (w_{ij} + w_{ji})^{-1} \qquad 1.25$$

and so 1.22 may be written as

$$dn_1/dt = -\sum_{\substack{j=1 \\ j\neq i}}^{p} \frac{\Delta n_{ij} - ((n_i + n_j)/(n_{io} + n_{jo}))\Delta n_{ijo}}{2T_{ij}} \qquad 1.26$$

and the solution of 1.26 for the time varying population of level i will be sum of exponential terms of the form:

$$n_i(t) = n_{io} + \sum_{\substack{j=1 \\ j\neq 1}}^{p} C_{ij} \exp -(t/T_{ij}) \qquad 1.27$$

which must be evaluated numerically.

In an experiment, the relaxation behaviour of a particular level will frequently be dominated by one of the T_{ij}'s, having

a large amplitude constant C_{ij}, and this will be the time constant of the observed relaxation recovery, although more than one exponential may be observed, but in the simpler two level case, 1.27 effectively reduces to eq. 1.20, which contains only one exponential.

Waller (1932) made a calculation of T_1 in which he considered that the spin and orbital angular momenta of a paramagentic ion were completely decoupled, and that the spin was influenced by the lattice vibrations (phonons) only by their modulation of the dipolar coupling. This led to results which were several orders of magnitude larger than the experimental results obtained from studies of r.f. susceptibilities by Gorter (1936) at Leiden University, although the two main processes (direct and Raman relaxation) were shown to agree in form with Waller's predictions.

Later work by Heitler and Teller (1936) postulated that the modulation of the crystalline Stark effect by the phonons would provide a stronger relaxation mechanism, but still led to relaxation times that were too long when compared to experiment. Fierz (1938), Kronig (1939) and Van Vleck (1940) subsequently refined the theory of the mechanism which is largely accepted now, that the lattice vibrations modulate the crystalline field at the paramagentic ion due to their displacement (strain) of

the surrounding ions of the host lattice, and hence couple the phonons to the orbital momentum of the paramagnetic ion, and residual spin-orbit coupling then results in an overall coupling between the phonons and the spin, this being the mechanism whereby each individual spin transfers its energy to the lattice, with no co-operative effects from the other spins to which it is coupled.

At the time Van Vleck thought that the comparison between his calculations and the results of the Leiden group for the Ti^{3+} ion "miserable", although this apparently was due to decomposition problems associated with the alum itself, for subsequently this theory has had much success in describing the relaxation behaviour of a wide range of paramagnetic systems.

The theory was amplified by Mattuck and Strandberg (1960), using a modification of Van Vleck's approach to derive a spin-Hamiltonian formalism for the transition group ions, and Orbach (1961) proposed a third process involving real excited states of the ion, which is especially relevant in describing the relaxation of the rare earth ions. These theories of relaxation will be dealt with in further detail in Chapter 2, but some of the results of them will be quoted here.

In dealing with the relaxation of a single ion to the lattice, three processes may be involved. These are the direct

process, the Raman process and the Orbach, or resonance relaxation, process. These processes do not involve any co-operative processes such as cross-relaxation, or exchange interactions between clusters of ions, and are usually applicable only to salts of low paramagnetic concentration.

In the direct process the spin relaxes from state $|b\rangle$ to state $|a\rangle$ and in so doing emits a single phonon of energy δ_{ab}, where δ_{ab} is the splitting in energy between the two states. Calculation of the transition probability for this process for a Kramers doublet (one in which the two spin states are time conjugates of each other of half integral quantum number) leads to the dependance of T_1 on temperature and applied magnetic field being

$$T_1 = aH^{-4}T^{-1} \qquad 1.28$$

while for a non-Kramers salt, the dependence is

$$T_1 = a'(\delta_{ab})^{-2}T^{-1} \qquad 1.29$$

Where δ_{ab} is proportional to the applied magnetic field, then T_1 is inversely proportional to H^2.

The Raman process involves the scattering of a phonon of energy $h\nu'_p$ to energy $h\nu''_p$ where $h\nu''_p - h\nu'_p = \delta_{ab}$. This is equivalent to the absorption of the phonon of $h\nu'_p$ by the spin in state $|b\rangle$, causing a transition to a virtual state $|c\rangle$, followed by the emission of the $h\nu''_p$ phonon, and relaxation of

the spin to state $|a\rangle$. The calculated dependences for T_1 for this process are, for a Kramers salt,

$$T_1 = bH^{o}T^{-9} + b_1H^{-2}T^{-7} \qquad 1.030$$

the dependence of $H^{-2}T^{-7}$ only being relevant under certain circumstances, as discussed by Orbach (1961a). For a non-Kramers salt the dependence is

$$T_1 = b'H^{o}T^{-7} \qquad 1.31$$

The third relaxation process, the Orbach, or resonance relaxation, discovered by Finn, Orbach & Wolf (1961) is also a two phonon process, involving the absorption of a phonon $h\nu_p'$ by the spin in state $|b\rangle$, and its transition to a close lying excited level $|c\rangle$, with a splitting Δ above the ground levels, and then subsequent relaxation of the spin to state $|a\rangle$, with emission of a phonon $h\nu_p''$, where, as for the Raman process, $h\nu_p'' - h\nu_p' = \delta_{ab}$, but the state $|c\rangle$ is a real state, not a virtual one. This process is only important if the splitting Δ is less than the Debye energy, $k\Theta_D$, which is that of the highest energy phonon in the lattice phonon spectrum. In this case, the dependence of T_1 on temperature is exponential;

$$T_1 = c \exp\ (-\Delta/kT) \qquad 1.32$$

for both Kramers and non-Kramers salts, and the magnetic field depends on both internal hyperfine and dipolar fields, as well as applied field (Orbach, 1961b).

In a system in which all these processes are operative, the overall dependence of relaxation time on field and temperature will be

$$T_1^{-1} = aH^4T + bH^0T^9 + b_1H^2T^7 + c \exp(-\Delta/kT) \qquad 1.33$$

for states which half integral time conjugates of one another, otherwise, for non-Kramers salts,

$$T_1^{-1} = a'H^2T + b'H^0T^7 + c' \exp(-\Delta/kT) \qquad 1.34$$

The results quoted above all relate to relaxation in a perfect lattice. Due to the complexity of describing an imperfect lattice quantitatively the problem of calculating T_1 in this case has not received very much detailed attention. The effects on T_1 of imperfections in the lattice such as strain, mosaic misorientation and charged defects have however received some attention experimentally, and generally have been shown to contribute to the inhomogeneous line width of the resonance lines, and also to reduce the relaxation time.

With respect to eqns. 1.33 and 1.34, the temperature dependence of T_1 has received exhaustive study in many paramagnetic systems, and the various dependencies, T^{-1}, T^{-7} etc. have been established under conditions which conform to theoretical predictions, but the field dependence has received relatively little study, although Davids & Wagner (1964) showed that potassium cobalticyanide containing Fe^{3+} obeyed eqn. 1.28

very closely, displaying a $T_1 \propto H^{-4}$ dependence for the direct process at helium temperatures from 4GHz. to 12 GHz. A major difficulty in observing the field dependence over a large range of H is that the frequency of observation is proportional to the magnetic field (eq. 1.09), and therefore several spectrometers operating in different microwave frequency bands are required.

It was decided to measure the dependence of T_1 on magnetic field in a range of artificial ruby samples grown by various methods, and to relate this to their degree of crystalline imperfection, for the following reasons;

(i) Very little attention has been paid experimentally to this field of study.

(ii) The limitations, mentioned in sec. 1.4, on high frequency maser action due to the reduction of T_1.

(iii) Other workers have found little definite frequency dependence of T_1 in ruby at lower frequencies.

(iv) There was already existing an evaluation of imperfections in a range of ruby samples in the Department.

(v) Suitable equipment was partly in existence in this Department.

This has involved measurements of T_1 at X, J, K, Q and O bands (9, 16, 22, 35 and 70 GHz) with existing and recently built spectrometers, using the pulse saturation method (Davis,

Strandberg & Khyl, 1958), and the pulse response technique developed in this Department (Brown & Thorp, 1967). All the measurements have been made at helium temperatures, in order to observe the direct relaxation in ruby. The theory, a description of the apparatus and techniques, and results, are contained in the succeeding Chapters.

Chapter 2

THE THEORY OF PARAMAGNETIC RELAXATION

2.1 Introduction

As noted in section 1.5, the first attempt to calculate the spin-lattice relaxation time was made by Waller in 1932, using a model in which the lattice vibrations modulated the dipolar interaction directly, and although this work demonstrated the existance of the direct and Raman processes, the relaxation times that it yielded were several orders of magnitude larger than experimental results. Later work by Van Vleck (1940) gave a more exact form to the theories originated by Heitler & Teller, Fierz and Kronig, that the dominant mechanism is the modulation of the crystalline electric field by the phonons.

Van Vleck performed specific calculations for Cr^{3+} and Ti^{3+} ions in alums, and this was generalised by Mattuck & Strandberg (1960) to cover all iron transition group ions, using a spin Hamiltionian formalism, but retaining the same physical model as Van Vleck. An account of this single ion theory to show the derivation of the transition probability and relaxation time from a phonon-spin interaction Hamiltonian will now follow.

2.2 The spin-lattice relaxation time

As this is a single ion theory, the effects of spin-spin interactions are ignored, making it strictly applicable only to very dilute systems. Also the effects of lattice

distortion due to the presence of the paramagnetic ion, which may be of different size to the ion that it has replaced, are disregarded, although Klemens et.al.(1963) have pointed out that this assumption may be fallacious, but this point will be returned to later.

The perturbation treatment applied to an ion in a lattice will depend upon the relative magnitudes of the crystalline potential at the ion site, V_c, the energy of the free ion, $\mathcal{H}_o$, and the spin-orbit energy, $\lambda \underline{L}.\underline{S}$. Three cases may be distinguished.

1. $\mathcal{H}_o > \lambda \underline{L}.\underline{S} > V_c$ which is a weak crystal field, and is found in the rare earth ions, which have a filled outer shell of electrons which shield the spin-orbit interaction from V_c.

2. $\mathcal{H}_o > V_c > \lambda \underline{L}.\underline{S}$, this is the case of a medium crystal field, and is that found in the transition element ions under most circumstances.

3. $V_c > \mathcal{H}_o > \lambda \underline{L}.\underline{S}$ is the strong crystal field condition, which occurs in the case of ions with unfilled 4d and 5d shells, and for some 3d ions, where there is a considerable degree of covalent bonding.

The following theory considers case 2, the medium crystal field, and for such an ion V_c and $\lambda \underline{L}.\underline{S}$ can be considered as successive perturbations on $\mathcal{H}_o$, and in the lattice, a total Hamiltonian of the form

$$\mathcal{H} = \mathcal{H}_l + \mathcal{H}_o + V_c + 2\beta \underline{S}.\underline{H} + \lambda \underline{L}.\underline{S} + \beta \underline{L}.\underline{H} \qquad 2.1$$

may be written, $\mathcal{H}_l$ being the lattice vibrational energy,

β the Bohr magneton, $\underline{S}$ and $\underline{L}$ the spin and orbital angular momenta of the ion, λ the spin-orbit coupling constant, and $\underline{H}$ the applied magnetic field.

2.2.1 The phonon field

The vibrations of a lattice can be described by a Hamiltonian involving independent modes of vibration, which is:

$$\mathcal{H}_1 = \sum_p \left(\tfrac{1}{2}\hbar\omega_{p1}\left(\alpha^*_p\alpha_p + \alpha_p\alpha^*_p\right) + \tfrac{1}{2}\hbar\omega_{p2}\left(\beta^*_p\beta_p + \beta_p\beta^*_p\right)\right.$$
$$\left. + \tfrac{1}{2}\hbar\omega_{p3}\left(\gamma^*_p\gamma_p + \gamma_p\gamma^*_p\right)\right) \qquad 2.2$$

where α_p, α^*_p etc. are the Bose annihilation and creation operators, and for each value of p there are three distinct modes, of angular velocities ω_{p1}, ω_{p2} and ω_{p3}, one of which may be regarded as longitudinally polarised, the other two being orthogonal transverse modes. By using the commutation rules for the Bose operators, the Hamiltonian can be rewritten

$$\mathcal{H}_1 = \sum_p \hbar\omega_p\alpha^*_p\alpha_p + \hbar\omega'_p\left(\beta^*_p\beta_p + \gamma^*_p\gamma_p\right) \qquad 2.3$$

ω_p now being the angular frequency of the pth. longitudinal mode, and ω'_p that of the pth. transverse mode. A simplification of this description of the lattice energy which is frequently made in relaxation theory is to assume the Debye model for the lattice, in which $\omega_p = \omega'_p$, although usually $\omega_p > \omega'_p$, and p then becomes the phonon mode number, and $\omega_p = v|\underline{k}_p|$ where v is the velocity of sound in the lattice, and $\underline{k}_p$ is the propagation vector for the pth. mode. This assumption is equivalent to

assuming that the lattice is isotropic and dispersionless, that all the phonon modes have the same velocity, longitudinal or transverse, and that all the atoms in the lattice have the same mass and amplitude of vibration.

The allowed energies of a mode are now the eigenvalues $\hbar\omega n$ of $\hbar\omega\alpha^*\alpha$, and the eigenstates of the complete lattice may now be written as $|n_1,n_2,n_3,\ldots n_p\ldots\rangle$ where n_p is the number of phonons in the pth. mode (the occupation number). The lattice Hamiltonian can now be written

$$\mathcal{H}_1 = \sum_p \hbar\omega_p(\alpha_p^*\alpha_p + \tfrac{1}{2}) \qquad 2.4$$

and the phonon annihilation and creation operators have non-zero off diagonal matrix elements given by

$$\begin{aligned}\alpha_p^* \,|\ldots n_p\ldots\rangle &= (n_p+1)^{\frac{1}{2}}\,|\ldots n_p+1\ldots\rangle \\ \alpha_p \,|\ldots n_p\ldots\rangle &= (n_p)^{\frac{1}{2}}\,|\ldots n_p-1\ldots\rangle \end{aligned} \qquad 2.5$$

using the Debye model, the density of phonon modes in the crystal is

$$\rho(\omega) = dn/d\omega = \frac{3\omega^2 V}{\pi v^3} \qquad 2.6$$

providing ω is less than the Debye frequency, $2\pi v(3N/4\pi V)^{1/3}$, where V is the volume of the crystal, containing N atoms. The average thermal equilibrium occupation number of the pth. mode is given by the Bose-Einstein formula:

$$\bar{n}_p = (\exp(\hbar\omega_p/kT) - 1)^{-1} \qquad 2.7$$

If the equilibrium position of an ion in the lattice is designated by a vector $\underline{r}$, and the displacement from this

position in the a direction due to the phonon induced strain by u_{ra}, where a can be any of the Cartesian directions x,y,z, then u_{ra} can be written, after Klemens (1958), as:

$$u_{ra} = (2\hbar/M)^{\frac{1}{2}} \sum_{p} (\omega_p)^{-\frac{1}{2}} \phi_{pa} (\alpha_p + \alpha_p^*) \cos(\underline{k}_p . \underline{r} + \Delta_p) \qquad 2.8$$

where M is the mass of the crystal, ϕ_{pa} is the a component of the unit polarisation vector for the pth. mode, and Δ_p is an arbitrary phase factor for the pth. mode.

2.2.2 The crystalline electric field modulation

The crystal field potential at the paramagnetic ion will be modulated by the displacements of the neighbouring atoms due to the lattice vibrations described above. If the nearest neighbour cluster only is considered, the vibrations may be described in terms of the normal coordinates, Q_f, of the cluster with respect to the paramagnetic ion (Van Vleck, 1939), and the modulation of V, the crystal field, may be expanded as a power series in terms of Q_f's.

$$V = V_o + \sum_f \frac{\partial V}{\partial Q_f} \cdot Q_f + \frac{1}{2} \sum_{ff'} \frac{\partial V^2}{\partial Q_f \partial Q_{f'}} \cdot Q_f Q_{f'} + \ldots\ldots \qquad 2.9$$

where V_o is the static crystal field at the spin. The Q_f are linear combinations of the ordinary displacements of the nearest neighbours:

$$Q_f = \sum_{la} B_{fla} \, \delta r_{la} \qquad 2.10$$

where δr_{la} is the displacement in the a (= x, y, z) direction of the lth nearest neighbour, at vector position r_l with respect to the spin, assumed for simplicity to be at the same position

as the paramagentic ion nucleus. Using 2.8, the δr_{la} can be expanded in terms of the normal phonon modes, using the long-wavelength approximation, (Ziman, 1960) that the phonon wavelength is much larger than the interatomic spacing within the neighbour cluster, and so,

$$\delta r_{la} = (2h/M)^{\frac{1}{2}} \sum_{p} (\omega_p^{\frac{1}{2}}/v)\, \phi_{pa}(\alpha_p + \alpha_p^*)\underline{K}_p.\underline{r}_l \sin \Delta p \qquad 2.11$$

where $\underline{K}_p$ is the unit vector in the $\underline{k}_p$ direction, and the substitution $|\underline{k}_p| = \omega_p/v$ has been made.

Hence, substituting eq'ns 2.10 and 2.11 into 2.9, the expression for the dynamic lattice potential becomes

$$V = V_o + \sum_{fp} V_f A_{fp}(\alpha_p + \alpha_p^*) + \sum_{ff'pp'} V_{ff'} A_{fp} A_{f'p'} (\alpha_p + \alpha_p^*)(\alpha_{p'} + \alpha_{p'}^*) + \ldots \qquad 2.12$$

In which expression $V_f = \frac{\partial V}{\partial Q_f}$, $V_{ff'} = \frac{\frac{1}{2}\partial^2 V}{\partial Q_f \partial Q_{f'}}$

and $A_{fp} = \left(\frac{2\hbar\omega_p}{Mv^2}\right)^{\frac{1}{2}} \sin \Delta_p \sum_{la} \phi_{pa} B_{fla} \underline{K}_p.\underline{r}_l$.

2.2.3 The transition probability

With reference to eqn. 2.1, the total Hamiltonian can now be written as;

$$\mathcal{H} = \sum_p \hbar\omega_p(\alpha_p^*\alpha_p + \tfrac{1}{2}) + \mathcal{H}_o + V_o + 2\beta \underline{S}.\underline{H} + \lambda \underline{L}.\underline{S} + \beta \underline{L}.\underline{H} + \sum_{fp} V_f A_{fp}(\alpha_p + \alpha_p^*) + \sum_{ff'pp'} V_{ff'} A_{fp} A_{f'p'} (\alpha_p + \alpha_p^*)(\alpha_{p'} + \alpha_{p'}^*) \qquad 2.13$$

which may be subdivided into three parts, $\mathcal{H}_L$, $\mathcal{H}_S$, $\mathcal{H}_I$, the lattice Hamiltonian, involving only lattice parameters, the

spin Hamiltonian, (c.f. eq. 1.4) which describes the ground state energy levels of the ion, and involves only parameters of the paramagentic ion in the static crystal field of the host lattice, and the interaction Hamiltonian, which involves mixed parameters, and can be regarded as describing energy conserving transitions between the eigenstates of $\mathcal{H}_S$ and $\mathcal{H}_L$.

$$\mathcal{H}_L = \sum_p \hbar\omega_p \left(\alpha_p^* \alpha_p + \tfrac{1}{2}\right) \qquad 2.14$$

$$\mathcal{H}_S = \mathcal{H}_o + V_o + 2\beta \underline{S}.\underline{H} + \lambda \underline{L}.\underline{S} + \beta \underline{L}.\underline{H} \qquad 2.15$$

$$\mathcal{H}_I = \sum_{fp} V_f A_{fp} (\alpha_p + \alpha_p^*) + \sum_{ff'pp'} V_{ff'} A_{fp} A_{f'p'} (\alpha_p + \alpha_p^*)(\alpha_{p'} + \alpha_{p'}^*) \qquad 2.16$$

The calculation of the relaxation transition probability involves computing the matrix elements of $\mathcal{H}_I$ between simultaneous eigenstates of $\mathcal{H}_S$ and $\mathcal{H}_L$, which are given by the solutions of eq. 2.15, for $\mathcal{H}_S$ and eqn. 2.5 for $\mathcal{H}_L$.

2.2.3.a. The direct process

The first term in 2.16 is the largest, and usually the second part is unimportant. As this is purely an electric interaction term, it is operative only on the orbital moment of the paramagentic electron, and can thus be referred to as the orbit-lattice interaction, $\mathcal{H}_{ol}$. If two eigenstates of $\mathcal{H}_S$ are designated $|a\rangle$ and $|b\rangle$ (paramagentic energy levels), and a spin is initially in state $|b\rangle$, then under the action

of $\mathcal{H}_{ol}$ a transition may be made to state $|a\rangle$, energy being conserved by emission of a single phonon, of energy $\hbar\omega_p = \delta_{ab}$: i.e. phonon mode p goes from occupation number $|n_p\rangle$ to $|n_p + 1\rangle$.

Under first order time dependant perturbation theory the transition probability per unit time for this process is given (Landau & Lifshitz, 1959) by;

$$w_{ba} = 2\pi/\hbar^2 \, |\langle a, n_p+1| \, \mathcal{H}_{ol} |b, n_p\rangle|^2 \, \rho(\omega) \qquad 2.17$$

Using eqns. 2.5 and 2.6 to substitute into 2.17, and summing over all ions having a spin in state $|b\rangle$, and also summing over all phonon modes

$$w_{ba} = \frac{3\,\delta_{ab}^3}{2\pi\rho v^5 \hbar^4} \, |\langle a|\mathcal{H}_{ol}|b\rangle|^2 N_b (n_{ab} + 1) \qquad 2.18$$

where N_b is the population of state $|b\rangle$, ρ is the density of the crystal and n_{ab} is the Bose-Einstein occupation number (eq.2.7) evaluated for $\hbar\omega = \delta_{ab}$.

The transition probability for the reverse process, the absorption of a phonon by a spin in state $|a\rangle$, and a transition to state $|b\rangle$, must be subtracted from 2.18 to give a net rate of change N_b, with time, and then, providing that $\delta_{ab} \ll kT$, the relaxation time for the transition from $|b\rangle$ to $|a\rangle$ becomes;

$$1/T_1 = \frac{3\,\delta_{ab}^2 kT}{\pi\hbar^4\rho v^5} \, |\langle a|\mathcal{H}_{ol}|b\rangle|^2 \qquad 2.19$$

The distinction must now be made between Kramers and non-Kramers ions, for the above expression, 2.19, is valid only when the matrix element between states $|a\rangle$ and $|b\rangle$ is non-zero, which it is for states which are not time conjugates of one another (non-Kramers salts), which may be connected by the selection rule $\Delta m = 1$. Thus, for a non-Kramers ion, T_1 is inversely proportional to the absolute temperature, and to the square of the energyseparation of the eigenstates $|a\rangle$ and $|b\rangle$. When the energy levels are varying linearly with magnetic field, then the Zeeman splitting δ_{ab} is proportional to applied field, and so T_1 will be inversely proportional to H^2.

For a Kramers salt (one with ions having an odd number of electrons in their unfilled shell), it has been shown (Orbach, 1961c, Van Vleck, 1940) that it is a result of the behaviour of Kramers conjugate states under time reversal symmetry that the matrix element in 2.19 vanishes in zero magnetic field; this was referred to as quadrupole selection by Mattuck & Strandberg, and, after Van Vleck's original work, in which he noted the cancellation of various terms bringing about this zero result, it is sometimes known as Van Vleck cancellation.

In order to calculate T_1 in this case the presence of a magnetic field is necessary in order to break the time conjugate

nature of the Kramers doublet, $|\pm\tfrac{1}{2}p\rangle$, by admixture of higher excited states, $|q\rangle$, etc. of the ion, lying Δ_q above the ground doublet; matrix elements so obtained are reduced by a factor $\langle q|(\underline{\mu}.\underline{H})|\pm p\rangle / \Delta_q$, and the relaxation time is reduced by the square of this, so giving, using $g\beta H = \delta_{\pm p}$,

$$1/T_1 = \frac{12\beta^2 g^2 H^4 kT}{\pi\rho v^5 h^4 \Delta_q^2} \; |\langle q|\mu|-\tfrac{1}{2}p\rangle|^2 \, |\langle -\tfrac{1}{2}p|\mathcal{H}_{ol}|q\rangle|^2 \qquad 2.10$$

where μ is the magentic operator in the direction of $\underline{H}$.

From this it may be expected that for an ion with $S > \frac{1}{2}$ the only strongly allowed relaxation transitions will be those between levels of different Kramers doublets, while for an $S = \frac{1}{2}$ ion, the relaxation time will be inversely proportional to the temperature, as for a non-Kramers ion, but will be inversely proportional to H^4, which dependence has been shown in Fe^{3+} by Davids & Wagner (1964), as mentioned in section 1.5.

2.2.3.b Two phonon processes

The direct process, outlined above, can only use phonons of energy δ_{ab}/h, which constitute only a very small part of the phonon spectrum, as usually $\delta_{ab} \ll kT$, and the peak of the spectrum is around kT/h, the density of states being proportional to ω_p^2 (eq.2.6). The normal two phonon process, referred to as the Raman process by analogy with optical spectroscopy, compensates for this by using all of the phonon spectrum.

A spin, initially in state $|b\rangle$, can make a relaxation transition to state $|a\rangle$ by inelastic scattering of phonons. Thisproceeds by absorption of a phonon of energy $\hbar\omega_p$, effecting a virtual transition to a very short lived state $|c\rangle$, which, having a very short lifetime, has, by the uncertainty principle, ill defined energy, and is therefore not a true orbital state of the ion, but a virtual state. Almost simultaneously the spin relaxes to state $|a\rangle$, with the emission of a phonon of energy $\hbar\omega_q$, with the energy constraint;

$$\delta_{ab} = \hbar(\omega_q - \omega_p) \qquad 2.21$$

As long as $\delta_{ab} \ll kT$, this enables almost all of the phonon spectrum to be used. The computation of w_{ab} requires the use of the first term in eq. 2.16 to second order in time dependent perturbation theory, and the second term to first order. As in the case of the direct process, the first term is usually dominant, and only this will be considered. The effective orbit-lattice interaction for the two phonon processes is now of the form (Orbach, 1961a);

$$\mathcal{H}_{o12} = \sum_i \mathcal{H}_{o1}|i\rangle\langle i|\mathcal{H}_{o1}/(E_o - E_i) \qquad 2.22$$

where $|i\rangle$ is any intermediate state, and E_o and E_i are the energies of the initial and intermediate states. The transition probability is given by

$$w_{ab} = 2\pi/\hbar^2 \left| \langle a, n_q+1 \right| \sum_i \frac{\mathcal{H}^q_{ol} |i\rangle\langle i| \mathcal{H}^p_{ol}}{E_o - E_i} \left| b, n_p \right\rangle \Big|^2 \rho(\omega_p)\rho(\omega_q) \qquad 2.23$$

where $\mathcal{H}^x_{ol} = \sum_{fx} V_f A_{fx} (\alpha_x + \alpha^*_x)$, $x = p, q$.

In a similar way to the evaluation of eq. 2.18, summing over all spin sites containing $|b\rangle$ state spins, and subtracting the transition probability for the reverse process, the relaxation time is found to be

$$\frac{1}{T_1} = \frac{9}{4\pi^3\rho^2 v^{10}} \int_0^{\omega_D} \int_0^{\omega_D} \left| \sum_i \frac{\langle a|\mathcal{H}^q_{ol}|i\rangle \langle i|\mathcal{H}^p_{ol}|b\rangle}{\hbar\omega_p - \Delta_i} + \frac{\langle a|\mathcal{H}^p_{ol}|i\rangle\langle i|\mathcal{H}^q_{ol}|b\rangle}{-\hbar\omega_q - \Delta_i} \right|^2 \times$$

$$\rho(\omega_p)\ \rho(\omega_q)\ d\omega_p\ d\omega_q \qquad 2.24$$

where Δ_i is the energy splitting from the ground state to the i'th intermediate state.

Providing that the denominator of the integrand does not vanish (i.e. $\hbar\omega_p \neq \Delta_i$), and that $\Delta_i \gg kT$, and that there is no cancellation over the excited states $|i\rangle$, $\hbar\omega_p$ and $\hbar\omega_q$ can be ignored compared with Δ_i, and for non-Kramers ions the simplification;

$$\frac{1}{T_1} = \frac{9(6!)}{4\pi^3\rho^2 v^{10}} \left(\frac{kT}{\hbar}\right)^7 \left| \sum_i \Delta_i^{-1} \left(\langle a|\mathcal{H}^q_{ol}| i\rangle \langle i|\mathcal{H}^p_{ol}| b\rangle + \langle a|\mathcal{H}^p_{ol}| i\rangle \langle i|\mathcal{H}^q_{ol}| b\rangle \right) \right|^2 \qquad 2.25$$

is obtained, containing the well known result that T_1 is inversely proportional to T^7, and independent of magentic field

(or ground state splitting) for Raman processes in non-Kramers ions.

However, when $|a\rangle$ and $|b\rangle$ are time conjugate states of half integral quantum number, the excited states $|i\rangle$ will also occur as time conjugate pairs, at the same energy, Δ_i, and consequently when $|i\rangle$ is one state, say $|c\rangle$, only one pair of matrix elements in 2.24 will be non-zero, and when $|i\rangle$ is the other state, say $|d\rangle$, the other pair of matrix elements will be non-zero, of equal magnitude to the other pair, and of opposite sign (Orbach, 1961a). Quantitatively,

$$\langle a|\mathcal{H}^p_{ol}|d\rangle\langle d|\mathcal{H}^q_{ol}|b\rangle = -\langle a|\mathcal{H}^p_{ol}|c\rangle\langle c|\mathcal{H}^q_{ol}|b\rangle \quad 2.26$$

Although $\omega_p \cong \omega_q$, $\hbar\omega_p$ and $\hbar\omega_q$ are of opposite sign, preventing the sum of matrix elements being completely zero, and resulting in the reduced relaxation time for Kramers ions;

$$\frac{1}{T_1} = \frac{9!(kT)^9}{\pi^3\rho^2 v^{10}\hbar^7}\left|\sum_i \Delta_i^{-2}\langle a|\mathcal{H}^q_{ol}|i\rangle\langle i|\mathcal{H}^p_{ol}|b\rangle\right|^2 \quad 2.27$$

where the summation is only over states $|i\rangle$ which are time conjugate pairs. This gives the result that for Kramers salts, the relaxation time is inversely proportional to T^9, and again independent of δ_{ab} and H. It has been shown by Kronig & Bouwkamp (1938) that if the time conjugate nature of the Kramers states is broken by admixture of other states by an applied magnetic field, as discussed for the direct process, then T_1

should be proportional to $H^{-2}T^{-7}$ for Kramers ions. This however will only be a significant addition to 2.27 if other excited states of the ion are lying close to intermediate states $|i\rangle$.

A further Raman type process was proposed by Orbach & Blume (1962), which would occur in multilevel systems of Kramers doublets, when the intermediate states $|i\rangle$ are ground level states, not orbital states, and $\Delta_i \ll \hbar\omega_p$. Under the criterion $\lambda(\lambda/\Delta) > kT$, where λ is the spin-orbit coupling constant and Δ the crystal field splitting, a dependence $T_1 \propto T^{-5}$ is obtained at the low temperature end of the Raman region, but this is more important for the rare earth ions and third transition group ions than the first and second transition groups.

In 1961, Finn, Orbach and Wolf explained the relaxation behaviour of Ce^{3+} in cerium magnesium nitrate as a specialisation of the two phonon process when $\Delta_i < k\theta_D$ (θ_D is the Debye temperature), and the intermediate state $|i\rangle$ is a real excited orbital state of the ion. Under these conditions the denominator of the integrand in 2.24 vanishes as phonons of energy $\hbar\omega_p = \Delta_i$ are now able to enter into the relaxation process, and this implies a resonance between the phonon modes and static paramagnetic energy levels. The phonons involved are principally those of energy Δ_i, and energy is conserved at each step of the relaxation process, as well as overall. The situation is analogous to that found in optical resonance fluorescence

(Heitler, 1957), and the vanishing denominator is circumvented by introducing a finite lifetime h/Γ_i for the spin in the intermediate state, under the influence of $\mathcal{H}_{ol}$. The integrand of 2.24 will have two peaks, at $\hbar\omega_p = \Delta_i$ and at $\hbar\omega_p = kT$, but the former will be a narrower peak, and consequently, although an additive term to the normal Raman process, the resonance relaxation will be dominant, and the relaxation time for this process can be expressed as;

$$\frac{1}{T_1} = \frac{3}{2\pi\rho v^5} \cdot \frac{(\Delta_i/h)^3}{(\exp(\Delta_i/kT)-1)} \left[\frac{\langle a|\mathcal{H}^q_{ol}|i\rangle \langle i|\mathcal{H}^p_{ol}|b\rangle|^2}{|\langle a|\mathcal{H}^q_{ol}|i\rangle|^2 + |\langle i|\mathcal{H}^p_{ol}|b\rangle|^2} \right] \quad 2.28$$

which shows the characteristic exponential dependence of T_1 on temperature of $T_1 \propto \exp(\Delta_i/kT)$ for this process.

2.3 The phonon bottleneck

In the preceeding theory it has been assumed that the energy transmitted from the relaxing spins to the phonon modes is immediately transmitted out of the crystal to the surrounding refrigerant bath, thus not perturbing the phonon mode occupation numbers, and allowing them to be replaced by their thermal average values. This situation may not necessarily be so in the case of direct processes, and possibly Orbach relaxation, as both of these processes use only a very narrow resonant frequency band of phonons, and so, at liquid helium temperatures, where the specific heat of the phonons is very much less than

that of the spin system, there may occur a rise of 'phonon temperature' in this frequency band, corresponding to a phonon occupation number $\bar{n}'_p$, where

$$\bar{n}'_p = (\exp(h\omega_p/kT_p) - 1)^{-1} \qquad 2.29$$

where $h\omega_p = \delta_{ab}$ for the direct process, and T_p is the phonon temperature. Energy communicated to these resonant phonon modes can only be dissipated by direct radiation to thebath, or by inelastic scattering into different phonon modes.

In these circumstances there will exist the so called 'phonon bottleneck', when the observed relaxation behaviour will be dominated by the relaxation of the 'hot' phonons in selectively heated modes, which may be much slower than the true spin-phonon relaxation. The mechanisms which limit the phonon lifetime have been considered both theoretically and experimentally. Van Vleck (1941a & B) considered the scattering of phonons at the crystal surface to be the principal cause of bottlenecking, and that the phonon-phonon interaction, which would distribute the energy through the phonon modes, and so remove the heating of the resonant modes, is insufficient to break the bottleneck. Faughan and Strandberg (1961) give a theoretical treatment of the phonon bottleneck, and derive expressions for the conditions under which a steady state non-equilibrium phonon distribution will occur. They also consider the limitations on phonon life-

time due to phonon-phonon collisions, defects in the crystal, and absorption and scattering of phonons at the crystal boundaries, concluding that the latter is the principal mechanism in shortening the phonon lifetime, depending on the degree of acoustic mismatch at the junction of the crystal and helium bath.

Experimentally they attempted to observe the production of a non-equilibrium distribution of phonons in magnesium oxide doped with Cr^{3+} and in ruby, by observation of the diffusion of non-equilibrium phonons between two microwave cavities in a single sample. They did not see this effect, and estimated the rise in temperature of the phonons in contact with a saturated spin transition to be less than $0.04^{o}K$ in magnesium oxide, and less than $0.02^{o}K$ in ruby, at $4.2^{o}K$. Similar results were obtained when the crystals were polished to increase the reflection of phonons back into the sample, and their final conclusion was that the most probable reason for not observing the bottleneck is that the density of phonon states is not a Debye spectrum, but in fact that there are many more phonons of microwave frequencies to take part in the direct process than would be expected.

Nash (1961) observed relaxation times in copper Tutton salts which were dependent on crystal size, and ascribed these to phonon bottleneck. Scott and Jeffries (1962) derived the

spin-phonon and phonon-bath rate equations for the coupled spin-phonon-bath system:-

$$\frac{d\,\Delta n}{dt} = -\frac{1}{T_1}(\Delta n - \Delta n_o) - \frac{1}{T_1}\frac{n_o}{\bar{n}_p+\frac{1}{2}}(\bar{n}'_p - \bar{n}_p) \qquad 2.30$$

$$\frac{d\bar{n}'_p}{dt} = -\frac{1}{T_{ph}}\frac{\sigma(\bar{n}_p+\frac{1}{2})}{\Delta n_o}(n - n_o) - \frac{1}{T_{ph}}\cdot\left(\frac{n}{n_o}+1\right)(\bar{n}'_p - \bar{n}_p) \qquad 2.31$$

the notation being as used in section 1.5; T_{ph} is the phonon-bath relaxation time, and σ is the bottleneck factor, which may be defined as:-

$$\sigma = (E_s/T_1)/(E_p/T_{ph}) \qquad 2.32$$

where E_s is the Zeeman energy of the spin system, and E_p is the energy of the phonon system. If $\sigma \ll 1$, then the phonons are strongly coupled to the bath, and the observed relaxation is the spin-lattice (spin-phonon) relaxation, but if $\sigma \gg 1$, then there is a strong bottleneck.

The solutions of 2.30 and 2.31 have two time constants, T_b and T'_b, where $T_b \cong T_1 + t_1$, and, assuming $\sigma \gg 1$, and $E_s \gg E_p$,

$$t_1^{-1} \cong \frac{6\delta\nu k^2T^2V}{T_{ph}\pi^2Nv^3\hbar^3} \qquad 2.33 \qquad\qquad T_b'^{-1} \cong \frac{A\pi^2Nv^3\hbar^3}{6\delta\nu k^2TV} \qquad 2.34$$

where $\delta\nu$ is the linewidth of the resonance (which is approximately equal to the width of the phonon frequency band to which the spins transmit their energy in the direct process), N is

the number of spins in crystal volume V. After disturbance of the spin system to produce a population difference, Δn, the principal change in $\bar{n}_p'$ occurs with time constant T_b', which is much shorter than the time constant T_b for Δn, and so after Δn has almost returned to Δn_o, the thermal equilibrium value, both spins and phonons have reached a common temperature above that of the bath, and relax exponentially to the bath temperature with time constant T_b. In the case of there being no bottleneck, $T_b \cong T_1$, and in the case of a severe bottleneck $T_b \cong t_1$, and in this case a temperature dependence of $T_b \propto T^{-2}$ for the observed relaxation will be seen.

This was confirmed by Scott and Jeffries, who observed this dependence for the first time in rare earth ions in lanthanum magnesium nitrate, the most severe bottleneck occurring with the Pr^{3+} ion. They estimated that T_{ph} was of the order t/v where t is the thickness of a sample and v the velocity of sound in the sample, and thus ascribed the phonon lifetime to inelastic scattering of phonons at the crystal surface into other phonon modes.

Bottlenecking of the Orbach process has very rarely been observed because the phonons used in this process are of higher energy than those of the direct process and are better able to interact with phonons of similar frequencies, due to anharmonicity of the lattice, and so lose their energy.

Since the Raman process uses essentially all of the phonon spectrum, it is hardly to be expected that it could be bottlenecked in any way.

2.4 Modifications due to lattice defects and strain

Apart from the phonon bottleneck, which is more a consideration of the environment and experimental conditions surrounding a sample, than of the sample itself, all of the foregoing theories deal with paramagentic ions in what is regarded as a crystallographically perfect diamagentic lattice. This assumption of a perfect lattice is unlikely to be true in the case of a real material however, as the paramagentic ion itself will not be of the same mass as the ion it replaces in the lattice, and it will therefore constitute a defect site, causing distortion of the symmetry of the surrounding ligand ions, and also modification of the lattice waves. In addition, any material grown at high temperature by flame fusion, vapour phase or Czochralski methods, which includes the artificial gem-like materials such as rutile, sapphire, spinel, garnet and of course ruby, will contain a high number of crystallographic imperfections due to the thermal stresses involved in the growth method. Imperfections such as dislocations, grain boundaries and misorientations of the crystal axes within a single sample will contribute to microscopic strain in the lattice,

and this will have the effect of altering the interionic spacing between the paramagentic ion and its neighbours, and also of altering the symmetry of the ion site.

The disturbance of the crystalline field at the paramagnetic ion due to the alteration of the normal positions of the ligands will have the effect of introducing terms proportional to the lattice strain at the ligand ion into the expressions given in eq. 2.12 et.seq. In 2.12 $\underline{r}_l$ represents the distance of a ligand ion from the paramagentic ion, and if the ligand suffers displacement in the direction of $\underline{r}_l$ due to a compressive or extensive strain ϵ , then 2.12 may be rewritten as;

$$\underline{r}^s_{la} = (2h/M)^{\frac{1}{2}} \sum_p (\omega_p^{\frac{1}{2}}/v)\phi_{pa}(\alpha_p + \alpha^*_p)\underline{K}_p.\underline{r}_l(1 \pm \epsilon)\sin\Delta_p \qquad 2.35$$

where the superscript s denotes the case of a strained lattice. Hence, if the same strain is assumed to act isotropically at all the ligands,

$$A^s_{fp} = (2\hbar\omega_p/Mv^2)^{\frac{1}{2}}\sin\Delta_p \sum_{la} \phi_{pa}B_{fla}\underline{K}_p.\underline{r}_l(1 \pm \epsilon) = A_{fp}(1 \pm \epsilon) \qquad 2.36$$

and hence in the direct process, the interaction Hamiltonian for the strained case will be

$$\mathcal{H}^s_{ol} = \sum_{fp} V_f A^s_{fp}(\alpha_p + \alpha^*_p) = \mathcal{H}_{ol}(1 \pm \epsilon) \qquad 2.37$$

The static part of the crystalline potential, V_o, which appears in the spin Hamiltonian, $\mathcal{H}_S$, will also be modified by static strain; V_o can be written (Hutchings, 1964) as:

$$V_o = \sum_{1n} \frac{q_1 r^n}{r_1^{(n+1)}} \cdot \frac{4\pi}{2n+1} \sum_{m=-n}^{+n} (-1)^m Y_n^{-m}(\theta_1,\phi_1) Y_n^m(\theta_1,\phi_1) \qquad 2.38$$

where r_1, q_1, are the distance from the paramagentic ion nucleus, and the charge, respectively, of the 1th ligand in the unstrained case, r is the distance of the paramagentic electron from its nucleus, and the Y_n^m are normalised spherical harmonics of the angular positions (θ_1,ϕ_1) of the ligand ion with respect to the paramagentic nucleus. If an isotropic strain $\underline{\varepsilon}$ is assumed to act on the ligand ions, displacing them along their radius vectors $\underline{r}_1$, then $\mathcal{H}_S$ can be rewritten for the strained lattice;

$$\mathcal{H}_S^s = \mathcal{H}_o + 2\beta \underline{S}.\underline{H} + \lambda \underline{L}.\underline{S} + \beta \underline{L}.\underline{H} + V_o\left(\sum_n (1 \pm \underline{\varepsilon})^{-(n+1)}\right) \qquad 2.39$$

For a 3d ion the only values of n which have to be considered are n = 0, 2, 4. (Bleaney & Stevens, 1953). There will therefore be introduced into the eigenstates of $\mathcal{H}_S^s$ terms in $(1 \pm \underline{\varepsilon})^{-(n+1)}$, which will appear in the expression for the direct process transition probability;

$$w_{ba}^s = 2\pi/\hbar^2 \left| \langle a.K\left(\sum_n (1\pm\underline{\varepsilon})^{-(n+1)}\right),(n_p+1) \left| \mathcal{H}_{o\parallel}^s \right| b.K\left(\sum_n (1\pm\underline{\varepsilon})^{-(n+1)}\right),n_p \rangle \right|^2 \rho(\omega) \qquad 2.40$$

where K is a constant arising from the diagonalisation of $\mathcal{H}_S^s$, and w_{ba}^s is the transition probability for the strained

lattice, which may be written as a power series in $(1 \pm \varepsilon)$;

$$w_{ba}^{s} = A(1 \pm \varepsilon)^{-4} + B(1 \pm \varepsilon)^{-6} + C(1 \pm \varepsilon)^{-8}) \qquad 2.41$$

where A, B, C are contributions to the strained transition probability from the unstrained expression. It may be seen that a compressive strain, $-\varepsilon$, gives rise to an increase in the transition probability, i.e. to a decrease in the spin lattice relaxation time, which effect has been observed in the series of ruby samples studied in this thesis.

An additional effect of lattice defects such as interstitial ions and substitutional ions, which are of different mass from those that they replace, is modification of the assumed Debye spectrum of phonon modes. This involves the introduction of extra phonon modes, which may either be localised at the defect site, or propagated through the lattice, and also scattering of normal phonon modes at the defect site. Kochelaev (1960) has considered the scattering of phonons at defect sites as producing much larger relative displacements between ions than the normal modes of a perfect lattice. He considers this as having the greatest effect on the direct process, and derives an expression for the transition probability which is independent of magnetic field (c.f. eq.2.19), and inversely proportional to the distance between the paramagnetic ion and the defect site: consequently the relaxation time is dependent on the concentration of the paramagentic

ions and on the density of defect centres in the crystal.

Klemens (1962) and Castle et. al. (1963) have considered the effects of localised phonon modes created at defect sites. Montrell and Potts (1955) showed that when a substitutional impurity is more than 20% lighter than the atom it replaces, a new high frequency lattice mode arises, localised near the impurity since its frequency is above the Debye cut off frequency, which prevents the mode propagating through the lattice. This localised mode will affect the relaxation of a paramagnetic ion associated with the defect. Since the probability of excitation of a high frequency mode decreases with the decreasing temperature, the principal effect will be at higher temperatures on the Raman process. This involves interaction of the localised phonons with the normal modes, and decay of the local mode into two normal modes after interaction with the spin. This hasbeen considered by Feldman et. al.(1965) who find that for temperatures less than θ_i,

$$T_1^{-1} \propto \omega_i (h\omega_i/Mv)^3 .1/\delta_{ab} .\exp(-\theta_i/T) \qquad 2.42$$

where θ_i is the temperature associated with the local mode frequency, ω_i, in the same way as the Debye temperature is with the Debye cutoff frequency. The exponential temperature dependence predicted in 2.42 was observed by Feldman et. al. in the light ions H^- and D^- in calcium fluoride.

In the case of low frequency local modes, where $\omega_i < \omega_D$, the defect vibration will not be localised to the defect, but will be able to propagate through the lattice, and also interact with other defects. The calculation of the lattice strains produced and the frequencies involved uses the theory of a forced, damped oscillator, (Castle et. al. 1963) and results in a complex temperature dependance for T_1:

$$T_1^{-1} \propto \left[(T/\theta_D)^7 J_6(\theta_D/T) + B((T/\theta_D)^3 J_2(\theta_D/T) - (T/\theta_D)^3 J_2(\theta_i/T) + (T^{11}/\theta_i^8\theta_D^3) J_{10}(\theta_i/T))\right] \quad 2.43$$

the first term being the normal Raman process for a non-Kramers salt, and the additional terms arising from the local modes. The dependencies of T_1 on temperature in the Raman region have been observed in Cr^{3+} in magnesium oxide by Castle et. al. (1961) and in defect centres produced in irradiated quartz by Klemens et. al. (1963).

2.5 Cross-relaxation and co-operative effects

None of the foregoing theory considers interactions between paramagentic ions, which must be taken into account to discuss the concentration dependent relaxation effects which occur in all but very magnetically dilute samples. These processes are dependent on variation of the distance between paramagnetic ions in the lattice, and under the above heading there can be considered cross relaxation, exchange interaction

and ion clustering.

Cross relaxation can take place between the energy levels of two different paramagentic species, or between the levels of a single multilevel spin system. If two spin systems, a and b, have the same energy splitting between two levels in each system (but not necessarily the same absolute energy), then, calling these levels $|1\rangle$ and $|2\rangle$, and $|3\rangle$ and $|4\rangle$, a spin in the upper level of a, $|2\rangle$, can relax to the lower level, $|1\rangle$, while simultaneously a spin in the lower level of b, $|3\rangle$, is excited to the upper level, $|4\rangle$. The rate equations for these levels must now include cross-relaxation terms, e.g. for level $|1\rangle$; (c.f. eq. 1.17a)

$$(dn_1/dt)_{cr} = w_{cr}(n_2n_3 - n_1n_4) \qquad 2.44$$

which would be an additive term to eq. 1.17a, w_{cr} being the cross relaxation transition probability. In equilibrium, eq. 2.44 requires that $n_2/n_1 = n_4/n_3$, which implies that the two spin systems have the same spin temperature, since the energy gap is the same in each. The cross-relaxation transition probability can be related to a cross-relaxation time, T_{ab}, which is approximately $T_{ab} \cong 1/w_{cr}$, although the time response of a system under cross relaxation is not usually a simple exponential. Cross-relaxation is an energy conserving process which does not involve the lattice at all, and is therefore essentially temper-

ature independent. The mechanism for the effect is a weak dipolar coupling between the spins, which can absorb or donate sufficient energy to enable cross-relaxation to take place between pairs of levels which are not of exactly the same energy splitting. If one transition in, say system a, is excited by a pulse of microwave radiation under resonant conditions, then spin-spin relaxation will bring that transition of system a to internal equilibrium, as noted in section 1.5, and then the two systems, a and b, will come to a common spin temperature in the cross-relaxation time, T_{ab}, and then they will relax to their thermal equilibrium populations, with their spin-lattice relaxation times, T_{1a} and T_{1b}.

T_{ab} is usually much shorter than the spin-lattice relaxation time, and therefore shows itself as a fast initial recovery after the disturbance of the spin populations of a transition. If one of the species present has a very short T_1 compared with the other, then this will tend to dominate the observed relaxation behaviour of the other transition, as cross-relaxation attempts to keep both systems at the same spin temperature. Even if the fast relaxing species is of very low concentration compared to the slower relaxing species, spin-spin processes in the majority ions, which are generally very fast, will tend to transfer energy to the fast relaxing centres from more distant neighbours, and so still shorten the observed relaxation of the majority ions.

If the energy splittings of the levels of a single multi level species are equal, or nearly so, then cross relaxation can take place between the levels of the single species, and also if the levels are harmonically related in energy, within the single species, or between two different species, then multiple spin flips can occur (involving more than two simultaneous spin transitions) with energy conservation, as noted in section 1.5.

A further mechanism which can cause relaxation is phonon induced modulation of the exchange interaction between two paramagnetic ions. The exchange interaction is very strong, and extremely sensitive to interionic spacing, but is very short range, and has most effect between paramagnetic ions which are nearest neighbours. As discussed by Gill (1962) and Al'tshuler (1963), modulation of isotropic weak exchange alone will not induce relaxation, but small anisotropies due to crystal field, dipolar interactions, or the exchange itself, must be introduced to allow spin flips to occur. In the case of strong exchange, when the ions are neighbours, and referred to as an exchange coupled pair, the pair have their own spectrum of energy levels, within which relaxation may occur. It has been suggested by Van Vleck (1960) that the exchange coupled pairs may act as intermediate fast relaxing centres, to which normal uncoupled spins may cross-relax. The complexity of the pair

spectrum is such that the required energy equivalence for cross-relaxation to take place from the spectrum of the unpaired ions can almost always be satisfied. The energy splittings involved in the exchange spectrum are of the order of those required by the Orbach process, and this relaxation process may therefore be operative at the exchange coupled pair. This will bring high energy phonons into the relaxation, and so provide a possible by-pass of any phonon bottleneck in the relaxation of the unpaired ions. This process will be strongly concentration dependent, since the number of pairs will increase with increasing concentration. However even in nominally dilute samples, there may occur clustering of paramagentic ions at defect sites or grain boundaries, where it is energetically favourable for substitutional ions to be situated, and hence localised increases of concentration may occur, quite independently of the macroscopic concentration of the sample, and these 'exchange pockets' may dominate the relaxation behaviour of the material.

Chapter 3

THE MEASUREMENT OF RELAXATION TIMES: APPARATUS I

3.1 INTRODUCTION

The first experimental attempt to measure the variation of paramagentic susceptibility with the frequency of an applied magnetic field was made by Kammerlingh Onnes and Breit at Leiden in 1924. Their results were inconclusive; and it was left to Gorter (1936), working at the same University, to establish positively the existence of paramagnetic relaxation, by measurement of the variation in the power absorbed in a sample with the frequency of the applied magnetic field. These experimental results were several orders of magnitude less than the theoretical predictions of Waller (1932), although they did establish the existence of the direct and Raman processes of relaxation, as predicted by Waller.

With the discovery of paramagnetic resonance by Zavoisky in 1945, the major field of interest in magnetism became the study and interpretation of spectra, and the evolution, on the theoretical side, of the theory of crystalline fields and their capability to explain the observed resonance spectra. The study of paramagentic relaxation fell somewhat into abeyance until the late 1950's, when the advent of the solid-state maser (Basov & Prokhorov, 1955; Bloembergen, 1956; Scovil et. al., 1957) and the practical devices stemming from it, made the

study and explanation of relaxation, which enters critically into the efficiency of maser devices, a vital field of research in magnetism. At this time there were developed several techniques for measuring relaxation times under resonant conditions, which approximate closely to those in an actual maser cavity. In contrast to the pre-war results of the Dutch physicists, which yielded an average relaxation time for all the transitions of an ion, the resonant methods give information about a single transition only, and are able to give further information about departures of relaxation behaviour from the single ion theories described in Section 2.3 et. seq.. A summary of these techniques follows, succeeded by a description of some of the experimental techniques used in the present work.

3.2 METHODS OF MEASURING RELAXATION TIMES

The methods of measuring relaxation times fall into four general categories:

(i) Non-resonant techniques

(ii) Resonant C.W. techniques

(iii) Resonant pulse techniques

(iv) Ultrasonic techniques

The methods will be described under these sub-headings, the third category containing those used in this thesis.

3.2.1. Non-resonant techniques

The non-resonant method of measuring relaxation times was invented by Gorter (1936), and was initially used to test the theoretical predictions of Waller (1932). The method consists of measuring the frequency dependence of the components $\chi'(\omega)$ and $\chi''(\omega)$ of the total susceptibility $\chi(\omega)$ which are related by,

$$\chi(\omega) = \chi'(\omega) - i\chi''(\omega) \qquad 3.1$$

$\chi'(\omega)$ determines the magnitude of dispersive effects in the sample, and $\chi''(\omega)$, the absorption of power in the sample. The thermodynamic theory of relaxation given by Casimir and Du Pre (1938) assumes that the spin system and the lattice are two separate thermodynamic systems, each in internal equilibrium; the spin system equilibrium being maintained by spin-spin relaxation. Following these assumptions, the theory results in the following expressions for χ' and χ'':

$$\chi'(\omega) = \chi_{ad} + (\chi_o - \chi_{ad})/1+\omega^2\tau^2) \qquad 3.2a$$

$$\chi''(\omega) = (\chi_o - \chi_{ad})\omega\tau/1+\omega^2\tau^2 \qquad 3.2b$$

and the rate of energy absorption per unit volume of the sample is $P = \frac{1}{2}\omega\chi''(\omega) H_1^2$, where ω is the angular frequency of the alternating magnetic field, of intensity H_1, χ_{ad} and χ_o are the adiabatic and static susceptibilities and τ is the relaxation time. τ is dependent on the 'specific heat' of the spin system and the constant relating the energy transfer between spins and lattice to the difference of spin and lattice temperatures, and is an average relaxation time of

all the paramagnetic transitions in the sample.

The practical realisation of the method has many forms, some given by Gorter (1947), but usually the sample is placed in a coil which is fed with an alternating current, producing an alternating magnetic field, which is usually aligned parallel to a static magnetic field. The frequency of H_1 is varied at frequencies in the vicinity of τ^{-1}, and the changes in χ' and χ'' can be detected in a variety of ways. The original method of Gorter was to detect the absorption of power due to χ'' by a calorimetric method, and to detect the effects that χ' has on the frequency of the sample coil due to changes of its inductance. Alternatively, bridge methods of determining the changes of coil resistance and inductance, and phase sensitive detection of the effects of the components χ' and χ'', which are in phase quadrature, have been used.

None of these methods are as sensitive as modern resonance techniques, the limit of detection for useful results being of the order of 10^{17} spins at liquid helium temperature, compared with 10^{10} - 10^{12} spins for the best modern resonance spectrometers. Consequently, the method has found application principally to magnetically concentrated materials, within its principal limitation of only measuring a relaxation time averaged over all the spin transitions of the material.

3.2.2 Resonant C.W. techniques

3.2.2.a C.W. Saturation

This method of determining paramagnetic relaxation times is due to Eschenfelder and Weidner (1953), and is an adaption of a method used for measuring nuclear magnetic relaxation times. (Bloembergen et.al. 1948). The method depends upon the solution of the Bloch equations, and writing the imaginary part of the susceptibility as:

$$\chi'' = \tfrac{1}{2}\pi \chi_o \nu_o g(\nu) s_{ij} \qquad 3.3$$

where s_{ij} is the saturation factor for the transition from level i to level j, and only these two levels are considered to take part in the relaxation process. ν_o is the resonant frequency, and $g(\nu)$ is the normalised lineshape function, whence, from equation 1.6, the power absorbed in a sample may be written as:

$$P_a = -\tfrac{1}{2}\pi^2 \chi_o \mu_o \nu_o^2 H_1^2 g(\nu) si_j \qquad 3.4$$

If the lineshape of the resonance is Lorentzian, $g(\nu)$ may be written

$$g(\nu) = 2T_2/(1 + 4\pi^2(\nu_o - \nu)^2 T_2^2) \qquad 3.5$$

T_2 being the spin-spin relaxation time, which experimentally is related to the half-power linewidth, $\Delta\nu_{\frac{1}{2}}$, by $T_2 = 1/\pi\Delta\nu_{\frac{1}{2}}$. The saturation factor, s_{ij}, can be equated to the stimulated emission probability w_{ij} and the spin-lattice relaxation time T_1:

$$s_{ij} = 1/(1 + 2w_{ij}T_1) \qquad 3.6$$

W_{ij} may be calculated from knowledge of the r.f. magnetic field at the sample (eq. 1.7)

Thus, in theory, the spin-lattice relaxation time may be calculated from knowledge of the saturation factor, which in turn may be deducted by measuring the power absorbed in the sample as a function of the r.f. field present at the sample (eq. 3.4). The r.f. field is a function of the power incident upon the cavity, and the power absorbed is a function of the power reflected from the cavity. In practice, the magnetic Q of the cavity with the sample on resonance, Q_m, and the off-resonance loaded Q, Q_L, must be calculated from measurements of the incident power, P, and the reflection coefficient, R, of the cavity. The measurement of P is an absolute measurement, and is difficult to do: methods which have been used usually involve a directive feed to a barreter or bolometer, or to a calibrated thermistor bridge. The data was evaluated by Eschenfelder and Weidner by plotting Q_m/Q_L against $P(1-R)^2$, the gradient of which is proportional to T_1. The actual values of H_1 at the sample may be calibrated by placing a standard sample, such as DPPH, in the cavity at the sample position, and evaluating H_1 from the known relaxation times of the standard sample.

A major difficulty in the use of this method is the determination of the lineshape factor, which may not be Lorentzian, and will be an intermediate between this and Gaussian

if the line is inhomogeneously broadened. In this case the theory only applies to a component spin packet of the overall linewidth (a homogeneously broadened component line of the overall lineshape envelope). In addition, not all systems obey the Bloch equations, and saturation of the absorptive and dispersive components of the susceptibility may occur at widely varying power levels, as shown by Portis (1953). The method also requires the use of small samples, otherwise the value of H_1 will vary over the volume of the sample, and a consequence of this is a reduction in the signal strength (Q_m/Q_L). At low temperatures the amount of power which may have to be dissipated in the cavity and sample to ensure saturation may lead to uncertainty over the temperature of the sample. Lloyd and Pake (1954) have given a detailed theory of this method, taking account of the participation of all the energy levels in the relaxation process.

3.2.2.b C.W. saturation with A.C. modulation

This method is a modifcation of the C.W. saturation technique which bears a superficial resemblance to the non-resonant method. A 100% amplitude modulated microwave signal is used to saturate the transition being studied, and this induces magnetisation of the sample, which, when the modulating frequency is less than $1/T_1$, produces an alternating component of magnetisation in the same direction as the applied static field. This component is detected by a small

coil appropriately orientated immediately adjacent to the sample. As the modulating frequency approaches $1/T_1$, insufficient spins are able to relax between cycles of the microwave field to enable the magnetisation to follow the power variation in the cavity, and consequently the amplitude of the signal from the detector coil decreases. At sufficiently high frequencies the spins do not follow the power modulation at all, but experience only an average applied magnetic field, and the time varying magnetisation of the sample reduces to zero, as does the coil signal. The method was invented by Herve and Pescia (1960), and has been used at modulating frequencies up to 30 MHz. by Herve (1963).

3.2.2.c. Static susceptibility under resonant conditions

Candela and Mundy (1965) describe a method of measuring the variation of static d.c. susceptibility as a function of the microwave power absorbed by a sample at resonance. They give an expression for the spin-lattice relaxation time:

$$T_1 = MH_o^2((\chi_o - \chi_p)/P_a K) \qquad 3.7$$

where M is the mass of the sample, H_o is the static magnetic field, χ_o and χ_p are the susceptibilities of the sample at zero microwave power and when it is absorbing power P_a. K is a constant depending on the units used for the other parameters.

The susceptibility is measured by an electromagnetically controlled beam balance which determines the force acting on

the sample in the static field H_0, and power absorption in the sample is calculated from measurements of the power incident on and reflected from the cavity, using calibrated thermistor bridges in directional couplers.

3.2.3 Resonant pulse techniques

Like the resonant C.W. techniques, the resonant pulse techniques enable the relaxation of a single transition to be measured. However, the great advantage of the pulse techniques is that they enable the time varying population difference of a pair of levels to be observed directly, instead of yielding a relaxation time averaged over all the relaxation processes taking place between the two levels, as do the C.W. techniques. The pulse methods do not depend on the assumptions of a physical model such as the Bloch equations, upon which the C.W. methods depend. The majority of modern relaxation measurements are now made using pulse techniques, as they enable deviations of the relaxation process from the single ion theories to be observed in far greater detail than the other methods, and can therefore give a truer picture of the actual form of the relaxation process.

3.2.3.a D.C. Magnetisation technique

This was the earliest pulse technique used, and was developed by Damon (1953) and Bloembergen and Wang (1954). The technique uses a detector coil, adjacent to the sample in the cavity, which detects the component of d.c. magnetisation

of the sample parallel to the applied magnetic field, in much the same way as the method of Herve and Pescia (Sec. 3.2.2.b). The saturating microwave radiation is applied as a high power pulse, which causes the magnetisation of the sample. At the end of the pulse the spins begin to relax, and so the magnetisation decays exponentially, being proportional to the population difference of the two levels being observed. The e.m.f. induced in the detector coil is proportional to the time derivative of the magnetisation, and so, when the e.m.f. is passed through an integrating amplifier, the result is a measure of the time dependent relaxation of the spin system. The main difficulty of the method is the processing of the signals from the detector coil, which are very small, but the microwave system is very simple; a high power magnetron feeds a simple bridge spectrometer which enables the resonance condition to be established, the whole detection system being external to the microwave circuit. Feng and Bloembergen (1963), using this method at 9 and 24GHz., observed cross relaxation effects in ruby.

3.2.3.b. The pulse saturation technique

This is one of the most widely used methods for measuring relaxation times, and has found application to many materials, having relaxation times ranging from microseconds to seconds. The method was first described by Davis, Strandberg and Kyhl (1958), but many variations of the apparatus, using the same

basic technique, have subsequently been described. The essence of the method is to apply a high power pulse of resonant microwave radiation to the sample, which saturates, or partially saturates, the transition being observed. The behaviour of the spin system after the saturating pulse is monitored by a low-level resonant microwave signal from a reflex klystron, which causes negligible disturbance of the populations of the levels. If the pulse produces complete saturation, equalising the populations of the two levels, then no power is absorbed from the monitor klystron at the end of the saturating pulse, or, if only partial saturation is produced, the monitor absorption signal is reduced. As the spins relax after the pulse, and the population difference is restored towards thermal equilibrium, as described by eq. 1.20, so the power absorbed from the monitor increases, being proportional to the population difference, and this may be described by a time dependent susceptibility component $\chi''(t)$, which obeys the equation

$$\chi''(t) = 1 + (\chi''(0) - 1)\exp(-t/T_1) \qquad 3.8$$

where $\chi''(0)$ is the value of $\chi''(t)$ at the end of the pulse. The monitor signal output from the spectrometer is proportional to $\chi''(t)$, and when displayed on an oscilloscope gives an exponential trace (provided simple spin-lattice relaxation is occurring). If $\chi''(\infty)$ is the unsaturated value of

$\chi''(t)$ (i.e. the monitor signal level when the spin system has fully returned to thermal equilibrium), then the gradient of the plot of $\log_e(1 - \chi''(t)/\chi''(\infty))$ against time, derived from the oscillograph of the recovery, is the spin-lattice relaxation time. Any deviation of the above graph from a straight line is an indication of departure from simple spin-lattice relaxation, but in general faster processes, such as cross relaxation, will have died away shortly after the end of the pulse, and so the single exponential resulting in the tail of the recovery oscillograph will give a measure of the slowest process present which is usually the spin-lattice relaxation time.

The experimental apparatus used for this technique has had many forms, of varying complexity, involving one, two or three valves. The basic apparatus is a convential bridge spectrometer, employing either a hybrid tee or a circulator, with the addition of a high power pulsing facility at the same frequency as the signal klystron. The pulse source may be either a klystron or magnetron, as used by Davis et. al., or a microwave amplifying valve may be used to produce pulses from the signal klystron, as in the X-band spectrometer described in Section 3.3. Alternatively, as described by Ruby, Benoit and Jeffries (1962), a diode switch across the wave guide may be used to alter the power level of the signal klystron, providing a high

power saturating pulse when switched on, and a highly attenuated low power monitor signal when switched off, due to leakage. The use of a waveguide switch eliminates the necessity to stabilise a high power valve, and lock its frequency to that of the monitor klystron. If a very high power pulse source is used, some protection, such as a T.R. cell, must beprovided before the receiver to protect the diodes, but often powers of less than a watt provide sufficient saturation of the sample, and this precaution is unnecessary. The use of a single klystron superheterodyne receiver, such as described by Brown, Mason and Thorp (1965) eliminates the necessity for a local oscillator klystron and its attendant frequency control. If a single klystron spectrometer is operated with a diode switch to produce the saturating pulses, this results in the greatest simplicity of operation, as no frequency stabilisation between valves is needed. Such a single klystron superhet. spectrometer for measuring relaxation times is described by Llewellyn, Whittlestone and Williams (1962), and a single klystron spectrometer for pulse saturation measurements using a crystal video receiver is described in Chapter 4.

A very similar technique to pulse saturation, using the same basic principle, is described by Giordmaine, Alsop, Nash and Townes (1958). Two kylstrons are frequency swept

across the resonance, the first giving a high power saturating signal (not a square pulse) to the sample as it passes the resonant frequency, and the second, which reaches the resonant frequency a variable time after the first valve signal provides a low power monitor signal, gives the instantaneous population difference between the two levels, as it passes resonance. As the time interval between the two valves signals reaching resonance is varied, so a point by point picture of the relaxation recovery is built up. Bowers and Mims (1959) describe a method of saturating a transition at one frequency, and observing the relaxation recovery at a different frequency.

3.2.3.c.Inversion recovery

This method is due to Castle, Chester and Wagner (1960), and uses the technique of adiabatic rapid passage. The sample, in a cavity, is placed in a magnetic field which is below the resonant value corresponding to the frequency of a low power monitor klystron. An auxiliary sweep coil, fed with an alternating current, repeatedly sweeps the magnetic field rapidly through resonance, and a high power klystron provides a pulse at the same frequency as the monitor, which is synchronised to arrive as the sample is brought to resonance. This pulse inverts the populations of the levels being observed, and initially maser action occurs, the monitor signal being

amplified each time the magnetic field passes through resonance. As the spins relax the monitor signal passes through zero, at which point the levels are saturated (their populations are equal), and returns to the normal thermal equilibrium absorption value. The locus of the points of the monitor signal peaks after saturation is an exponential, as is the continuous trace of the pulse saturation experiment, the locus giving the relaxation time in the same way. This method was extended from the original 9 GHz. of Castle et. al. to 34GHz. by Thorp, Pace and Sampson (1961).

3.2.3.d. Pulse Response

This method was developed by Brown and Thorp (1967) to enable measurements of relaxation times to be made at very low power levels, obviating the requirement of a high power microwave source, which is a major difficulty at very high frequencies. The original equipment is described in Section 3., but the underlying theory is a simple derivation from the rate equations for a two level system. Rate equations can be written to include both relaxation and stimulated transition probabilities; using the notation of Sec. 1.5:

$$dn_1/dt = -w_{12}n_1 + w_{21}n_2 - W_{12}n_1 + W_{21}n_2 \qquad 3.9a$$

$$dn_2/dt = w_{12}n_1 - w_{21}n_2 + W_{12}n_1 - W_{21}n_2 \qquad 3.9b$$

These can be combined into a single rate equation, using

equation 1.21, and the fact that the stimulated transition probabilities are equal for upward and downward transitions, yielding

$$d\Delta n/dt = (- (\Delta n - \Delta n_o)/T_1) - 2W_{12}\Delta n \qquad 3.10$$

This equation can be rearranged to give

$$d\Delta n/dt = -(\Delta n - (1 + 2W_{12}T_1)^{-1}\Delta n_o)/(1/T_1 + 2W_{12})^{-1} \qquad 3.11$$

which has a solution of exponential form, with a time constant, τ, which is $\tau = (1/T_1 + 2W_{12})^{-1}$. Since W_{12} is proportional to the microwave power incident on the sample (eq.1.7), τ will become dependent on the incident power when $W_{12} \sim 1/T_1$, but if the observation is made at such a low power that W_{12} is negligible compared with $1/T_1$, but sufficient for useful absorption signals to be obtained, then $\tau = T_1$. An exact measurement would measure τ as a function of power, followed by extrapolation to zero power. Equation 3.11 describes the response of a spin system to a low level pulse of microwave power. Initially the system is in thermal equilibrium, and the power absorption at the beginning of the pulse is very strong, being proportional to the population difference, which is a maximum. As the sample absorbs power, and spins are excited into the upper level, so decreasing the population difference, the absorption decreases exponentially to its steady state value, and analysis of the exponential appearing

on the top of the oscillograph trace of the reflected signal from the sample, in the same way as a pulse saturation trace, gives the relaxation time.

3.2.4. Ultrasonic techniques.

In 1963 Dobrov and Browne reported measurements of acoustic absorption in ruby at microwave frequencies up to 10 GHz. They used quartz, and at lower frequencies barium titanate, transducers bonded to the ruby crystals to generate monochromstic coherent phonons and measured the absorption of these by the crystal, by reflection and transmission methods, as a function of magnetic field. When the resonance condition is fulfilled, the spins will absorb quanta of acoustic energy from the phonon field in the same way as an electromagentic field will simulate transitions.

From these abosrption coefficients and measured spin-phonon lineshapes they derived the magnetoelastic tensor, and hence the spin-lattice relaxation time. Their results were in general longer than relaxation times measured by other techniques, but could be reconciled with theory, and the effect of exchange coupled pairs.

3.3 Apparatus and experimental techniques - Introduction

The remainder of this Chapter describes the three spectrometers which already existed in this Department, which were used to measure relaxation times in a range of ruby specimens.

All the measurements were made at liquid helium temperature in order to observe the direct relaxation process. The X-band (9.3 GHz.) and Q-band (35.5 GHz.) spectrometers were conventional superheterodyne spectrometers, adapted to the pulse saturation method of measuring T_1. The O-band (70 GHz.) spectrometer used the pulse response method, and crystal video detection. Chapter 4 describes the design, construction and operation of two spectrometers, operating in J-band (16GHz.) and K-band (22 GHz.), puspose built to make relaxation measurements as simply as possible.

3.4. The X-band Spectrometer

The spectrometer used for relaxation studies at 9.3 GHz. was a conventional two klystron superheterodyne spectrometer, modified to make relaxation measurements using the pulse saturation technique by the addition of a travelling wave tube amplifier, operating in a pulse mode, to provide the saturating pulses.

3.4.1. The superheterodyne spectrometer

A diagram of the spectrometer circuit is given in Fig. 3.1. The spectrometer uses a rectangular reflection cavity operatinf in the TE_{012} mode, with a Q of approximately 1000. The cavity is split laterally $\lambda_g/4$ below the coupling iris, at a position where wall currents are a minimum, to enable samples to be introduced. Samples were placed on the narrow

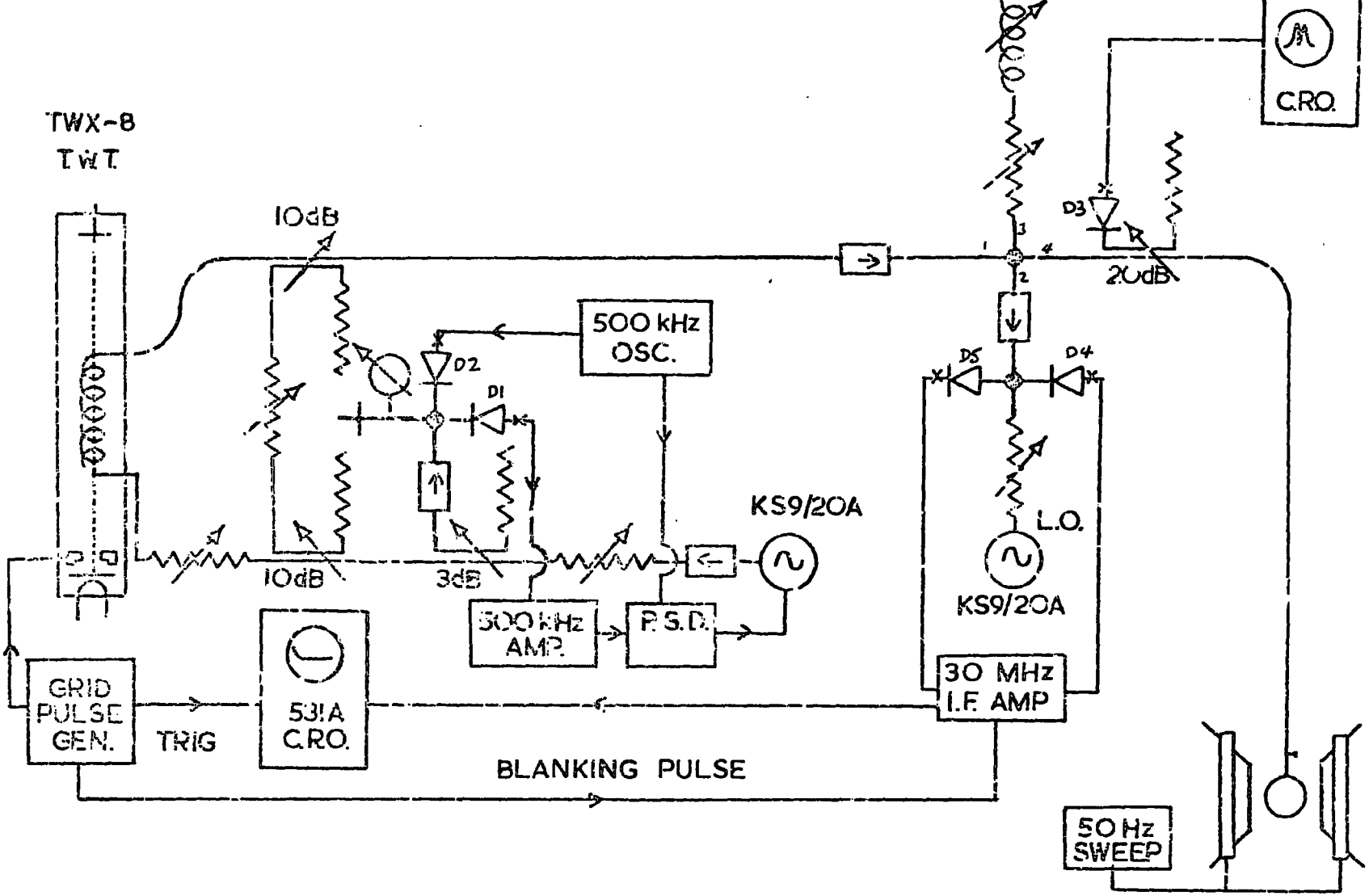

FIGURE 3.1 THE X-BAND SPECTROMETER

(for key see figure 3.1 supp.)

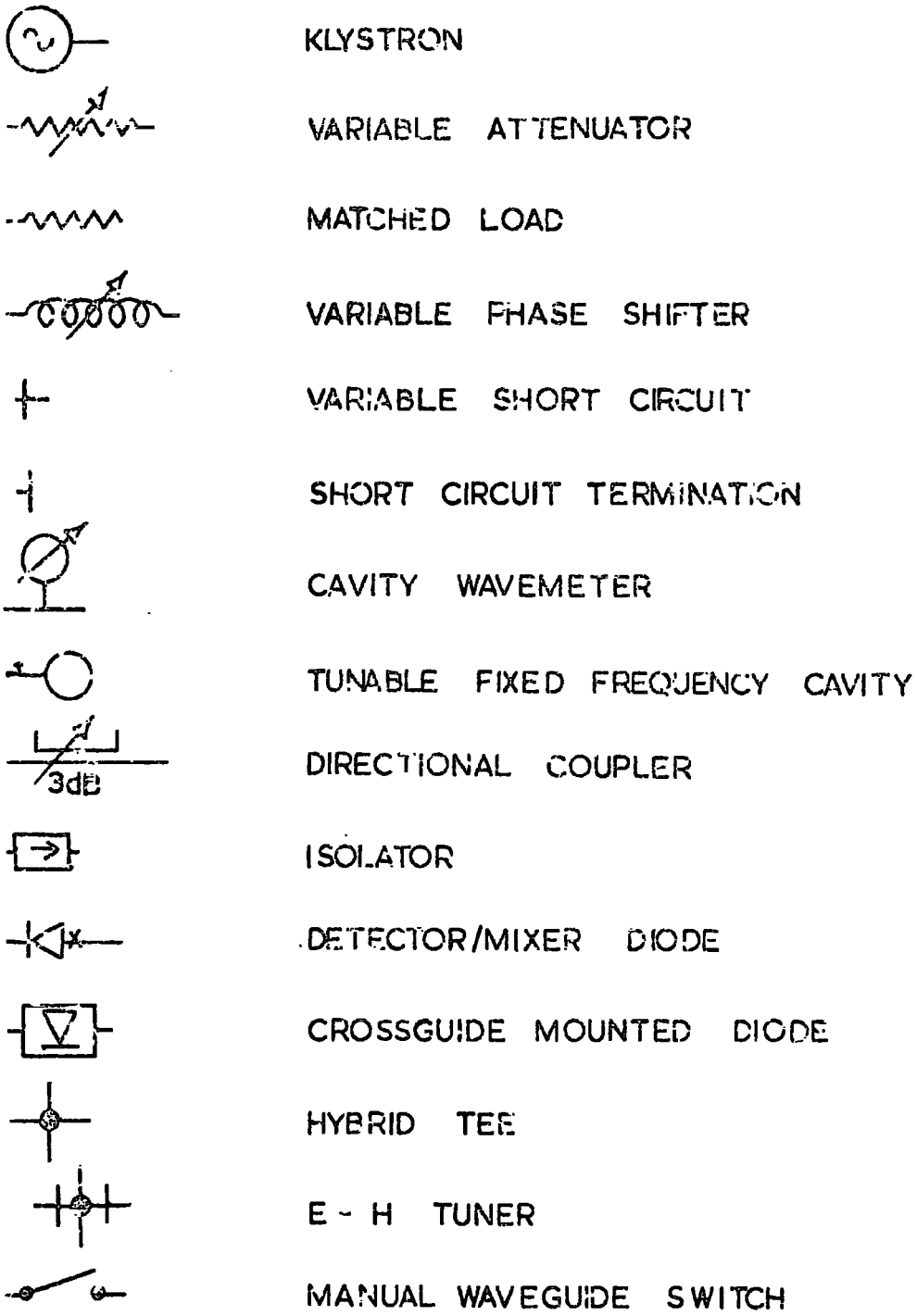

FIGURE 3.1supp SYMBOL KEY TO WAVEGUIDE CIRCUIT ELEMENTS

face of the cavity, just below the split, at a position where they intercepted the maximum vertical component of the microwave magentic field. The samples were attached by a smear of Apiezon vacuum grease, which has a sufficiently high viscosity to hold the sample in place at room temperature, and which freezes solid at liquid nitrogen or helium temperatures. The coupling mechanism consists of a circular coupling hole, centrally positioned in the waveguide, in a 0.010" brass iris, with a single 8 BA tuning screw mounted in the centre of the broad face of the waveguide, immediately above the iris. The coupling to the cavity was set by sweeping the signal klystron reflector voltage at 50Hz. so as to display the klystron mode as reflected from the cavity to diode D3 (Fig. 3.1.) on an oscilloscope. The klystron was then mechanically tuned to centre the cavity abosrption dip on the mode display, and the tuning screw adjusted to bring the tip of the absorption dip to the baseline of the display. This indicated that all power incident on the cavity at its centre frequency was being absorbed in the cavity - i.e. the coupling was 100%, and the cavity presented a matched termination to the waveguide.

Microwave power from the signal klystron, a KS9/20-A giving an output of 20mW, enters arm 1 if the bridge hybrid tee, and is equally divided between arms 2 and 3. Arm 3 is referred to as the balance arm, and by adjustment of the phase

shifter and attenuator the power reflected from arm 3 into arm 4, the receiver arm, can be arranged to be of equal amplitude and opposite phase to any power reflected from the cavity, on arm 2, into arm 4. Any power reflected back into arm 1 is absorbed in the isolator. In this condition no power reaches the detector diodes of the balanced mixer, and the bridge tee is said to be balanced. When the magnetic field is brought to resonance the sample absorbs power and alters the reflection coefficient of the cavity, and upsets the balance of the bridge, causing an amount of power proportional to the absorption in the sample to reach the detector diodes. When the proportion of power dissipated in the sample is small compared to that dissipated in the cavity as a whole, then the signal at the detector is proportional to χ'', and hence to the population difference of the levels being observed.

The hybrid tee is sensitive to inbalance in both phase and amplitude, and both of these are present in the reflected signal from the cavity near resonance, the phase shifting arising from the dispersive component of the susceptibility. In order to observe only the absorptive component of the resonance, the bridge tee is unbalanced slightly in amplitude only. At the detector diodes of the balanced mixer, which are a pair of opposite polarity, CV 2154 and CV 2155, the absorp-

ption signal is mixed with radiation from the local oscillator klystron, operating at a frequency difference of 30MHz. from the signal. This provides a 30MHz. intermediate frequency signal input to the I.F. strip, where it is amplified and rectified, the final signal being displayed on an oscilloscope. Both the I.F. amplifier and the klystron power packs are parts of an ex.U.S.A.F. airborne radar set, AN/APG-30.

When operating as a normal spectrometer, the frequency of the signal klystron is locked to that of the experimental cavity by a phase locking sustem. A 500 KHz. low amplitude modulating voltage is applied to the signal klystron reflector, electronically sweeping the klystron frequency slightly either side of its centre frequency. When this frequency modulation, which is much less than the cavity bandwidth, is reflected from the cavity, it is converted into a 500 KHz. amplitude modulation on the signal. As the klystron centre frequency traverses the cavuty absorption curve, this a.m. changes its phase by 180° from the low frequency to the high frequency 3dB point, and has minimum amplitude at the cavity centre frequency. The 500 KHz. signal is fed back from the I.F. amplifier and further amplified by a tuned amplifier, and passed into a phase sensitive detector with a reference signal from the modulating oscillator. The outpur of the p.s.d. is a d.c. voltage which is proportional to the centre frequency deviation between the

klystron and the cavity, and of opposite polarity when the klystron frequency is on either side of the cavity centre frequency. By adjusting the phase of the reference signal, the polarity of the p.s.d. output may be corrected, allowing it to be applied directly to the klystron reflector as a correction signal.

Operation of the spectrometer in the pulse mode for relaxation studies requires frequency stabilisation external to the experimental cavity, since the signal level varies too much to allow the internal locking system to be used. A Pound a.f.c. system (Pound, 1946) is used, power being extracted from the main microwave circuit by a 3dB directive feed, and passed by an isolator to a hybrid tee. Arm 3 contains a diode, D1, which is fed with the same 500 KHz. modulating voltage as was applied to the klystron reflector, as described above. This frequency modulates the radiation reflected from this arm into arm 2, which contains an absorption wavemeter. The signal reflected from the wavemeter into arm 1 is amplitude modulated in the same way as that reflected from the experimental cavity in the internal locking system, and in arm 1 the amplitude modulated sidebands 500 KHz. above and below the klystron frequency mix with radiation at the klystron frequency, to produce a 500 KHz. signal at diode D2. This is amplified

and passed to the phase sensitive detector to produce the correction voltage as above.

The magnet system used on this spectrometer was a Newport Instruments 4 inch type A electromagnet, mounted on a low loading trolley providing 360 degrees rotation about a vertical axis through the centre of the pole gap. This, with its associated power supply provided fields of up to 5 kilogauss with a stability of 1 part in 10^4.

3.4.2. The Pulsing Equipment

The saturating pulses were produced by a travelling wave amplifier, M-O Valve Co. type TWX-8, which took its microwave input from the signal klystron, thus ensuring that the saturating pulses were of the same frequency as the monitor, with no additional a.f.c. equipment. The monitor signal by passed the T.W.T. via the 10 and 20 dB couplers, which reduced its power to a few tens of microwatts. A high voltage pulse generator delivered 750 volt pulses to the grid of the T.W.T., producing output microwave pulses of maximum power approximately 1 watt, with a rise and fall time of 1 μsec and a length variable up to 100 msec.

In order to provide protection for the superhet. receiver during the power pulse, an arrangement of multivibrator and monostable circuits delivered a blanking off pulse to the I.F.

amplifier, overlapping the power pulse by a few microseconds at either end. This resulted in a dead time of a few μseconds at the end of the power pulse when the initial relaxation recovery could not be seen, but as the relaxation times being studied were of the order of the tens of milliseconds, this did not affect these measurements. The power pulse was insufficient to cause any danger of burn-out of the detector diodes in the balanced mixer, and so no form of waveguide T.R. protection was required.

3.4.3. Cryogenic facilities

In order to make measurements at the temperature of liquid helium, 4.2°K, a glass double tail dewar system contained the cavity and its 0.010" wall German silver waveguide feed. The outer dewar was filled with liquid nitrogen, and allowed to pre-cool the inner dewar, which had a pumpable interspace, before transfer of liquid helium. The inner dewar was sealed to the cryostat head, and connected to a helium gas recovery system to allow the boil off from the dewar to be returned for re-liquification.

A common source of low frequency noise in spectrometers is boiling cryogenic fluid which finds its way into the cavity and waveguide, the bubbles of gas causing random changes in the dielectric constant of the filling of the cavity, and hence of its reflection coefficient. To prevent this the cavity

was surrounded by a brass can, fitted to a screwed ring above the coupling iris. The threads were well covered in Apiezon grease which froze solid during the pre-cooling with liquid nitrogen, preventing the entry of liquid helium when it was transferred to the inner dewar.

There was no provision for remote control of the cavity coupling or cavity frequency from the cryostat head when the cavity was cooled down. The frequency change due to contraction of the cavity was compensated for by alteration of the klystron frequency. The degree of coupling also altered on cooling down, and this was allowed for by setting off the coupling at room temperature to about 75%; on cooling the cavity to 4.2°K the coupling became very close to 100%.

The level of liquid helium in the inner dewar was monitored with a superconducting depth gauge. The gauge element was made by tinning 40 swg constantan wire with lead/tin solder, using Tricene flux. The enamelling was first removed from the wire; the most efficient solvent for this purpose was found to be Stripalene 713. At the temperature of liquid helium the lead/tin sheath of this wire, which has a critical temperature of about 7°K, becomes superconducting, but the passage of a small current (about 100mA) is sufficient to prevent any wire above the level of the liquid helium attaining the critical temperature. Thus, when the element is mounted perpendicular

to the surface of the liquid helium, that part which is above the surface retains the resistance of the constantan core, while that part below has zero resistance. A 100 mA transistorised constant current power supply was built to feed the element, the voltage developed by this current flowing through the sensor being proportional to the length immersed in liquid helium. Several element configurations were tried, involving both free mounted and enclosed wires, in single and multiple loops. The final design adopted was a strip of 1/16" paxolin, 14" long and 0.2" wide, with a .020" x .020" groove cut in either side, at a slight angle to each other, containing a single loop of lead/tin/constantan wire which passed through a small hole linking the two grooves at the bottom of the strip, and was soldered to small tags at the top of each groove. The whole was then coated with G.E. low temperature varnish (Oxford Cryogenics Ltd.) to prevent any accidental short circuit even though the wire was recessed in the paxolin. This element was small enough to fit the tail of the dewar, which a free standing element would not do with the cavity sealing can fitted, and has proved robust enough to withstand many cycles from room to liquid helium temperature without failure.

3.4.4. Operation and recording of data.

The samples were mounted in the cavity with the crystalline c-axis in the horizontal plane, which enabled the magnetic

field to be rotated with respect to the c-axis, allowing any polar angle to be selected easily. After cooling down to liquid helium temperature, the transition to be measured was found by modulating the magentic field at 50Hz. via auxiliary sweep coils on the magent poles, and slowly sweeping the magentic field to the resonant value to obtain a resonance display at 100 Hz. on the Tektronix 531A oscilloscope used. The particular transition was identified by reference to the graphs of resonance spectra, for ruby plotted as resonant magentic field versus polar angle for various frequencies, published by Schulz-du-Bois (1959).

The bridge was balanced, as described in Section 3.4.1., to remove any dispersive component, leaving only the absorption display. The 50 Hz modulation was removed, and the oscilloscope triggered from the front edge of the saturating pulse, which was usually 5 msec long. This resulted in an exponential trace when the static magentic field was precisely at the centre of the resonance line. The Y-amplification and the time base speed (operating on the calibrated ranges only) were adjusted to give a display of measurable height and which had decayed to a level baseline whilst still on the oscilloscope screen; the base line gives a measure of $\chi''(\infty)$ (Sec.3.2.3.b.). This oscillograph was then photographed with a Polaroid camera; a typical exponential relaxation recovery oscillograph is shown in Fig. 3.2, with the associated semilogorathmic plot

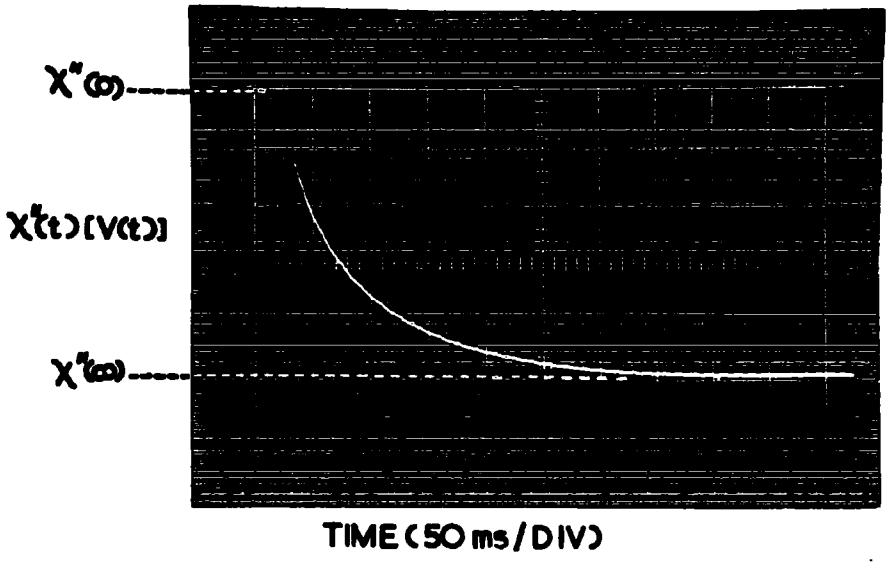

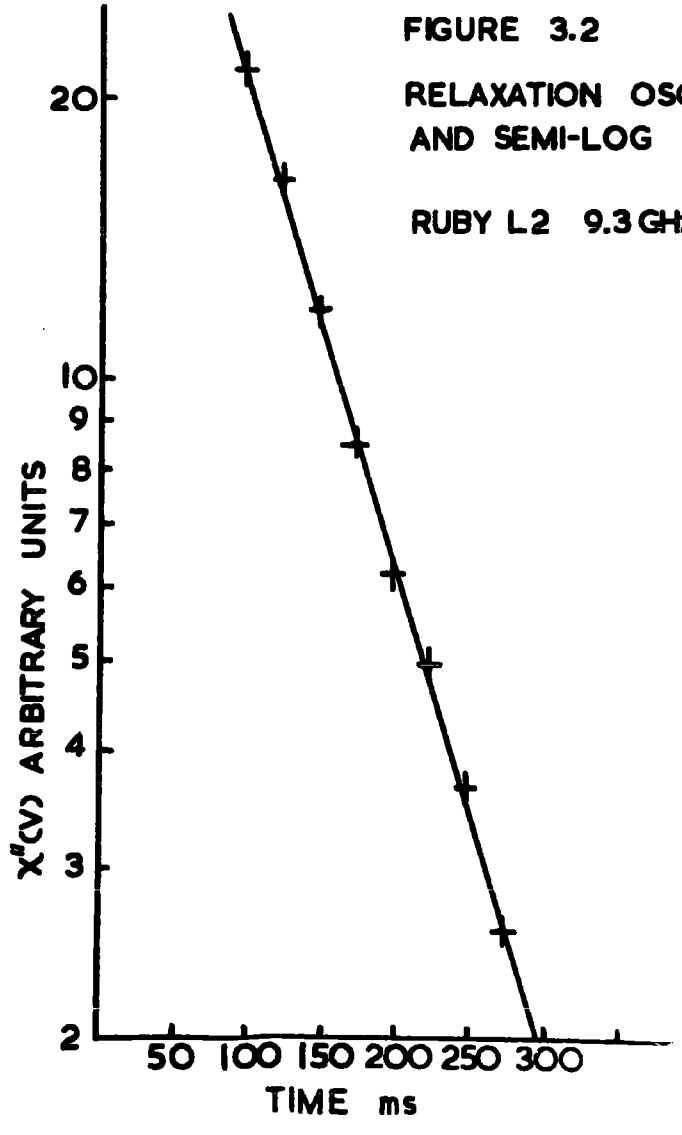

FIGURE 3.2

RELAXATION OSCILLOGRAPH AND SEMI-LOG ANALYSIS

RUBY L2 9.3 GHz T_1 = 83 ms

of absorption against time. The gradient of this line gives the value of the relaxation time and, as the figure which is a single straight line, shows this is a single exponential. Any deviation from a single straight line, either as a curve or multiple straight lines, would be an indication of the presence of other relaxation processes than the direct process. This was very infrequently observed in the present work, and when it did occur, the gradient corresponding to the tail of the exponential was used to give the value of the spin-lattice relaxation time, as mentioned in Section 3.2.3.b.

It is important that the monitor power should not cause any saturation of the resonance line being observed, and, to check this, the monitor power was increased by means of the attenuator in the by-pass arm, but this was not found to affect the relaxation times measured in the ruby samples used. A pulse repetition frequency (prf.) of 10 Hz was used for setting up the spectrometer, but actual measurements were made by single shot operation, to ensure complete recovery to thermal equilibrium of the spin system between saturating pulses. This also facilitated photography of a single relaxation recovery trace.

3.5. The Q-band spectrometer

This was a single klystron superheterodyne bridge spectrometer, operating at frequencies close to 35 GHz, adapted

for pulse saturation relaxation measurements by the addition of a second high power klystron. The basic spectrometer has been described by Brown et. al. (1965), although modified since, and in the form used for this work is shown diagramatically in Figure 3.3.

A conventional superhet receiver, as described in Section 3.4.1. employs a separate klystron as a local oscillator, the frequency difference between this and the signal klystron necessarily falling within the passband of the I.F. amplifier. The noise due to a point contact diode used as a mixer is inversely proportional to the I.F. frequency, whereas the noise introduced by an amplifier using a specific type of valve is approximately proportional to the frequency of operation. As discussed by Strum (1953), this results in a broad frequency band from 30 to 60 MHz where, from the point of view of noise, it is most advantageous to place the intermediate frequency, the exact optimum frequency depending on the characteristics of the microwave diodes and the amplifier design.

At X-band frequencies stabilisation circuits are well able to maintain a frequency difference of this magnitude between two klystrons, but at Q-band this becomes very difficult, and so the single klystron superhet, which was first described by Misra (1958) operating at X-band, has evolved.

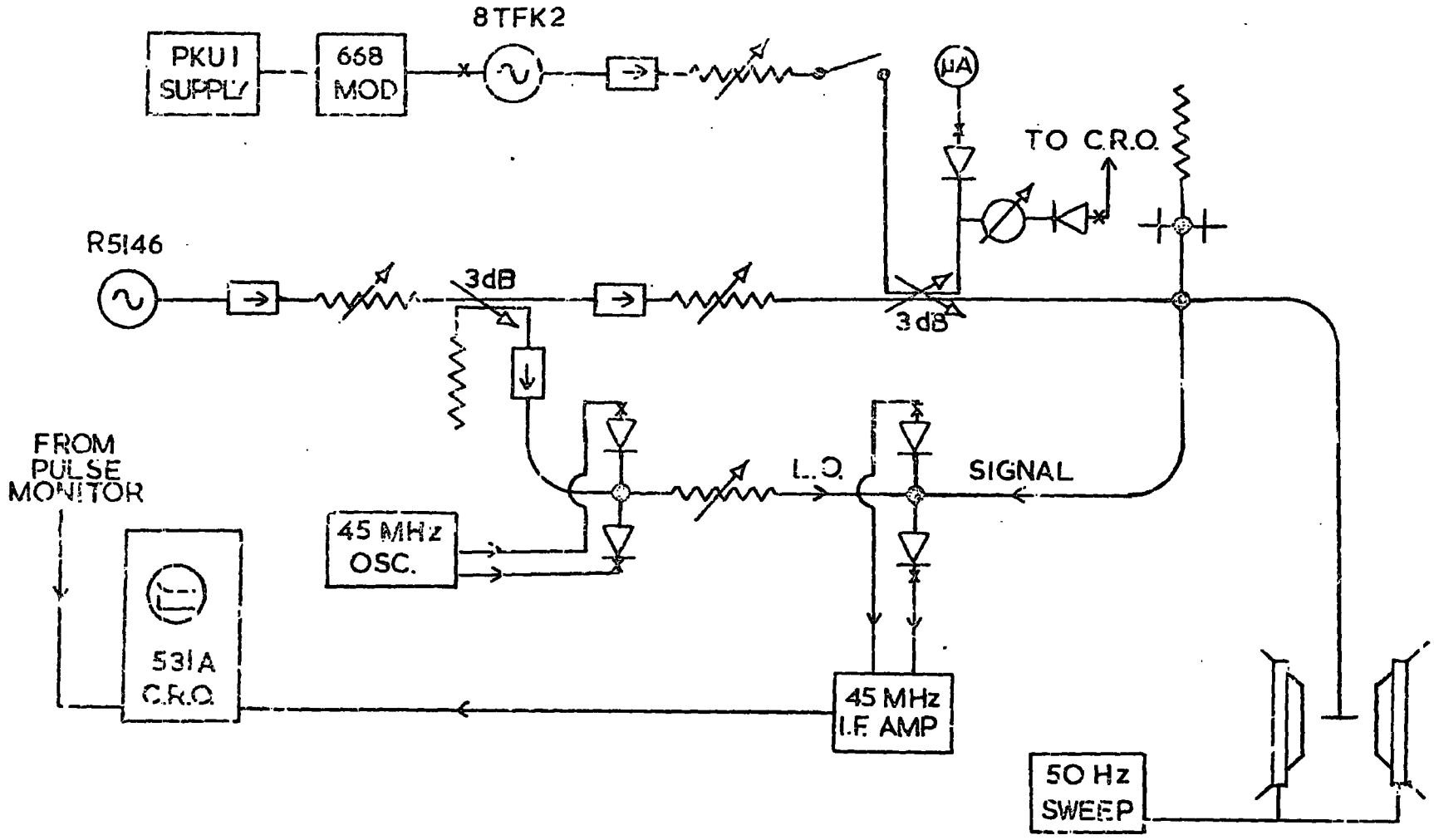

FIGURE 3.3 THE Q-BAND SPECTROMETER

(for key see figure 3.1 supp.)

3.5.1. The Single klystron superheterodyne spectrometer.

The spectrometer uses a hybrid tee bridge, as described in Section 3.4.1, but the balance arm contains an E - H tuner instead of an attenuator and phase shifter. This matching element consists of an unmatched hybrid tee, with moveable non-contacting short circuiting plungers in the E and H arms, and has the property of being adjustable to present an impedance of any magnitude, and therefore to match any given mis-match, and as such is ideally suited to balancing a microwave bridge. Both the local oscillator and signal power are dervied from one E.M.I. R5146 reflex klystron, which gives 20 mW output between 34 and 35.5 GHz. In the original version of the spectrometer described by Brown et. al. the l.o. power is contained in the sidebands at $(f_o \pm 45)$ MHz (where f_o is the klystron frequency), introduced by a transmission modulation diode driven at 45 MHz. This modulation diode was a standard Q-band detector/mixer cartridge diode, VX3136, G.E.C. Ltd., placed in a transmission waveguide mount (Hilger and Watts W 865), which, when driven by a 1 volt r.m.s. 45 MHz signal (the maximum available from the r.f. generator), produced some 1% modulation of the monitor power. A 3dB directive feed then split the power, half providing the monitor signal, and the sidebands in the other half providing the local oscillator input to the balanced mixer, which contained a pair of diodes of opposite polarity, GEM 8

and GEM 9 (Mullard). This arrangement had some disadvantages, notably the presence of the sideband frequencies in the monitor signal at the sample, which could have caused some modulation broadening of the resonance lines, although this was not observed in ruby. The advantage of the local oscillator frequency being self-tracking, and the simplicity of operation which this effected was, however, a very great advantage. The design was criticised by Buckmaster and Dering (1966) on the grounds of degradation of sensitivity due to the sidebands on the monitor signal, and the spectrometer was subsequently modified to remove this objection, this being the version in Fig. 3.3.

The modulation to produce l.o. sidebands was removed from the main microwave circuit to the sidearm, and took the form of a balanced modulator: effectively this was a balanced mixer assembly, containing a reverse polarity pair of diodes, VX3136 and VX3171, which were fed in parallel with the 45 MHz modulation signal. Microwave radiation entering the tee in the H arm divides equally into the two side arms, and is reflected from these, modulated at 45MHz by the diodes, back to the junction. There the sideband components, which are in antiphase, as the modulating diodes are of opposite polarity, add and pass out of the E-arm into the balanced mixer, while the fundamental frequency components, being still in phase, are passed back out of the H-arm to be absorbed in the isolator. The

supression of the fundamental in the local oscillator signal is around 40 dB, and this removes any standing bias at the mixer diodes due to the fundamental, causing them to act in the low-level, square law, conversion region, which results in the superhet output being proportional to the signal power from the spectrometer bridge.

The I.F. amplifier was an 11 stage stagger tuned amplifier originally designed for a two klystron superhet. receiver, and consequently having a bandwidth of 10 MHz. This was reduced to 3 MHz with a corresponding increase in gain and signal to noise ratio. After final stage detection the signal was displayed on an oscilloscope.

This spectrometer did not use a conventional cavity, but instead the sample was placed at the bottom of a short circuited length of .010" wall stainless steel waveguide which went to the bottom of the tail dewar system used. This design was dictated by the lack of space for a cavity in the original double glass dewars used for liquid helium temperature measurements in the small pole gap required of the electromagent in order to obtain the resonant fields (15 kG) required at Q-band frequencies. As fairly large samples were used, typically internal waveguide dimensions (.280" x .140") by 0.4" long, the improved sensitivity of a cavity was not essential, the r.f.

field strength in the ordinary waveguide being sufficient for good absorption signals to be seen. This eliminated the requirement of any a.f.c. system for the klystron, which was placed in an oil bath to reduce long term thermal drift, and the heaters were powered by a battery to minimise any 50 Hz modulation of the microwave power from a.c. heaters.

The magnet system used with this spectrometer was a Newport Instruments 8 inch type D water cooled electromagnet, with a C225 9 KW stabilised power control unit and d.c. generator. This produced a maximum field of 16 kilogauss in a 4.5.cm gap, and a homogeneity of the order of 1 part in 10^5 over a volume of a few ccs at the centre of the gap. Field homogeneity of this order is required to prevent avoidable inhomogeneous broadening of the resonance lines.

3.5.2. The pulsing system.

Saturating pulses of microwave power were supplied by a water cooled Elliott 8TFK2 drift tube klystron, providing up to 20 watts output power at frequencies near 35 GHz. This valve was powered by an Elliott PKU-1 klystron power supply, with a 668 Modulator unit to give modulation of the klystron cathode voltage. The pulse width was variable from 30 μs to 600 ms, with a p.r.f. between 0.15 Hz and 1 KHz, the fall time of the microwave pulse being about 3 μs. The frequency of the power

klystron was made coincident with that of the monitor klystron using a transmission absorption wavemeter, Midcentury Microwave type MC22/2A. The wave meter was first tuned to the monitor frequency using a microammeter connected to a diode on the absorption arm. The power klystron frequency was tuned until pulses were seen coming from the transmission arm, via the wavemeter cavity, these being displayed on an oscilloscope. The pulse height was carefully maximised, by tuning the klystron, indicating that the power klystron frequency was exactly in the centre of the wavemeter Q-curve. When the relaxation recovery was observed on one beam of the double beam oscilloscope, and the wavemeter transmitted pulse on the other beam, any drift of the power klystron frequency could immediately be seen as a decrease in the height of these pulses.

Due to the very low local oscillator power level virtually no mixing action takes place at the mixer diodes during the saturating pulse. For mixing to take place both the signal and local oscillator powers should be comparable, and the local oscillator power should be greater than the signal, or else the high power signal biases off the diodes so far that mixing is prevented. This resulted in very little input to the I.F. amplifier during the pulse, and hence no blanking off of the amplifier was required.

3.5.3. Cryogenic facilities

Originally this spectrometer was operated with a double glass tail dewar system, which, because of its fragility, and the lack of space in the inner tail due to the small magnet gap, was replaced by a stainless steel tail dewar, designed and built by Oxford Cryogenics Ltd. Fig.3.4 is a diagram of the cryostat indicating the essential details of its internal construction. The intermediate tail annulus is a heat shield, maintained at 77°K by the liquid nitrogen reservoir, removing the necessity for a liquid nitrogen jacket surrounding the tail, and provides sufficient room in the tail for waveguide sizes up to WG 16 (X-band). In operation, the vacuum interspace was evacuated to a pressure of less than 10^{-4} torr with a diffusion pump, which ensured a boil off of liquid nitrogen of less than 200 ml /hour, and enabled a temperature of 4.2°K to be maintained for over five hours by the transfer of about 2 litres of liquid helium.

Initial pre-cooling of the cryostat with liquid nitrogen took two to three hours, prior to which the central chamber was evacuated and filled with helium gas to act as an exchange fluid and exclude condensible vapours. Transfer of liquid helium from a travelling dewar was effected using a double walled metal syphon, and was monitored during transfer by the superconducting depth gauge, described in Section 3.4.3, which was sellotaped to

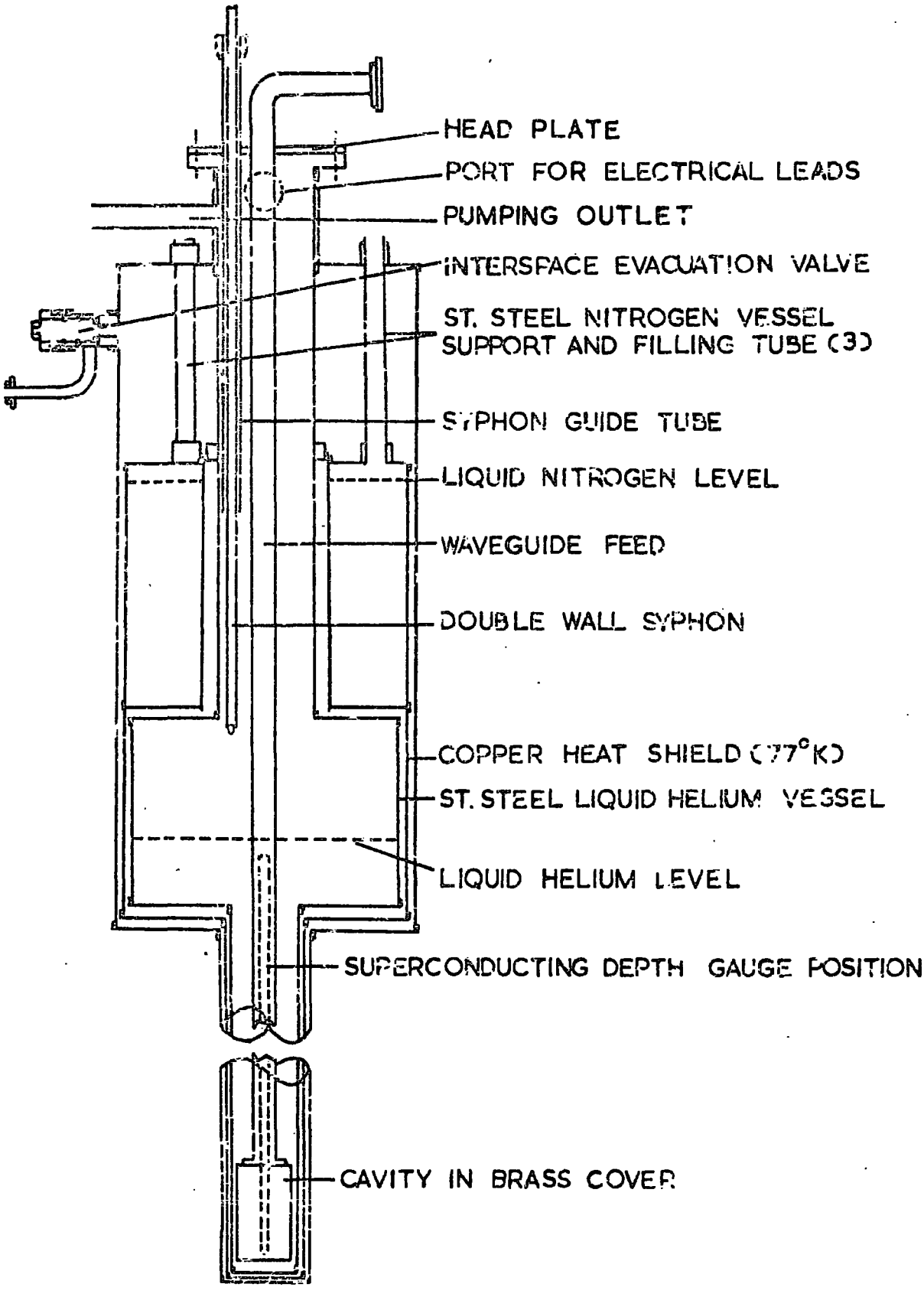

FIGURE 3.4 THE METAL TAIL CRYOSTAT

the waveguide.

3.5.4. Operation of the spectrometer

The orientation of the samples with respect to the waveguide and magnetic field was the same as for the X-band spectrometer described in Section 3.4.4., the c-axis being in the horizontal plane. Due to the very low Q of the length of waveguide containing the sample compared with a cavity, it was not found necessary to seal the bottom of the waveguide against the entry of liquid helium, as no significant decrease in low frequency noise was observed on sealing the short circuiting plunger with Wood's metal after insertion of the sample.

50 Hz field sweep was used to locate the required resonance lines prior to application of the saturating pulses. These produced exponential traces in the same way as at X-band when the magnetic field was precisely adjusted to the centre of the resonance line. In the absence of a cavity, balancing of the bridge to observe only an absorptive signal was not as simple as for the X-band spectrometer. The method used was to adjust the E - H tuner off resonance to produce a minimum d.c. level at the output of the amplifier, using the oscilloscope in the d.c. coupled mode. On bringing the magnetic field to resonance with 50 Hz field modulation superimposed, a 100 Hz resonance display was obtained; the E - H tuner was adjusted to maximise this as an absorption signal, consistent with the d.c. level of

the baseline of the display being the same on either side of the absorption line: This was checked by switching off the 50 Hz modulation, and slowly, sweeping through the resonance line with the magnetic field, paying close attention to the d.c. level of the signal immediately adjacent to the resonance line, the absence of any overshoot on both sides indicating true absorptive balance. To clarify this, Figs. 3.5.a and b are oscillograms of a 100 Hz resonance display with the brdige adjusted for, a, absorption, and b, dispersion, only, these displays being quite general for all the spectrometers described here. For initial setting up a fairly high p.r.f. (30 Hz) was used, but for photographic recording, using a Polaroid camera, the p.r.f. of the 668 Modulator was turned down as low as possible (0.15 Hz) enabling both the spin system to recover to thermal equilibrium between pulses, and the camera shutter to be opened and closed to record only a single trace, using the beam location indicator lights on the oscilloscope. Analysis of the photographs was exactly as described for the X band results.

3.6 The O-band spectrometer

This spectrometer was built specifically to measure relaxation times by the pulse response method, outlined in Section 3.2.3.d. The method and apparatus have been described by Brown and Thorp (1967). Due to the prohibitive cost of microwave valves operating in the 4 mm band (70 GHz) this spectrometer

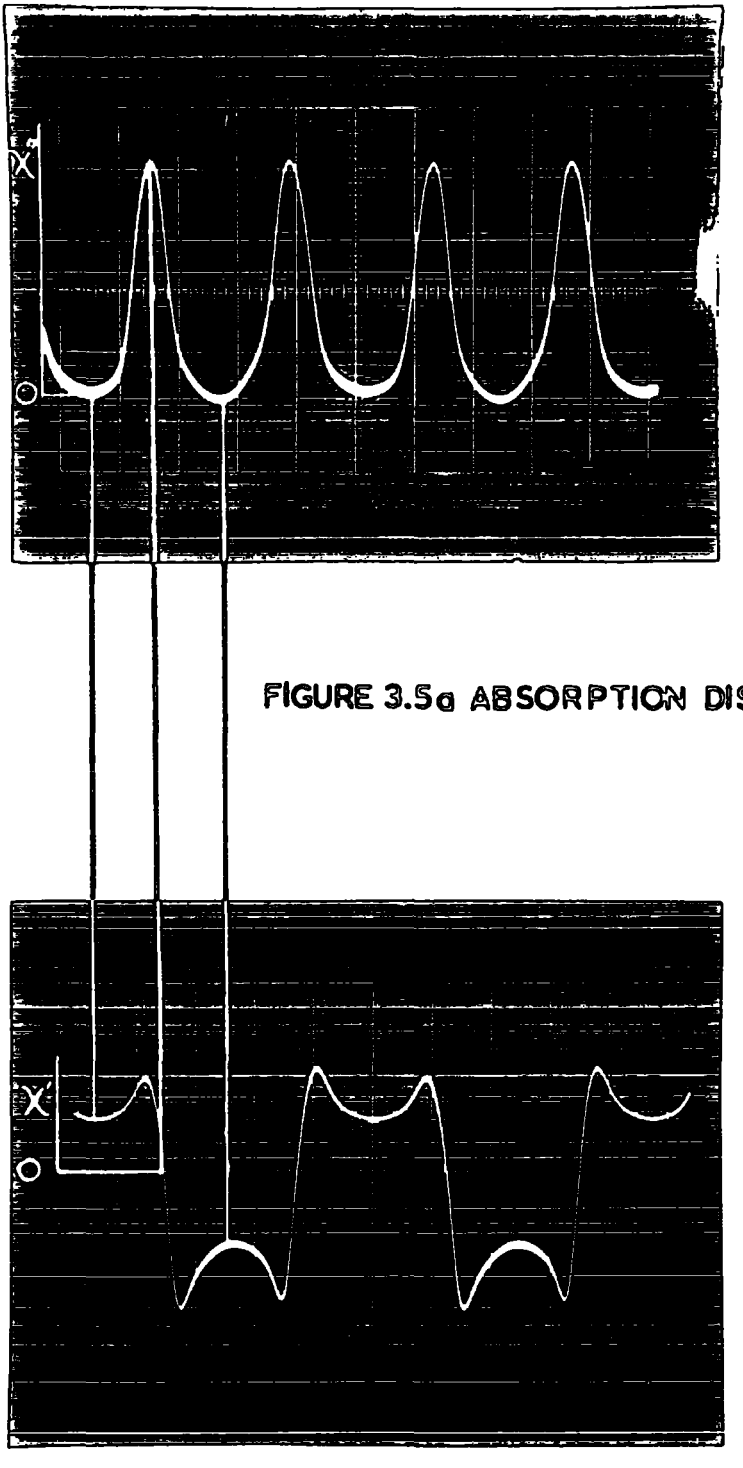

FIGURE 3.5a ABSORPTION DISPLAY χ''

FIGURE 3.5b DISPERSION DISPLAY χ'

used as a microwave source the first harmonic of a Q-band reflex klystron, generated by a cross-guide mounted diode and a waveguide taper, acting as a high pass filter. The requirements placed on the microwave pulse for the pulse response method are very stringent, and generating suitable pulses is the major practical difficulty with this technique. In order to observe the time varying response of the spin system, the frequency deviation across the pulse must be very much less than the linewidth of the resonance, in order to ensure that the same part of the line is being monitored throughout the pulse. Since the variation of the power absorbed by the sample is being monitored, the variation in pulse amplitude across the pulse must also be very small so as not to distort the exponential response. Grid modulation of a particular reflex klystron has met these requirements, but other methods of modulation which have been tried have not been successful.

3.6.1. The pulse response Q - band spectrometer

Figure 3.6 is a block diagram of the spectrometer. The hybrid tee bridge, matching and detector elements are all 4 mm (WG26) components, and as such the design is conventional. The balancing of the bridge was performed by an E - H tuner. The detector diodes used were Hilger and Watts W0948, in which the point contact diode is integral with the mount, which has

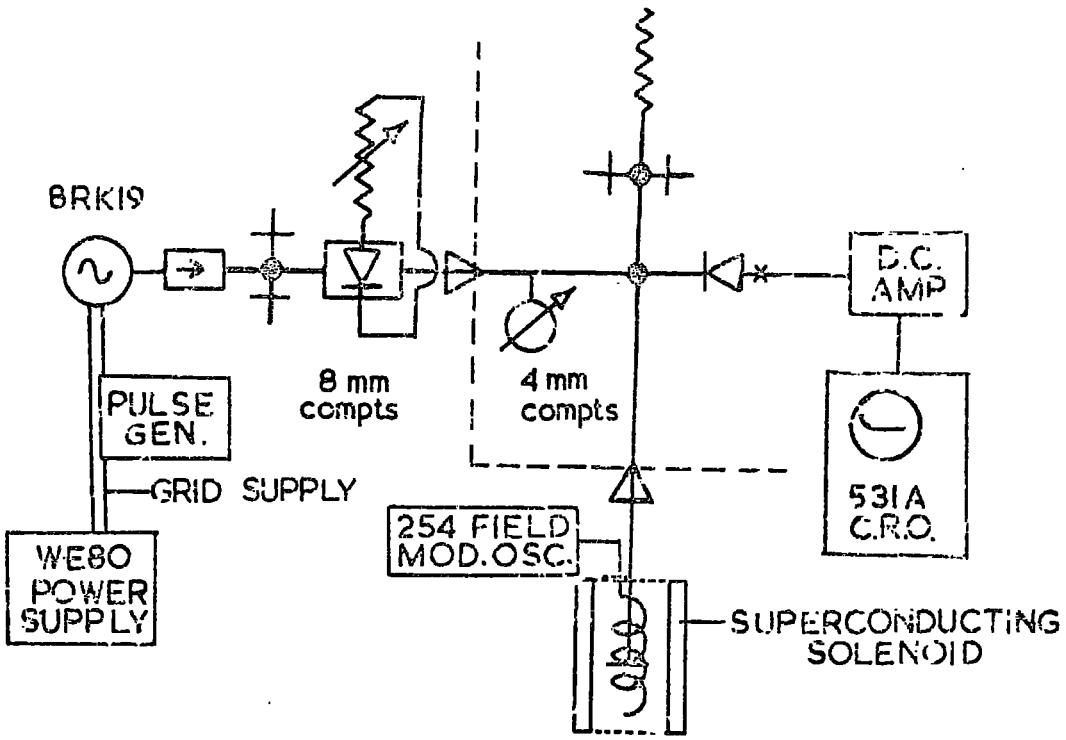

FIGURE 3.6 THE O-BAND SPECTROMETER

(for key see figure 3.1 supp.)

a tunable short circuit behind the diode. The germanium chip is mounted on a grub screw, which enables the relative position of the chip and tungsten whisker to be varied, and the whisker pressure also to be adjusted to maximise the output detected current. Periodic adjustment of the diode was necessary, as it was extremely sensitive to shock, which would degrade its performance by some 10dB from the optimum. These diodes were about 13 dB more sensitive than a tunable cartridge diode mount (Mid-century Microwave MC26/17), which employed a post and bar waveguide transformer to feed a 1N53 coaxial cartridge diode. The detector diode fed a high gain d.c. amplifier (Solartron A.A. 900), the output of which was displayed on an oscilloscope. This simple crystal-video receiver was well suited to relaxation studies with this spectrometer, as the signals were all at low level, thus not requiring a large dynamic range of the amplifier, and enabled the high gain of the amplifier to be used fully, producing a video display with a signal ratio of approximately 10 dB. The spectrometer did not use a cavity, due to the extreme complexity of operating an a.f.c. system at 70 GHz, but utilised a short circuited length of waveguide to contain the sample in the cryostat, as did the Q-band spectrometer, described in Sec. 3.5.1. The waveguide feed into the cryostat was WG22 (Q-band) .010" stainless steel wall waveguide, short circuited by a plunger,

on top of which was the sample. The 70 GHz radiation was launched into this size of waveguide by a WG26 to WG22 taper. This was done to reduce the attenuation of 4 mm waves, which was excessive in stainless steel walled WG26, but which was very much reduced by transmitting the waves in a higher mode than the fundamental, H_{01}, in the larger waveguide.

3.6.2. The grid modulated klystron source

The source of microwave radiation was an Elliott 8RK19 reflex klystron, giving a C.W. power of around 60 mW at frequencies near 35GHz. The choice of this klystron was crucial to the operation of the spectrometer, due to its grid modulation characteristics. Figures 3.7a and 3.7b are the grid characteristics of the 8RK19 and an E.M.I. R5146 Q-band reflex klystron as measured by Brown. From these it may be seen that the frequency deviation of the 8RK19 with change of grid-cathode voltage is minimal, whereas there is a linear relationship between the two for the R5146. This results in the 8RK19 giving grid modulated pulses which have no frequency deviation detectable by a high-Q wavemeter (Midcentury Microwave MC22/2A), indicating that the deviation, if any, is less than 5 MHz. The klystron was run with 8 volt pulses to bring the grid-cathode voltage just to the threshold of oscillation at -40 volts, where the power output was 3 mW, measured with a thermistor

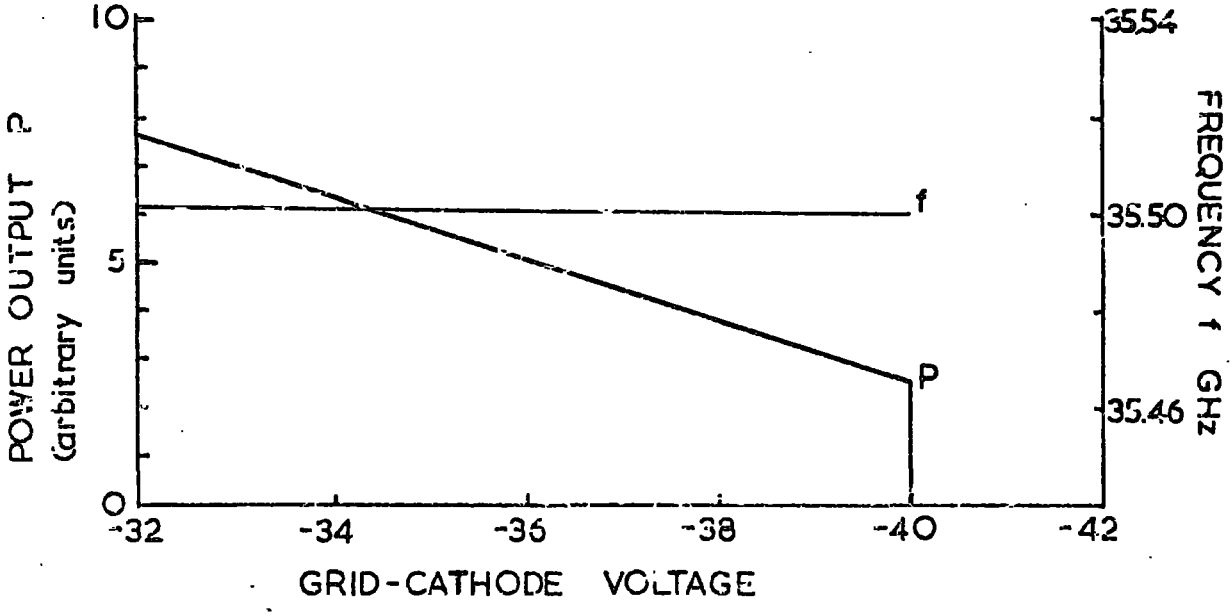

FIGURE 3.7a 8RK19 KLYSTRON GRID CHARACTERISTICS

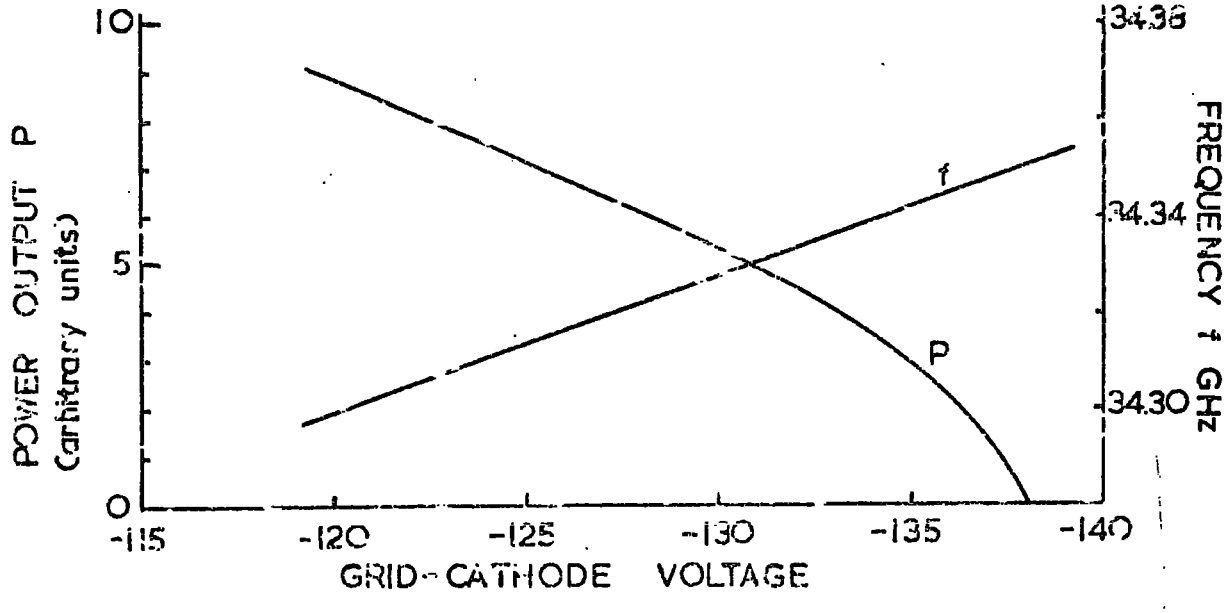

FIGURE 3.7b R5146 KLYSTRON GRID CHARACTERISTICS

bridge. Pulsing further up the grid characteristic produced more power, but at the risk of slightly greater frequency deviation.

Originally the pulses were transmitted to the grid via a blocking capacitor (an integral feature of the Microwave Instruments WE 80 power supply used), which introduced some resistance - capacitance differentiation of the applied pulse, and hence amplitude sag along the length of the output microwave pulse. Of necessity the pulses were some 40 ms long, as they had to be about 8 times longer than the relaxation time being measured, in order to display the baseline of the exponential properly, and this served to accentuate the sag towards the end of the pulse. This problem was removed by modification of the pulsing apparatus. A multivibrator/monostable pulse generator was built, and interposed in the grid supply line as shown in the circuit diagram of Figure 3.8. This pulse generator gave pulse lengths between 50 and 500 ms, with a rise time of 10 μs, and a p.r.f. between 10 Hz and 1 Hz and also had a single-shot facility. The unit was powered by PP3 dry cell batteries, and the whole was contained in a small box, insulated with heavy gauge polythene sheet. The control shafts were brought out on tufnol rods, and the input and output from the power supply to the klystron grid entered the box via the centre pins of UHF series coaxial connectors, which are insulated to withstand 3 KV. Since this

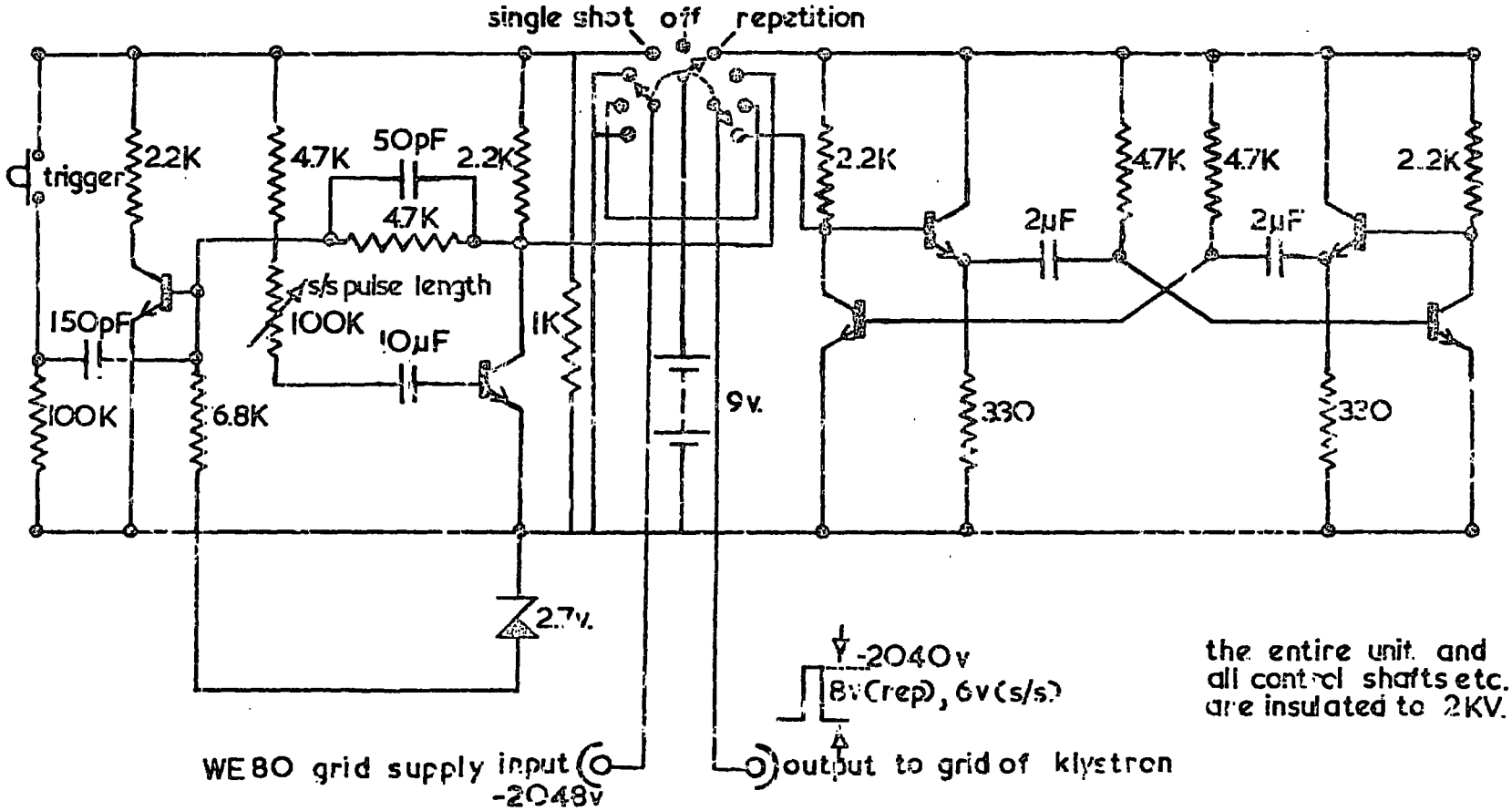

FIGURE 3.8 KLYSTRON GRID PULSING UNIT

generator was directly coupled to the klystron grid, all r - c coupling, and hence amplitude sag of the microwave pulse, were eliminated.

3.6.3. The harmonic generator

The 35 GHz pulses were fed onto the harmonic generator diode, which was a standard Q-band detector diode in a transmission mount; a Mullard GEM 9 diode was found to give maximum conversion efficiency. The E - H tuner before the diode mount replaced a phase shifter which had been used for matching, and was found to give improved matching to the mount, resulting in a 3 dB improvement in the output of 4 mm power. After the diode mount, a WG22 to WG26 waveguide taper acts as a high pass filter, the 35 GHz radiation not being propogated more than a few guide wavelengths in the WG26 waveguide, as it enters an evenescant mode, which attenuates exponentially. Harmonic conversion theory requires the diode to be connected in parallel with a load resistance. While leakage paths in the diode cartridge allow harmonic generation to take place when the diode is ostensibly open circuited, a 100 ohm load was found to maximise the 70 GHz output. The manufacturers of the diode mount and taper, Microwave Instruments Ltd., quote a conversion efficiency of -27 dB to the first harmonic (70 GHz), for this harmonic generator, which gives a figure of 6 μW for the output power pulse at O-band, from the 3 mW input pulse at Q-band.

3.6.4. The superconducting magnet and cryogenic system

In order to generate the magnetic fields required to observe $\Delta M = 1$ transitions in ruby at 70 GHz, which are of the order of 25 kilogauss, a superconducting solenoid was used, manufactured by International Research and Development Ltd. The solenoid was wound from niobium/zirconium alloy, with a critical temperature of $8^{\circ}K$, insulated and reinforced by interwindings of nylon. The solenoid had a bore of 19 mm diameter, which was sufficient to contain an auxiliary modulation coil wound on a tufnol former and, along the common axis of solenoid and coil, the Q-band low temperature stainless steel waveguide.

The superconducting magnet was energised by the same Newport Instruments control unit and generator used for the type D electromagnet of the Q-band spectrometer. The superconducting magnet was connected in series with the type D electromagnet, and a high current safety diode was connected in parallel with the solenoid. The safety diode has two functions; a) The solenoid has a normal resistance of 1500 ohms, which, connected to the control unit output, would cause run away of the generator and so the diode provides a low current path in series with the electromagnet. When the solenoid is superconducting, it short circuits the diode and the control unit therefore sees the correct load resistance at all times. b) If the superconducting

solenoid should go normal while energised, either because of a sudden change in the current, or from lack of liquid helium, then the energy stored in the magnetic field must be dissipated. This can occur safely in the diode, which also damps out any current 'ringing' which may occur, and prevents a voltage surge, which could be of kilovolts, and would destroy the control unit and the solenoid insulation.

The magnet was contained in a stainless steel cryostat, of similar internal construction to that in Fig. 3.4, without the tail, but a compartment 8" x 3½" dia. below the liquid helium reservoir to contain the solenoid. The solenoid was supported in position by a length of 1" dia. stainless steel tube which also contained the waveguide coaxially.

3.6.5. Operation of the spectrometer

The specimens used were the same as at Q-band, cut to fit waveguide WG22, with the c-axis in the horizontal plane. This restricted measurements to a polar angle of 90° only, due to the axial geometry of the solenoid. The samples were mounted on a short circuiting plunger, which was not sealed against the entry of liquid helium (see Sec. 3.5.4.). Operation of the cryostat was similar to the procedure with the tail cryostat used at Q-band; the interspace was first evacuated with a diffusion pump and the interior pre-cooled for several hours with liquid

nitrogen before the transfer of liquid helium. The depth of liquid helium was monitored with a superconducting depth gauge, similar to the one described in Sec. 3.4.3., but with the sensor element free mounted beside the solenoid.

The resonance lines were located by modulation of the magnetic field with the klystron operating in the C.W. mode, the auxiliary coil being driven by an Airmec type 254 high power oscillator at a low audio frequency. Fig 3.9 shows such an absorption display obtained at 70 GHz. The klystron was then switched to the pulsed mode of operation, and the voltages carefully adjusted to the working conditions discussed in Sec. 3.6.2. The E - H tuner was used to balance the bridge, the pulse disappearing when the bridge was completely balanced, and reappearing when amplitude unbalance was introduced to observe the absorption component of the resonance. When the field was adjusted precisely to the centre of the resonance line pulses with an exponential top were obtained on the oscilloscope. The pulse length was adjusted in conjunction with the oscilloscope timebase to give a display which showed the level baseline of the exponential, and the trace was then photographed with a Polaroid camera. A pulse response oscillograph is shown in Fig. 3.10, these being interpreted in the same way as pulse saturation oscillographs by a semilogarithmic plot of amplitude against time.

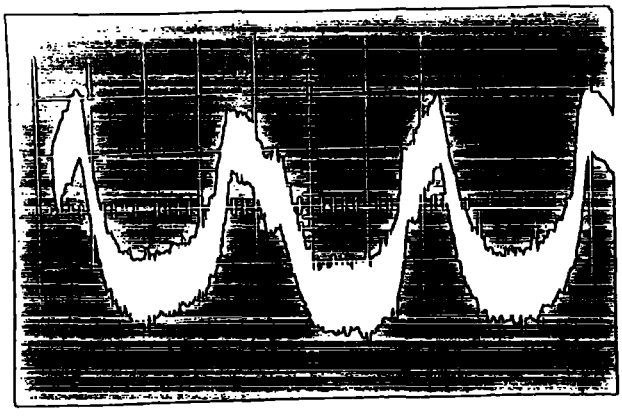

FIGURE 3.9

70 GHz ABSORPTION DISPLAY

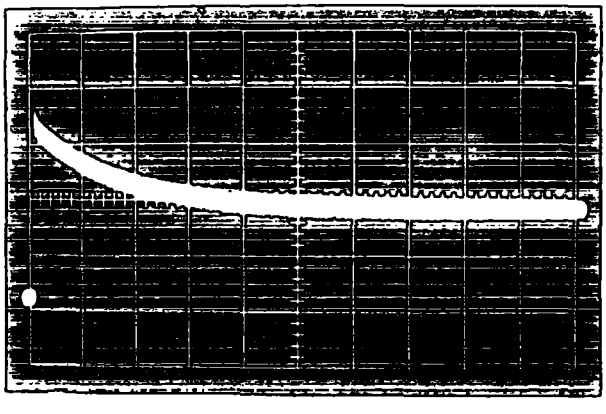

FIGURE 3.10

70 GHz PULSE RESPONSE TRACE

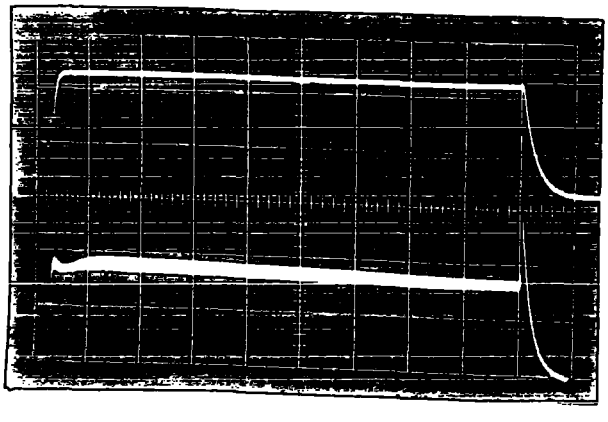

FIGURE 3.11

4TFK4 GRID PULSE
UPPER: WITHOUT WAVEMETER
LOWER: WAVEMETER SET AT
C.W. OPERATING FREQUENCY

3.6.6. The O-band klystron

Few measurements had been made with the spectrometer as described above before the 8RK19 klystron reached the end of its working life with a burnt out heater. The cost of replacement was found to be unrealistic, the price of the valve having increased by 600% due to mergers in the electronics industry and so an attempt was made to use an Elliott 4TFK4 O-band klystron for relaxation studies. This valve is a modification of the 8TFK2 drift tube klystron, with an additional 70GHz cavity coupled directly to the 35 GHz cavity, so as to extract the first harmonic radiation directly from the electron beam. The power output is approximately 250 mW at frequencies between 75 and 77 GHz. This lies above the frequency range of the first harmonic which could be extracted from any of the O-band reflex klystrons available and so eliminated the possibility of using the pulse saturation technique, with the 4TFK4 as the source of saturating pulses and the first harmonic of an R5146 providing the monitor power. The modulation characteristics of the valve are shown in Fig. 3.11, [redacted] oscillographs of a pulse from the 4TFK4 with and without a high-Q wavemeter (Midcentury Microwave MC26/2) set at the C.W. frequency of the valve, showing the frequency deviation across the pulse, which makes the 4TFK4 unsuitable for the pulse response method with directly pulsed operation.

The alternatives to internal modulation of the valve supply voltages are to use a waveguide switch external to the valve, or to pulse the magnetic field to the resonant value from just above or below. The coupling between the auxiliary coil and the superconducting solenoid was sufficient to cause the superconductivity to quench when the auxiliary coil was suddenly pulsed, so ruling out field pulsing. Neither a ferrite switch or a diode switch produce any frequency deviation in pulsed operation, but unfortunately neither of these devices are commercially available operating in the 4 mm frequency band. However, some Philco 1N2792 germanium mixer diodes were available which had been purchased to operate a 4 mm superheterodyne receiver. These had never been used, as the construction of the diode cartridge is based on RG-98/U (WG25) waveguide, the point contact diode being a fully encapsulated crossguide type, operable in either polarity as both contact pins are insulated from the body. Since the diode cartridge is completely traversed by the waveguide section, a [illegible] was designed for these diodes, and is shown in Fig. 3.12. The WG26/RG-98/U waveguide tapers were made by broaching annealed copper walled WG26 waveguide with a highly polished tool-steel former, and were made a close sliding fit to the longitudinally split mounting block. This enabled the tapers to be pushed up to the glass

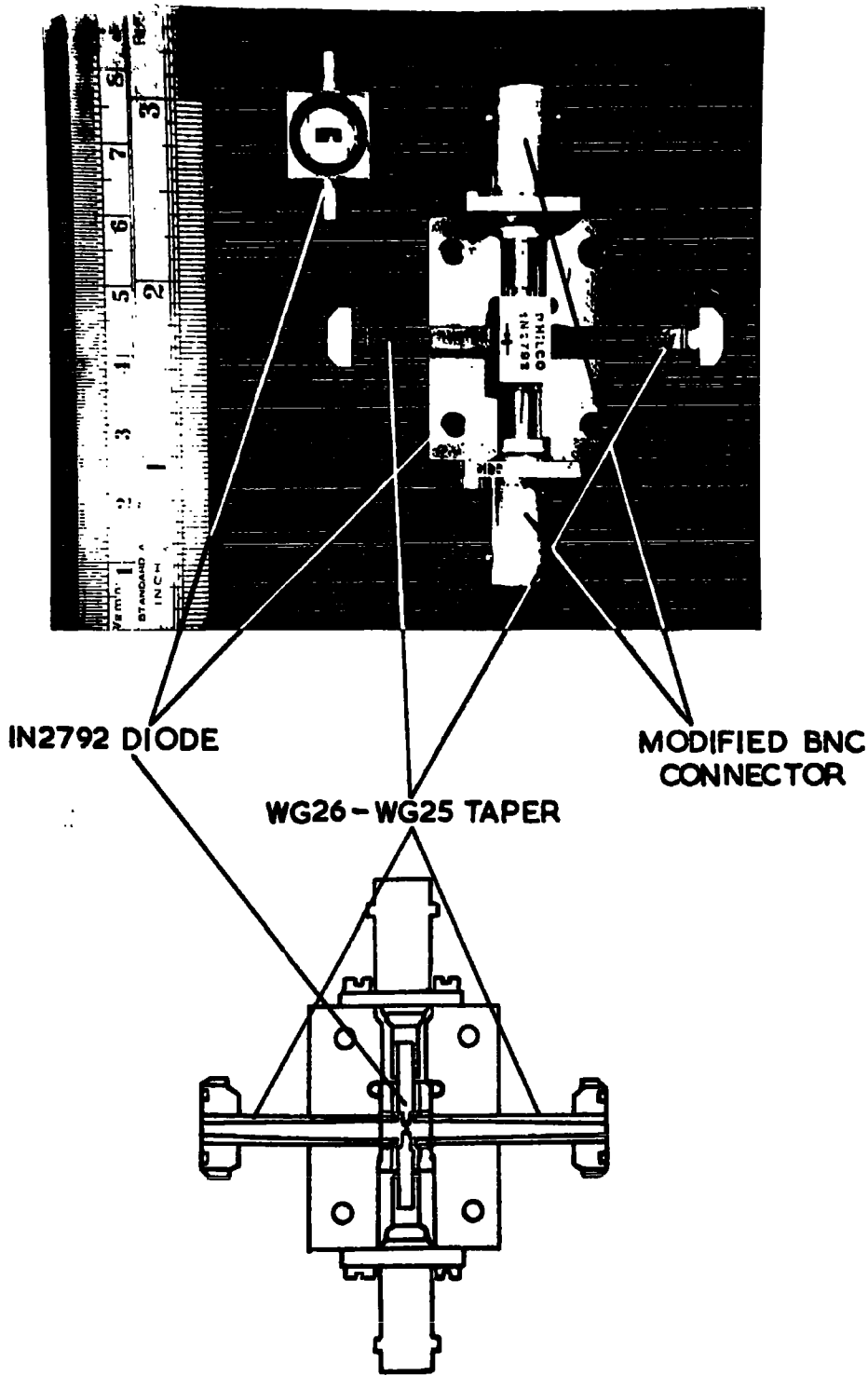

FIGURE 3.12 IN2792 DIODE TRANSMISSION MOUNT

windows of the IN2792 diode cartridge, which were recessed by .012", before clamping the whole assembly with the crossbolts. This diode was tested with both the 4TFK4 klystron at 76 GHz and the first harmonic of an R5146 Q-band klystron, 71 GHz, which is closer to the design frequency of the diode cartridge (69.75 GHz). An E - H tuner was used as a matching element before the diode, but at both frequencies it was found to give a maximum attenuation of 1.7 dB, with a reverse bias of 10 volts, to an unbiased insertion loss of -6dB. The insertion loss was reduced to -3 dB when the diode was forward biased with a current of 10 mA, giving an overall switching ratio of 4.7 dB. This is insufficient reverse bias isolation for the pulse response technique, as, even when the klystron output is attenuated to the microwatt level, sufficient leakage power passes the diode in the 'off' condition to cause disturbance of the spin system. This is also too low a switching ratio for the single klystron pulse technique, described in Chapter 4, as the leakage power level, which is used as the monitor signal, is too high for the 'on' pulse to cause sufficient additional saturation of the spin system to be detected as a departure from thermal equilibrium by the monitor. One possible explanation for the poor modulating performance of these diodes lies in the high reverse bias leakage current characteristic, shown in Figure 3.13.

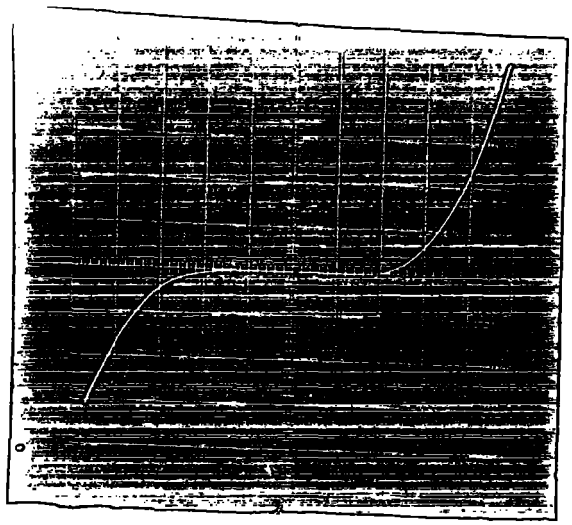

FIGURE 3.13 a

I-V CHARACTERISTIC OF IN2792 DIODE

FORWARD: 0.2v, 10 mA/DIV

REVERSE: 1v, 5 mA/DIV

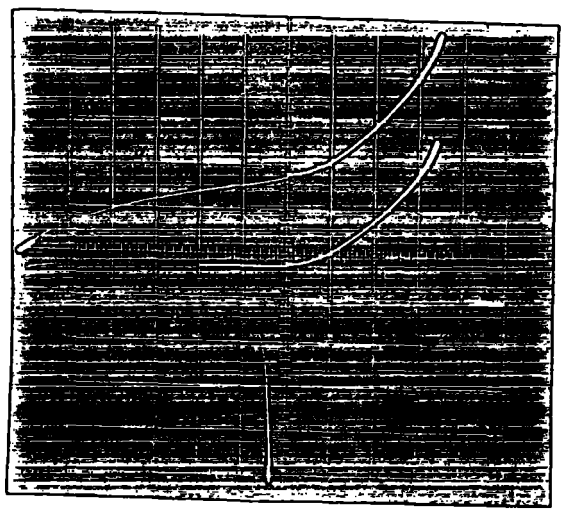

FIGURE 3.13 b

I-V CHARACTERISTIC OF O-BAND SWITCHING DIODE

FORWARD:
UPPER & LOWER; 2v, 20 mA/DIV

REVERSE:
UPPER; 20 v, 2 mA/DIV
LOWER; 20 v, 50 mA/DIV

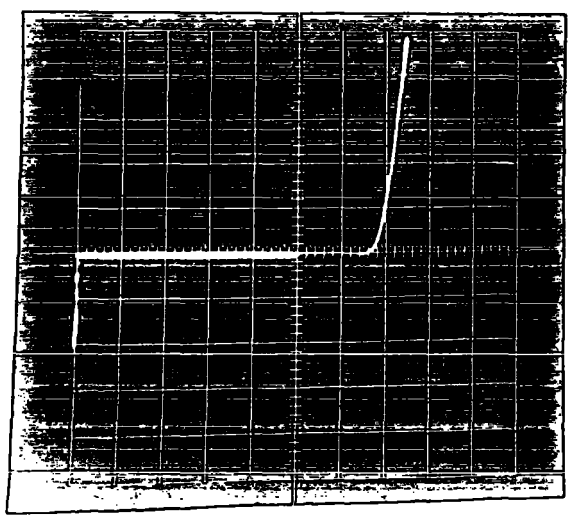

FIGURE 3.13 c

I-V CHARACTERISTIC OF L4756 DIODE

FORWARD: 0.5 v, 20 mA/DIV

REVERSE: 20 v, 0.2 mA/DIV

Another possible explanation for these poor pulsing characteristics was thought to be gross mismatching to the diode due to the use of tapers. Accordingly a wave guide mounted diode was constructed directly in WG26 waveguide in an attempt to obtain better pulses. The construction of the diode in its mount is shown in Figure 3.14; some of the techniques used in its manufacture are contained in Torrey and Whitmer (1948).

The semiconductor material used was single crystal n-type germanium, supplied as .006" thick wafers by the Koch-Light Co. These wafers were stated to have a resistivity of 40 ohm cm^{-1} and a dislocation density of 7.10^3 cm^{-1} and, as supplied, had a roughly lapped surface finish. A wafer cleaved to obtain a .030" square chip, which was washed in trichloroethylene before being soldered squarely to the brass 10 BA threaded header with lead/tin solder, using Tricene flux. This produces a mechanically sound ohmic contact, the solder forming an alloy at the interface with the germanium. Without further treatment this produces a very poor diode, and the rectifying face of the chip was therefore finished by lapping and etching. The header was screwed into the central sliding stem of a stainless steel polishing jig, which kept the face of the chip parallel to the abrasive surface, while allowing free movement in the vertical plane.

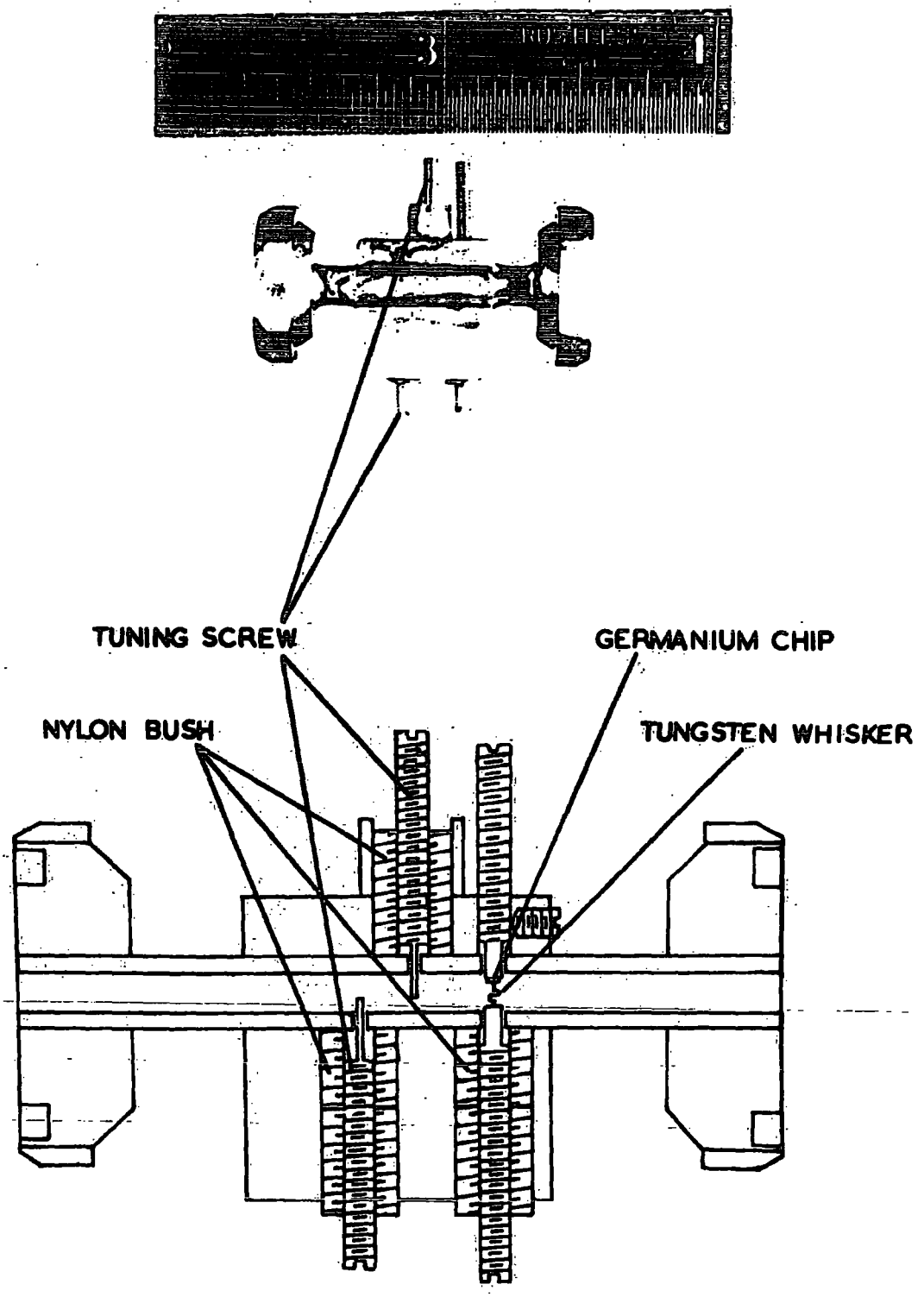

FIGURE 3.14 O-BAND MODULATING DIODE

The chip was lapped successively with wet 600 grit carborundum paste on a glass lap and 3,1 and ¼ micron diamond paste on a rotary lapping machine and finally polished with 0.1 micron alumina powder and water on a glass plate. The polished surface was etched with CP4 etchant to remove the work damaged layer, and enhance the carrier lifetime by removal of surface recombination states. CP4, normally made up of 3 parts hydrofluoric acid to 5 parts concentrated nitric acid and 3 parts glacial acetic acid, etched germanium very rapidly, but the addition of a further 6 - 8 parts of acetic acid as a moderator slows down the etching rate sufficiently to allow a very thin surface layer only to be removed, leaving a very high mirror finish.

The contact whisker was made from tungsten wire, supplied by Lamp Metals Ltd. It was not possible to crimp .001" wire into a whisker due to its excessive springiness, but .002" wire was easily shaped, either by hand with tweezers, or using a jig, to produce a double crimp. In order to solder the whisker into the mounting hole in its supporting post the tungsten was copper plated after crimping to shape, tungsten metal being virtually impossible to solder. The tungsten was first cleaned by electrolytic etching in Langmuir's solution (1 part sodium hydroxide to seven parts each sodium and potassium nitrite made up in 100 parts of water), the whisker being the anode and another piece of tungsten wire the cathode. Approximately 10 seconds

immersion with 20 mA current flowing cleaned the surface to a bright finish without undue erosion of the wire, and immediately after washing in distilled water the whisker was plated. An acid/sulphate plating bath was used, made up of 200 gm copper sulphate, 30 ml concentrated sulphuric acid and 12 grams of potash alum in 1 litre of distilled water. The whisker was made cathodic to a pure copper anode, and a thin adherent coating of copper formed in 1-2 minutes with the passage of about 1 mA.

The whisker was tinned, cut to length and then soldered into the supporting post, ensuring that the tip was as near coaxial as possible with the post. The copper plating on the crimp itself was removed by a brief dip in concentrated nitric acid, and the tip pointed electrolytically, using Langmuir's solution again, but with just the tip of the whisker touching the solution surface. The application of about 2 volts rapidly dissolves the tip to the point where the decrease in wetted area limits the current that can flow, and leaves the tip of the whisker with a very fine point, estimated to have a radius of the order of .0002" when viewed under a microscope.

Having prepared the germanium chip and the whisker on their respective headers they were assembled to the mount. The nylon bush holding the whisker support has the dual role of providing an insulating mount for this contact and, due to the resilience of the nylon, a 'dead', backlash free motion of the

whisker results when the support post is screwed in. Nylon bushes were fitted to provide this 'dead' motion for the tuning screws, the nylon also providing a self-locking action. The whisker was advanced until it just made contact with the chip of germanium, and then it was advanced approximately .001" further to establish contact pressure through compression of the crimp. Adjustment of the crimp compression could be made to less than .001" with the backlash free motion of the 10 BA screw, which has a pitch of 0.13".

The resulting diode had a forward resistance of 60 ohms and a back resistance of around 10^5 ohms, measured at 0.5 volt. The diode characteristic is shown in Figure 3.18b. Upon testing at 76 GHz, this diode was found to have a conversion efficiency, when used as a detector, very similar to that of the WO 948 diode/mount made by Hilger and Watts. Used as a modulator, the diode had an overall switching ratio of 7 dB, with a forward bias (ON) of 40 mA, and a reverse bias of 25 volts (OFF), the insertion loss when forward biased being 2.5 dB. Although somewhat better than the performance of the Philco 1N2792 diode used as a modulator, this did not provide sufficient reverse bias isolation to enable either pulse response or pulse saturation relaxation measurements to be made, for the same reasons as before. It is possible that the semiconductor material

used, germanium, is a limitation to better modulation characteristics at millimetric frequencies. Commercially available switching diodes now being produced for use at centimetric frequencies (Philco L4700 series, extending to K band, 26 GHz), utilise the higher resistivities available from epitaxial silicon grown on high conductivity substrates to offer switching ratios as high as 35 dB, compared to the performance of the previous generation of germanium switching diodes (Philco 1N3093) which gave a maximum ratio of 16 dB at X Band.

Unfortunately no facilities for silicon epitaxy were available, nor were any other suitable samples of germanium, or gallium arsenide, which has a very high mobility, and so this interesting line of research had to be discontinued.

CHAPTER 4

APPARATUS AND EXPERIMENTAL TECHNIQUES II

4.1 Introduction

Following the results of preliminary measurements of spin lattice relaxation times in ruby at the frequencies dealt with in Chapter 3 it was decided to extend the measurements into the frequency intervals between X-band and Q-band, as this appeared to be the major region of interest. The two frequency bands in this interval for which components are commercially available are J-band (12 - 18 GHz, based on WG 18 waveguide) and K-band (18 - 26 GHz, WG 20) and so spectrometers were built to operate at these frequencies. The initial intention was to use the pulse response method for both of these spectrometers, but the critical requirements placed on the microwave pulse prevented this, despite the apparent simplicity of the microwave circuit required. Consequently a single klystron pulse saturation technique was developed for both these instruments, using microwave switching diodes.

4.2. The J-band spectrometer

4.2.1. Design considerations

As originally conceived, this spectrometer was to use the pulse response technique developed for use at Q-band. Initial measurements of the grid modulation characteristics of a J-band

reflex klystron, E.M.I. R9625, indicated that they were similar to those of the R5146 described in Section 3.6.1., making this valve unsuitable for the technique for the same reasons. Accordingly, an E.E.V.C. K3102 reflex klystron was purchased, giving 45 mW output between 14.5 and 17.5 GHz. The modulation characteristics of this valve are shown in Figure 4.1, an oscillograph of a pulse from the valve with and without a wavemeter set at the c.w. operating frequency. This shows the frequency variation across the pulse width to be of the order of 50 MHz (the wavemeter used not being a high-Q type), thus rendering this valve also unsuitable for the pulse response technique with internal pulsing. However, microwave switching diodes have recently become available operating in this frequency band (Philco L4750 series) with a quoted isolation of 35 dB with power levels up to 2.5 watts. These promised to give sufficient isolation to enable the pulse response method to be used and the spectrometer was designed with this in mind.

Following the successful operation of the Q-band spectrometer (Section 3.6.1.) without a microwave cavity, it was hoped to adopt the same system at J-band. This was only partially successful however, for two reasons. In order to simplify the operation of the spectrometer and to keep the capital outlay as low as possible, this spectrometer was operated with

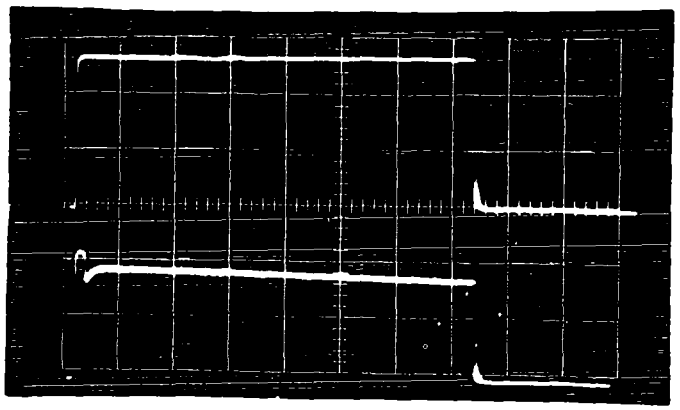

FIGURE 4.1 REFLECTOR MODULATED OUTPUT OF K3102 KLYSTRON

UPPER: WITHOUT WAVEMETER
LOWER: WITH WAVEMETER SET AT C.W. OPERATING FREQUENCY

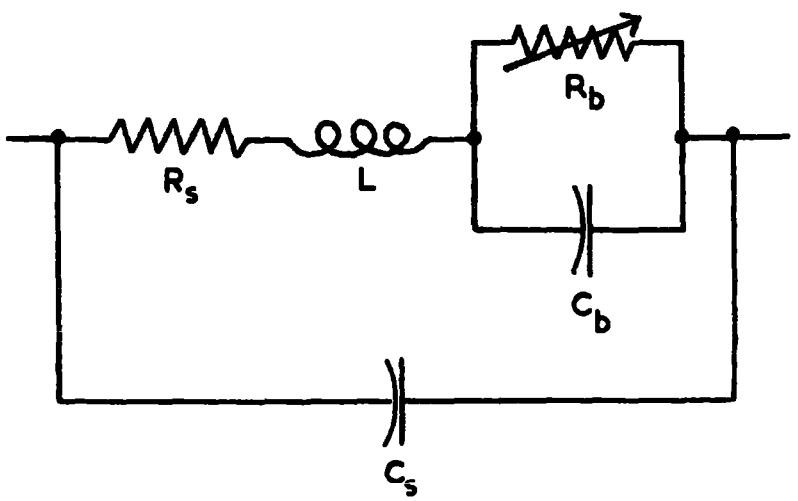

FIGURE 4.3a POINT CONTACT DIODE EQUIVALENT CIRCUIT

a simple d.c. amplifier/crystal video receiver instead of a superheterodyne receiver, as was the Q-band spectrometer. What the crystal video receiver gains in simplicity of operation and cost, having no l.o. with its attendant stabilisation or i.f. amplifier to be tuned, it loses in sensitivity compared with superhet. systems due to its wide r.f. bandwidth. This loss of sensitivity can be between 20 and 40 dB, depending on the power level at the detector and the degree of microwave 'bucking' employed at the diode (Feher, 1957). In addition, at Q-band the samples used filled the waveguide, and consequently had a large interaction with the microwave magentic field. At J-band, using the same samples, because of the longer wavelength, they do not have such a large volume of interaction with the microwave magnetic field, with a consequent reduction in the percentage of the incident power reflected to the bridge as a resonance signal.

Although the spectrometer was operated without a cavity, only very large samples gave sufficient signal to enable relaxation measurements to be made and the position of the sample above the short circuit termination of the waveguide was found to be critical, which it was not at Q-band - again because of the increased wavelength and reduced interaction. As a result of these preliminary measurements it was decided to operate the

system with a microwave cavity, which is described in Section 4.2.2. Introduction of a cavity raised the problem of frequency stability of the klystron and it was anticipated that an a.f.c. system would be required. However, tests with a cavity and the K3102 klystron as delivered indicated that short term drift was not as bad as expected, and so the klystron was stabilised by immersion in an oil bath to increase its thermal capacity and reduce the effect of thermal drift. The K3102 is a low voltage valve, and was run from a simple stabilised power supply, originally constructed to run a KS9/20-A X-band klystron. With this power supply and oil bath, the stability of the system was quite sufficient for the work proposed, a resonance signal being maintained without detectable drift or unbalance of the bridge for upwards of an hour once the oil bath had warmed up to its operating temperature. It is probable that greater stability could be attained either by temperature control of the bath, or by a microwave a.f.c. system, but these were not found necessary for the present work.

4.2.2. The experimental cavity

Due to lack of space in the tail of the metal cryostat used with this spectrometer a rectangular, rather than a cylindrical, cavity was used, the higher Q factors associated with cylindrical cavities not being needed as ultimate sensitivity was not the object. The introduction of a dielectric sample into an unfilled

cavity generally reduces its resonant frequency (Montgomery, Dicke and PUrcell, 1948) and so, as the samples used were of varying size, to allow constant frequency of operation the cavity was made tunable. A diagram of the cavity constructed is shown in Figure 4.2. Coupling was via a circular centered hole iris, and was varied by the capacitative tuning screw immediately above the iris. The tuning screw was mounted in a nylon bush to eliminate backlash and sideshake in its adjustment, which made tuning very tedious when the screw was originally threaded into the waveguide wall and secured with a locknut. The base of the cavity was a non-contacting plunger, which was removable with its leadscrew to allow the mounting of the samples on the plunger so as to lie against the narrow wall of the cavity. The insertion of the plunger enabled either TE_{101}, TE_{102} or TE_{103} modes to be selected across the tuning range of the klystron: operation was fixed at 16 GHz, the peak power putput frequency of the klystron, and the TE_{103} mode was usually used, as it had the highest Q (1200).

No provision was made for remotely varying the coupling at low temperatures, as it was intended to use the method described in Section 3.4.3., of 'setting off' the coupling at room temperature to become close to 100% at 4.2°K. This proved successful, and no modification was made to the cavity system.

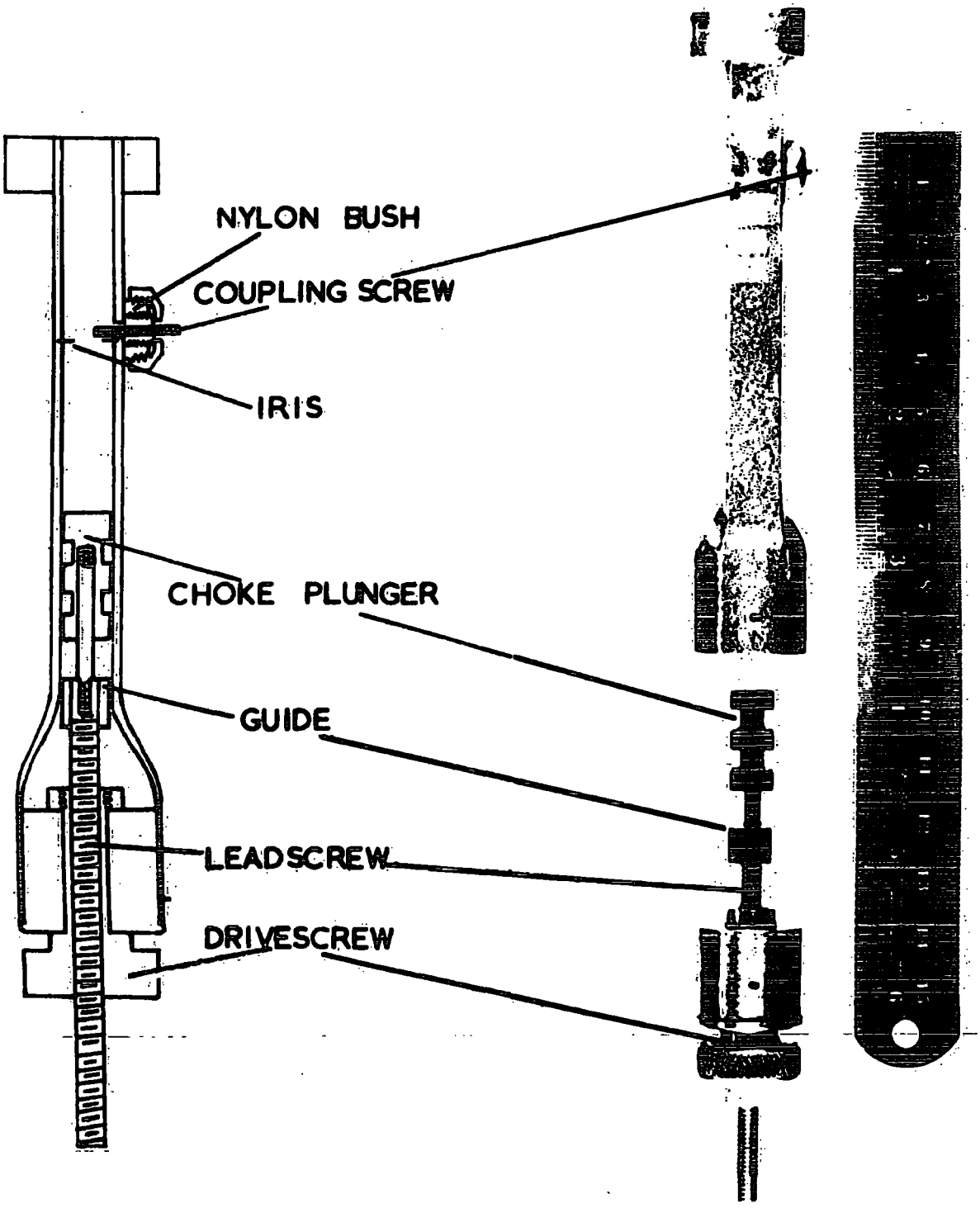

FIGURE 4.2 J-BAND CAVITY

Liquid helium was excluded from the cavity by a brass can screwed to a threaded ring above the cavity, a lip inside this can also acts as a locking ring to fix the cavity to the low temperature waveguide.

3.2.3. The switching diode

A point contact diode may be characterised by an equivalent circuit, shown in Figure 4.3a(i) L is the inductance of the contact whisker, and C_s the stray capacitance due to the mounting of the diode in its package. The effects of C_s can usually be eliminated by properly matching the diode to the waveguide, and can therefore be neglected. R_s is termed the spreading resistance, which is ohmic, and arises from the divergence of current flow lines into the semiconducting chip around the point of contact. R_b is the barrier resistance of the rectifying contact, arising from the formation of the barrier layer in the semiconductor at the contact and is variable with bias, being small (decreasing exponentially with voltage) in the forward direction, and large in the reverse direction. C_b is the barrier capacitance, which is also variable with bias, due to variations in the depletion layer thickness at the contact, and the storage and loss of charge in this layer.

When the diode is forward biased R_b becomes small, and C_b is shunted. The series circuit of R_s and L presents an

impedance such that the discontinuity is small, and little power is reflected from the diode. The residual mis-match, and dissipative losses in R_s and R_b cause the insertion loss of the diode. If the diode is reversed biased, R_b now becomes large, and is effectively shunted by C_b.C_b,R_s and L now form a series resonant LCR circuit with a much lower impedance than the waveguide, which results in a large proportion of the incident power being reflected. Thus, when forward biased the diode acts as an ON switch, and when reverse biased it is OFF.

To use the pulse response technique with this spectrometer a Philco L4756 switching diode was purchased. This has a quoted isolation of over 35 dB at 16 GHz, with an insertion loss of 0.5 dB. The transmission loss characteristic of this diode is very frequency sensitive due to the resonant nature of its design, as shown in Figure 4.3b, with the isolation/bias characteristic in Figure 4.3c. This simplified the design of a mount, shown in Figure 4.4, as one was not readily available commercially, since the diode was self tuned, but restricted the working frequency to being very close to the diode design frequency of 16 GHz in order to maintain the optimum isolation, required for the technique.

In practice, due to the requirement of operating at the cavity frequency, which altered as it cooled to helium temperature, it was very difficult to attain 35 dB isolation, the

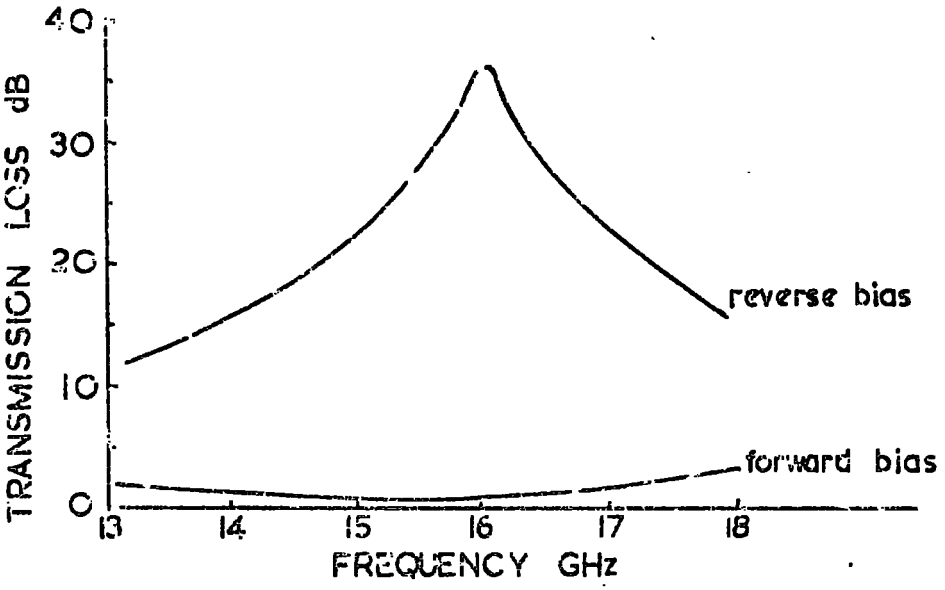

FIGURE 4.3b TRANSMISSION LOSS/FREQENCY CHARACTERISTIC OF L4756 DIODE

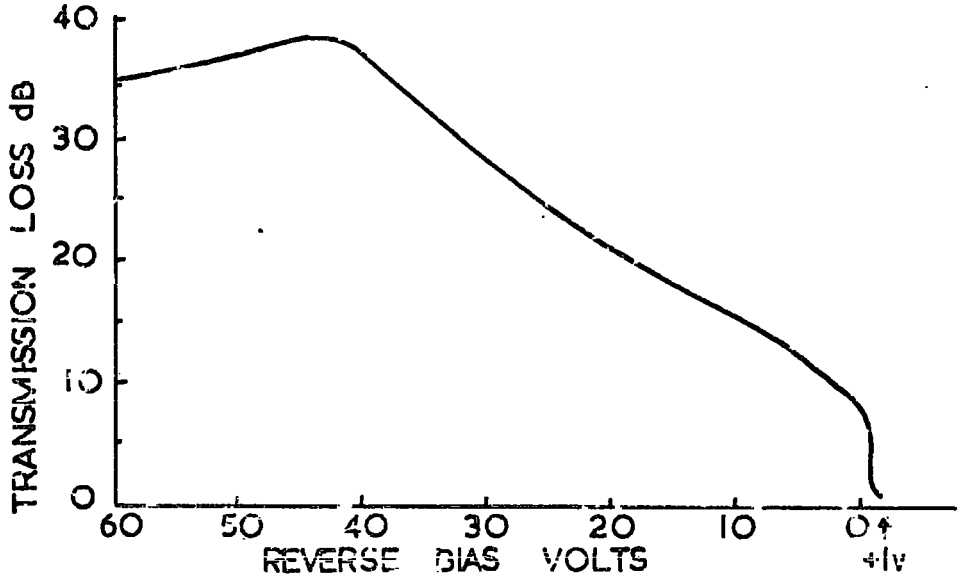

FIGURE 4.3c TRANSMISSION LOSS/BIAS CHARACTERISTIC OF L4756 DIODE

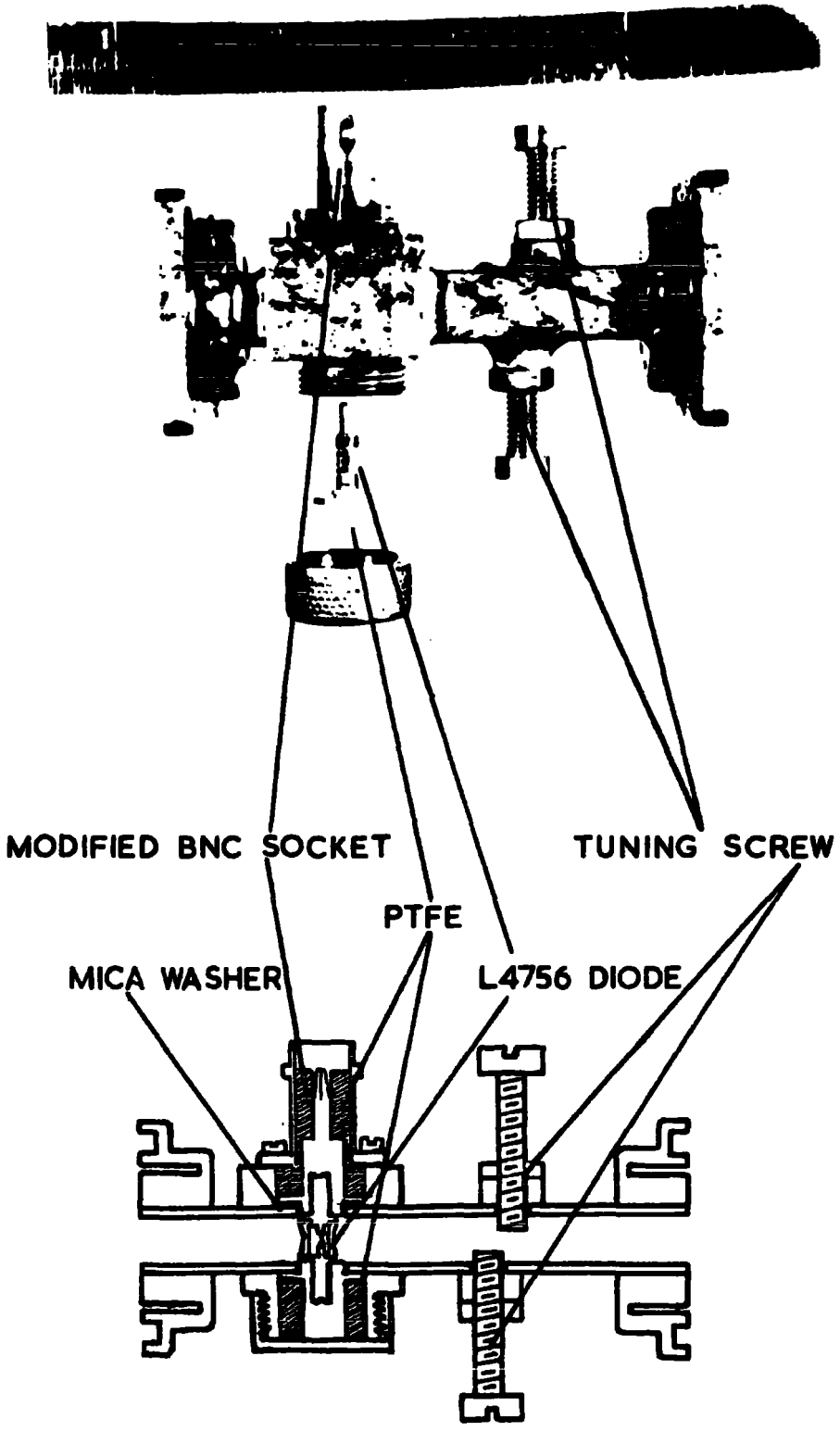

FIGURE 4.4 L4756 DIODE MOUNT

provision later of tuning screws on the mount being of little help. This resulted in extremely poor pulse response signals, which were too weak to be measurable. Therefore it was decided to use the leakage power past the switch in the OFF condition as the monitor power, and the ON pulse as the saturating pulse in the pulse saturation technique. This was successful. Although the output power of the K3102 klystron at the operating frequency was 40 mW, which was reduced by at least 3.5dB at the cavity, this produced sufficient disturbance of the populations of the energy levels to give easily detectable pulse saturation exponential traces for the $\Delta M = 1$ transitions.

To operate the diode under optimum conditions of maximum reverse bias attenuation and minimum forward bias insertion loss a transistor multivibrator pulse generator was constructed, giving a holding OFF voltage of - 45 volts, and a current controlled forward bias pulse of up to + 50 mA to the diode. This unit gave pulse lengths from 100 μs to 200 ms in switched variable ranges, with a p.r.f. from 30 Hz to 0.5 Hz, with a risetime of 4 μs and a fall of 400 ns. The rise and fall time of the microwave pulse were entirely limited by the pulse generator, the switching time of the diode being a quoted 10 ns. The reverse attenuation was varied by altering the reverse bias voltage, and the forward bias insertion loss by altering the

forward bias current (see Fig. 4.3c).

4.2.4. The spectrometer and ancillary facilities

The overall spectrometer circuit is shown in Figure 4.5. The bridge is a conventional hybrid tee type, balancing being effected by the E - H tuner. The auxiliary diode detector on the directive feed before the cavity was used for monitoring the cavity absorption during the initial setting up of the spectrometer. The d.c. amplifier used (Solartron A.A. 900) required a balanced input, floating with respect to earth and so the bridge detector mount was d.c. isolated from the main microwave circuit with a mica washer and nylon screws to locate the flanges.

The cryogenic system was the same as used for Q-band spectrometer described in Section 3.5.3., a stainless steel dewar containing the cavity, which was fed by internally silver plated .005" wall German silver waveguide. The same superconducting helium depth gauge as previously described was used. The magnet system was the Newport Instruments type D 8 inch electromagnet with 50 Hz sweep described in Section 3.5.1., the maximum field required at J-band being only 10 kilogauss.

Due to the restricted dynamic range of the d.c. amplifier, working at high gain to display the exponential recovery of the spin system with a monitor power level of approximately 20 μW, some difficulty was experienced with saturation of the amplifier

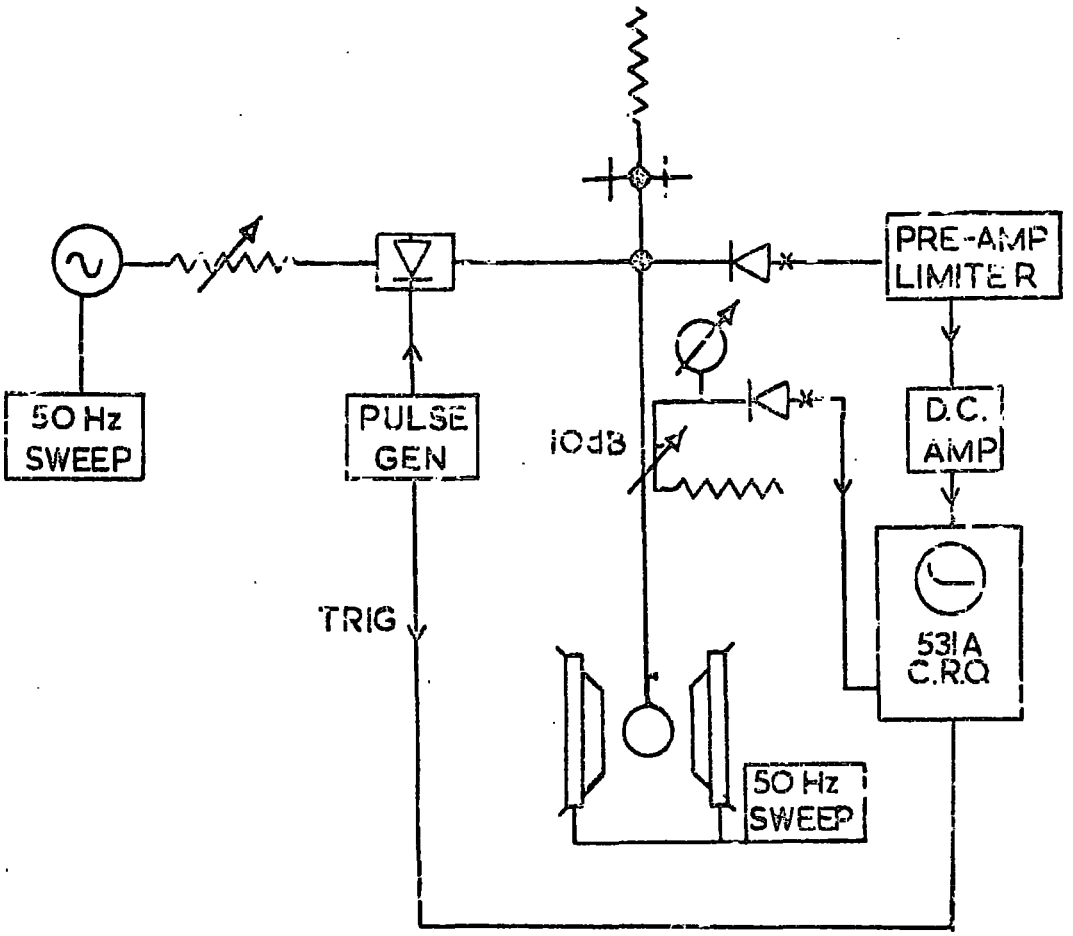

FIGURE 4.5 THE J-BAND SPECTROMETER
(for key see figure 3.1 supp)

by the saturating power pulse. By working very close to bridge balance little of the saturating pulse power reached the detector diode, but this also limited the available recovery signal. The preferred method of suppressing this saturation would have been to place another switching diode between the bridge and detector diode, and feed this with pulses in antiphase to those applied to the modulating diode, i.e. OFF during the saturating pulse, and ON during the monitor period, with slight overlap at either end of the saturating pulse. Another diode was not available, and so the problem was overcome with a low noise transistorised d.c. preamplifier/limiter (Nice, 1969), having a gain of 40 dB, and an output limited to 40 mV, which prevented the full output of the detector diode during the power pulse reaching the d.c. amplifier, but passed the full preamplified exponential recovery signal for further amplification and display. This unit was battery powered, and used low noise transistors. Using low noise 1N78B detector diodes for recovery of the micro wave signal, the majority of the noise in the system came from the A.A.900 amplifier (10 mV at maximum gain, 66 dB, with input shortcircuited).

4.2.5. Operation of the spectrometer

The ruby samples were mounted on the bottom plunger of the cavity with Apiezon grease and the plunger was then inserted

to find the TE_{103} resonance and locked in place, the klystron reflector voltage being swept at 50 Hz to display the mode on the oscilloscope. The cavity tuning screw was inserted to produce critical coupling and then retracted to give coupling of approximately 60%. This then produced near critical coupling at 4.2°K. The cavity was sealed in its brass can, the threads being coated with Apiezon grease. The cryostat was put in place and after pumping the interspace and filling the interior with helium gas, filled with liquid nitrogen to pre-cool for 2 - 3 hours. The cavity resonsnce was monitored during helium transfer, and the klystron mechanically tuned to return the cavity absorption to the centre of the mode display and ensure that the coupling had increased to approximately 100% after cooling.

The 50 Hz sweep was switched off and the reflector voltage adjusted to bring the klystron and cavity frequencies into exact coincidence. The resonance transition was then located using 50 Hz field sweep, and the bridge balanced to produce an absorption display, as detailed in Sec. 3.5.4. The sample was then exactly orientated with respect to the magentic field using the resonance absorption to find the c-axis direction precisely. Two methods were used for this: at polar angles of 0° and 90° the resonant field values for all ruby absorption lines show well

defined maxima or minima (Schulz-du Bois, 1959) and by rotating the magnet about its vertical axis and simultaneously adjusting the field value to follow the absorption line these may be located. The 90° and 0° positions can then be differentiated either by prior knowledge of the approximate location of the c-axis in the sample, or by the differences in the two spectra, no $\Delta M = 2$ or 3 transitions being visible at 0°. These maxima and minima are rather broad at J-band frequencies, and a much more precise method is to locate the 'double pump angle', 54°45', where the -3/2 to -1/2 and +1/2 to -1/2 transitions in ruby coincide at the same field value. This is a sharply defined position, as the spectrum is varying rapidly with polar angle in this vicinity, and may be located to within 0.1°. The magnet may then be rotated, using its vernier angular scale, by either 54.7° or 35.3° to exactly the 0° or 90° polar angle position. Using the resonance spectrum to locate the c-axis in this way removes uncertainties introduced by the twisting of the thin wall waveguide and the cutting of the sample, providing that the c-axis is placed as accurately as possible in the horizontal plane to start with.

Having located the required resonance, the field sweep was removed and the pulse generator switched on, the oscilloscope being triggered from the leading edge of the power pulse. The

field value was adjusted exactly to resonance to produce an exponential display on the oscilloscope, using a fairly high p.r.f. for ease of viewing while setting up. The amplifier gain and timebase were adjusted to produce as large an exponential trace as was commensurate with the noise level, and to display the baseline of the recovery. The p.r.f. was turned to the minimum to photograph the trace in order to minimise the possible effect of one pulse on the succeeding one. The analysis of the Polaroid photographs so obtained was the same as is detailed in Section 3.4.4.

4.3. The K-band spectrometer

This spectrometer was designed and built in parallel with the J-band spectrometer described in the previous Sections and shared some of the ancillary facilities, but differed somewhat in detail.

4.3.1. Factors affecting the design

This spectrometer was originally intended to use the pulse response technique for measuring T_1 and to exploit the low power requirement of the technique it was hoped to use the first harmonic of an X-band reflex klystron operating at 11 - 12 GHz, rather thanpurchase a much more expensive K-band klystron. Initial experiments were carried out using this source; the harmonic generator, manufactured by Midcentury Microwavegear Ltd., was an orthogonal guide type, the X-band guide having a bar and

post transformer feeding a straight post centrally mounted in the K-band guide, the post continuing above the waveguides into a tunable coaxial cavity containing the non-linear element, a 1N26 coaxial diode. This generator was fed by a 2K25 X-band klystron, which is quite unsuitable for electrode modulation, but it was intended to use a Philco 1N3482 X-band switching diode to produce the necessary pulses at X-band, these being converted to K-band pulses by the harmonic generator. However, the 1N3482 is a germanium diode and has an isolation ratio of only 18 dB, which allows too great a leakage for the pulse response method and the harmonic generator supplied too little power for the pulse saturation technique and so a K-band klystron was obtained. This valve was an unlisted experimental reflex klystron, kindly made available by the English Electric Valve Company, which is a scaled up version of the 8RK19 O-band klystron which had proved suitable for the pulse response technique at O-band. It was hoped that, as the electron optics of the two valves are similar, this valve would have similar grid modulation characteristics to the 8RK19, but unfortunately this was not so. Figure 4.6 shows oscillographs of the power output/grid voltage characteristic of the valve, the oscilloscope timebase voltage being used to sweep the grid voltage. As the upper trace shows, oscillation commences sharply at -60 volts, in a similar fashion to the 8RK19 (Fig. 3.7a), but superposition of the absorption curve of a

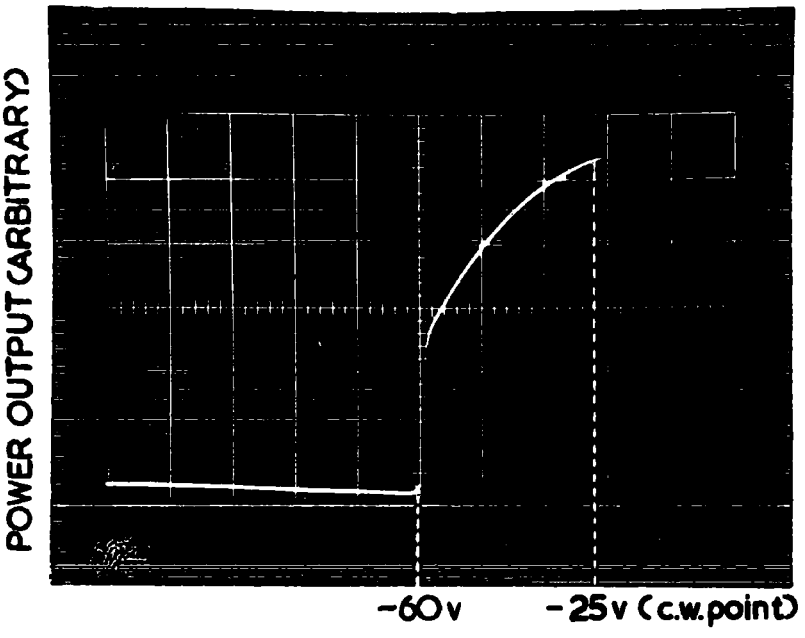

WITHOUT WAVEMETER

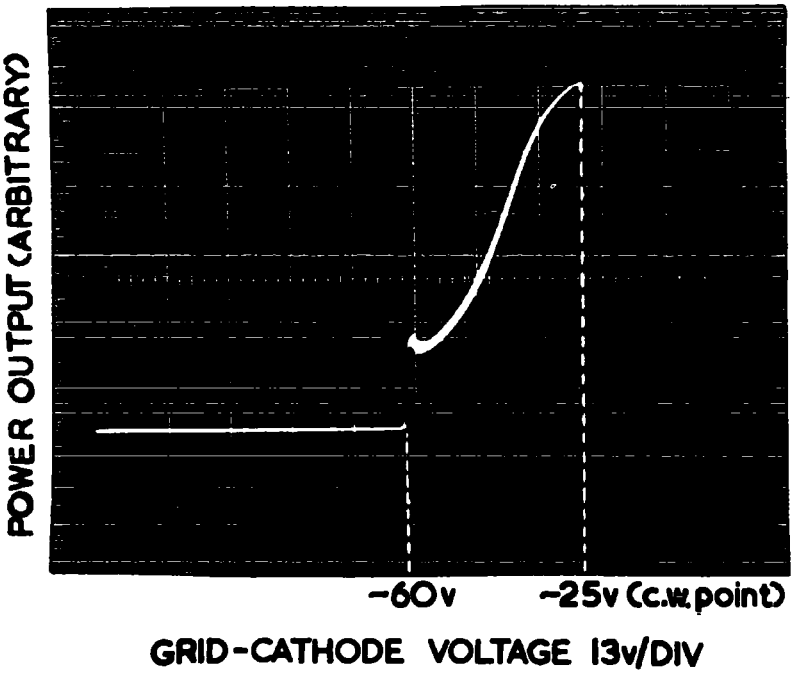

WITH WAVEMETER SET AT C.W. OPERATING FREQUENCY

FIGURE 4.6 K-BAND KLYSTRON GRID CHARACTERISTICS

high-Q wavemeter at the operating frequency in the lower oscillograph shows the considerable frequency deviation across the characteristic. Since the valve delivers over 80 mW between 21.35 and 22.33 GHz it was decided, following the experience with the J-band spectrometer, to use the pulse saturation technique, using switching diodes to control the power levels required. For the same reasons given in Section 4.2.1. it was necessary to use a microwave cavity to contain the sample in order to obtain sufficient sensitivity of operation.

4.3.2. Frequency stabilisation

Prior to delivery of the valve and in view of the great frequency instability of a simple spectrometer built using the harmonic generator as the source of K-band power, it was felt that an automatic frequency control (a.f.c.) system for the K-band klystron would be necessary for any e.s.r. work. This was built and tested using both the harmonic generator and 2K25 and the K-band klystron using a design due to Faulkner (1964), which has the advantage over the Pound system described in Section 3.4.1. of requiring fewer components and being somewhat simpler in operation. The microwave circuit is shown in Figure 4.7; the 50 kHz oscillator, amplifier and phase sensitive detector were simple transistorised units. The phase sensitive detector was transformer coupled to the oscillator and amplifier with transformers highly insulated between primary and secondary,

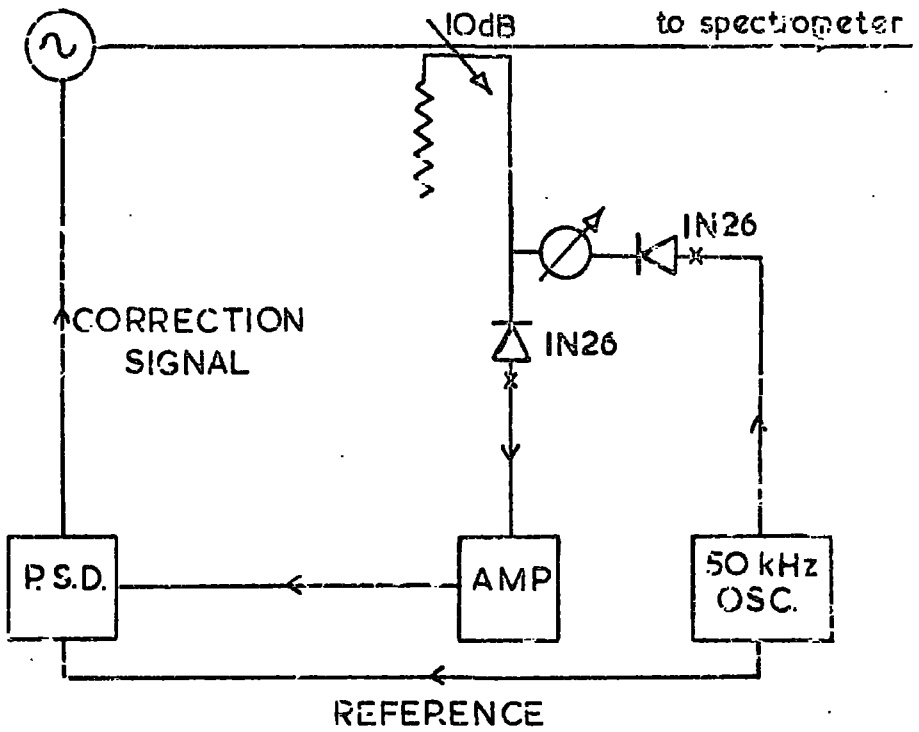

FIGURE 4.7 K-BAND A.F.C. SYSTEM

enabling the p.s.d. to be directly connected into the klystron reflector supply line, which was at 2.2 kV, the K-band valve being a high voltage type.

The principle of this a.f.c. system lies in modulation of the frequency of the reaction/transmission wavemeter cavity by the modulating diode terminating the transmission arm. This avoids the modulation of the klystron output which many a.f.c. systems require and avoids the complication of mechanical cavity modulation systems such as that described by Waring (1963). The original design required a phase shifter between the modulating diode and cavity, but this was found to be unnecessary using a tunable diode mount incorporating a variable insertion post in a slotted section of guide (Mid-century Microwave MC20/17), as this alone was sufficient to match the diode impedance to the cavity. Both modulating and detector diodes were 1N26 (Microwave Associates), the modulating diode drive being 1 v peak to peak at 50 kHz. When the modulating diode is correctly matched to the cavity and the klystron frequency coincides exactly with that of the cavity, the detector output is a very small signal at twice the modulating frequency, but when the klystron frequency drifts to eother side of the cavity centre frequency, a larger 50 kHz signal is produced, with opposite phase with respect to the modulating signal on either side of the

cavity centre frequency and this produces a d.c. output from the p.s.d. which acts, when applied with the correct polarity, as a correction voltage to the klystron reflector, returning the klystron frequency to that of the cavity. A high-Q K-band transmission/reaction wavemeter was not available with short delivery and so one was made, following the design of Bleaney et.al.(1947), using the H_{011} cylindrical mode. This places the transmission arm at 45^{o} to the main arm, so eliminating coupling of the H_{21} modes to the transmission arm. Coupling into the end wall of the cavity was via two small circular holes $\lambda_g/2$ apart in the narrow wall of the main guide, and symmetrically disposed about the centre of the end wall of the cylinder. Coupling to the transmission arm was by a centred circular iris at the end of the arm, forming part of the cavity side wall. The cavity end plunger was non-contacting, as there are no radial end wall currents with the H_{011} mode and was backed by a lossy tufnol ring to suppress unwanted coaxial modes behind the plunger. The entire assembly was made of brass, the interior surfaces being very highly polished and then silver plated, using a silver/cyanide solution and then repolished, which produced a Q of approximately 4000.

This a.f.c. system was first tested using the harmonic generator and proved successful in stabilising the frequency of

the source KS9/20A (2K25) X-band klystron, enabling a resonance display to be maintained for several hours, whereas previously a change in frequency would cause loss of the display within a few minutes. Although tested with the K-band klystron when delivered, this system was not finally found to be necessary, as, although the stability of the valve was not very good when allowed natural air cooling, drift sufficient to upset bridge balance but not to cause total loss of resonance occurring within about ten minutes, placing the valve in an oil bath, as was done for the K3102 J-band klystron, resulted in very good long term stability once operating temperature had been reached. Run in conjunction with a Microwave Instruments WE80 power supply, this klystron was capable of maintaining a resonance display for 4 - 5 hours if necessary, aided by the stability of the Newport Instruments C225 magent control unit and generator.

4.3.3. The experimental cavity

Initial experiments with this spectrometer were carried out using a rectangular TE_{10p} cavity of very similar design to that used at J-band (Fig.4.2.). This was somewhat longer and could therefore utilise higher modes, but it was found that the method of 'setting off' the coupling at room temperature to become 100% at helium temperature was not successful, due to the smaller, more critical dimensions involved at K-band. Therefore, a fixed frequency rectangular cavity with remotely variable coupling was

constructed, as shown in Figure 4.8. Figure 4.9 shows a plot of cavity Q versus mode number, p, for the rectangular TE_{10p} variable frequency cavity, which shows the increase in Q as the mode number rises. The Q factors were estimated using a commercial high Q wavemeter to determine the 3 dB width in frequency of the cavity absorption relative to the centre frequency which was kept constant at 21.5 GHz, this being the design frequency of the cavity, at which the K-band klystron gave maximum power output. As a compromise between high Q and convenient length, the TE_{104} mode was selected for the experimental cavity, but it was found necessary to make the bottom plunger of the cavity movable, due to the large and variable filling factor of the samples used. This caused a very large change in resonant frequency, taking it out of the tuning range of the klystron when the empty cavity resonated at 21.5 GHz and so a movable non-contacting plunger and locking screw were used to terminate the cavity.

The variable insertion capacitative tuning screw was retained, as this is capable of a wide range of matching, but was driven by a worm and spur gear. These were recessed into the threaded ring at the bottom of the stainless steel .010" wall low temperature waveguide, to which the modified K-band flange at the topof the cavity was clamped by a lip inside the brass can used to exclude liquid helium from the cavity. The worm was driven by a

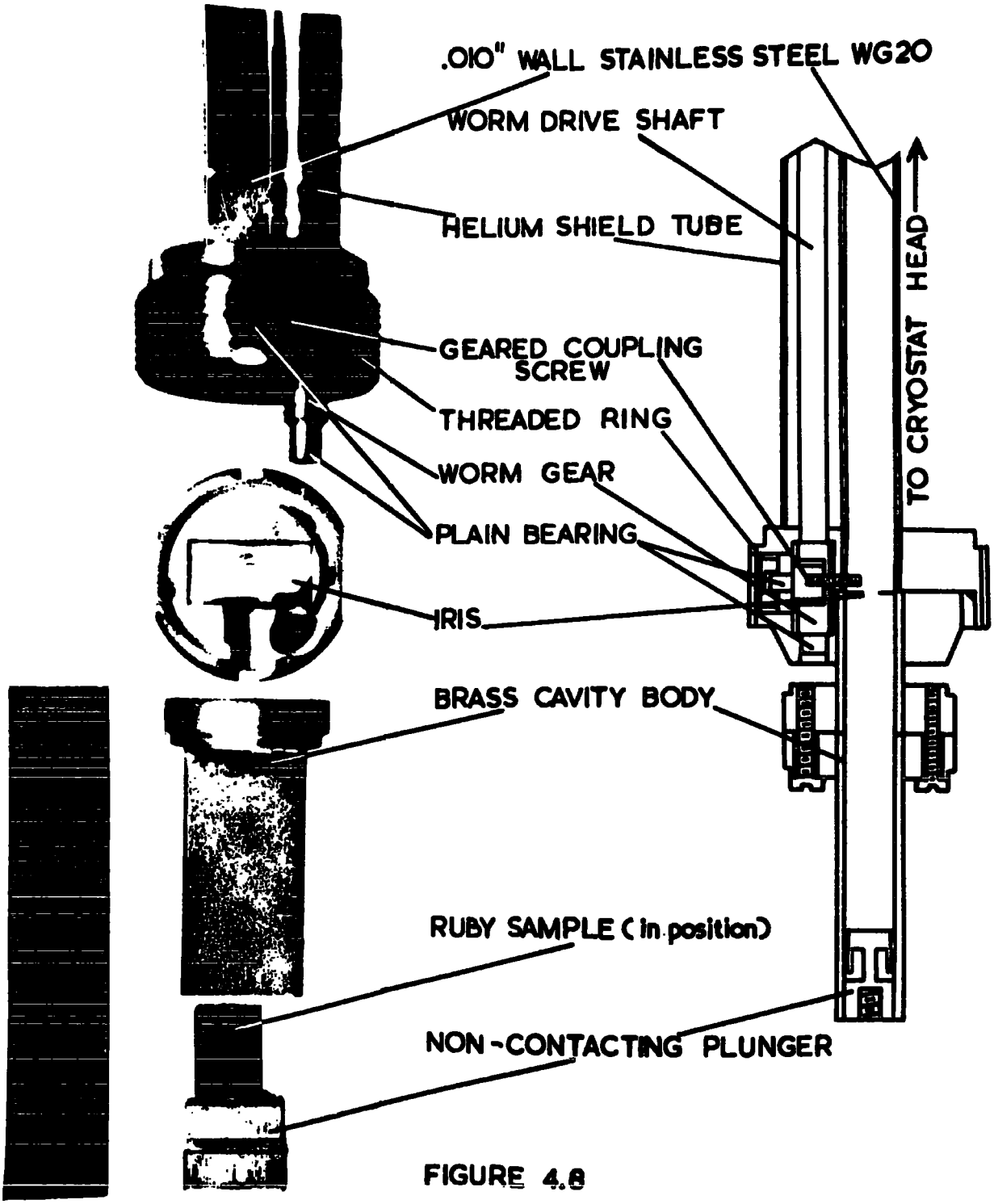

FIGURE 4.8

K-BAND REMOTELY VARIABLE COUPLING CAVITY

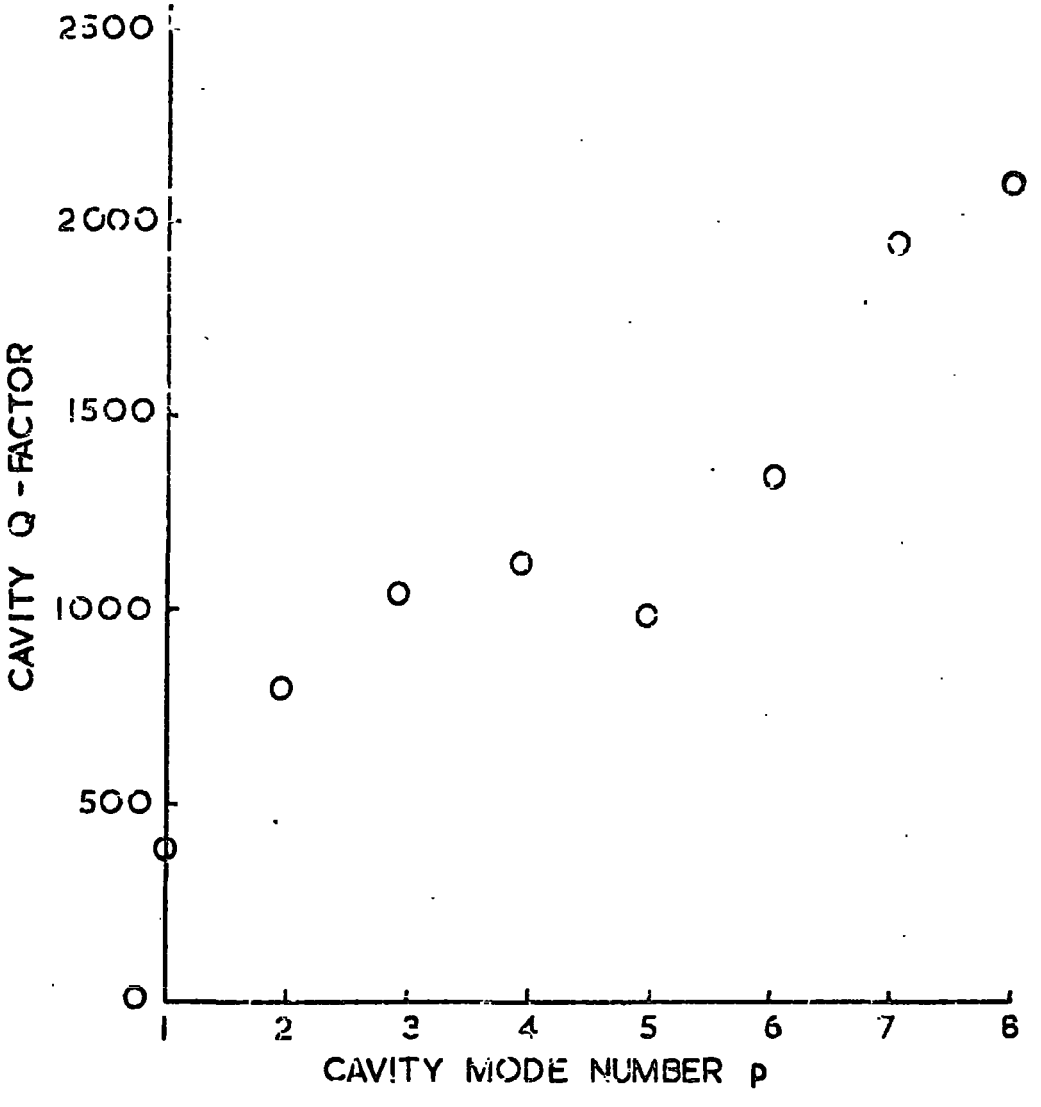

FIGURE 4.9 Q - FACTOR vs. MODE NO. FOR A RECTANGULAR TE_{10p} CAVITY AT 21.5 GHz

$\frac{1}{8}$" o.d. stainless steel tube, which ran up to the cryostat head within a .005" wall German silver guide tube which kept helium out of the mechanism. In use, the coupling drive was thoroughly de-greased in trichloroethylene to eliminate all traces of grease which would have frozen solid and siezed the mechanism at 4.2°K. The samples were mounted on the cavity plunger against the narrow wall with Apiezon grease and the plunger adjusted to bring the resonance of the filled cavity to 21.5 GHz before sealing the brass helium excluding can to the threaded ring with grease.

4.3.4. K-band pulse generation

Great difficulty was experienced in attempting to obtain a Philco L4760 series K-band swithing diode from the agents. Two alternatives to the original design intention wos therefore found. Firstly the J-band L4756 diode in its mount were matched to the K-band WG20 with two WG18/WG20 tapers, and used as a K-band switch. This was successful, despite the L4756 being designed specifically for 16 GHz operation. The two tuning screws on the mount were necessary to match the diode at 21.5 GHz, but a good match was found over the operating range of the spectrometer close to this frequency. This gave pulses with a switching ratio of about 24 dB with a forward bias insertion loss of approximately 1 dB. This, of course, does not appraoch the rated performance at its design frequency of the L4756 diode, but is comparable

with the specified switching ratio of the L4760 series of 28 dB, and proved adequate for pulse saturation experiments.

The second alternative was to make germanium point contact diodes in a crossguide mount similar to that tested at O-band and described in detail in Section 3.6.6. The design used was like that of Figure 3.14, the preparation of germanium chip and whisker of .002" tungsten wire being the same, but at this longer wavelength the two tuning screws, spaced $3\lambda_g/8$ apart, were mounted at the centre of the same broad face of the waveguide. The characteristics of this diode were similar to those of Figure 3.13b, showing a high inverse voltage breakdown (110 v), but considerably higher reverse leakage current than the commercial L4756 diode. This resulted in a switching ratio of about 20 dB, the insertion loss again being around 1 dB. The same diode pulse generator described in Section 4.3 was used to drive this diode, the reverse bias being 45 volts, and the forward bias current 50 mA.

Both of these systems allow almost full klystron power to pass in the ON condition, resulting in approximately 35 mW saturating power at the cavity and a reverse leakage monitor power level of approximately 200 μW. The larger monitor power and stronger saturating pulse than at J-band resulted in somewhat larger relaxation recovery signals than at J-band, sometimes no

additional amplification after the pre-amplifier/limiter being needed. As a check of whether the monitor power was too large and itself producing any appreciable saturation of the transition, the reverse bias was reduced, increasing the monitor power level, but down to 15 volts reverse bias no effect on the shape of the exponential recovery trace was observed.

4.3.5. The complete spectrometer and its operation

Figure 4.10 is a diagram of the K-band spectrometer. The circuit is virtually identical to that of the J-band spectrometer, the diode on the directive feed being used for setting up the cavity frequency and coupling. The detector diode on the hybrid tee bridge was attached with a Perspex coupling ring and mica washer to provide d.c. isolation for the balanced feed to the pre-amplifier and d.c. amplifier (Solartron A.A. 900). The bridge was balanced using the E - H tuner, after the diode modulator had been matched at the operating frequency, as this operation would upset bridge balance. The same stainless steel cryostat and Newport Instruments 8" type D electromagnet were used as at J and Q-band. After mounting the sample and finding the cavity resonance at 21.5 GHz using 50 Hz reflector voltage sweep on the klystron, the cryostat was assembled, evacuated and pre-cooled before the transfer of liquid helium. The klystron had to be re-tuned slightly to recentre the cavity frequency in

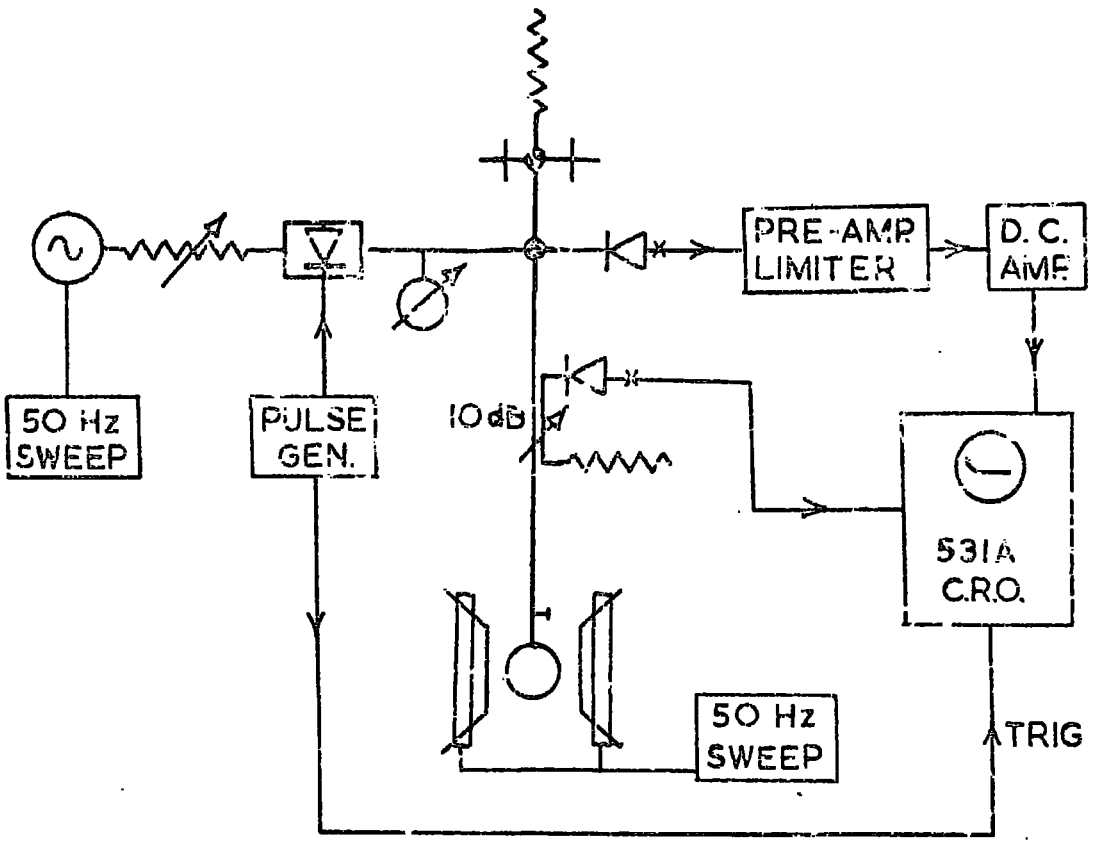

FIGURE 4.10 THE K-BAND SPECTROMETER

(for key see figure 3.1 supp.)

the klystron mode and the coupling adjusted to match the cavity. The required resonance was located with 50 Hz sweep of the magnetic field and the sample accurately orientated using the methods described in Section 4.2.5. The diode pulsing unit was then switched on, the field sweep removed and the magnetic field precisely adjusted to give exponential relaxation recovery traces, which were photographed on Polaroid film and analysed by a semi-logarithmic plot as detailed in Section 3.4.4. Using 1N78B detector diodes instead of the K-band diodes (both having the same co-axial packaging) gave somewhat better signal to noise and sensitivity in the spectrometer, which overall was rather more sensitive than the J-band spectrometer. For the ruby $\Delta M = 1$, $\Delta M = 2$ and $\Delta M = 3$ transitions in the same sample at room temperature, at a polar angle of 90°, the signal to noise ratios for the K-band spectrometer, measured from a 100 Hz oscilloscope absorption display, were 27, 18 and 11 dB, compared with the J-band spectrometer, with which the $\Delta M = 3$ transitions were not detectable above the noise, and the s/n ratios for $\Delta M = 1$ and $\Delta M = 2$ transitions were 20 dB and 9 dB.

Chapter 5
RESULTS AND DISCUSSION

5.1 Previous Data

The series of experiments described in Chapters 3 and 4 were performed on a range of samples of artificial ruby which had previously been subjected to crystallographic and e.s.r. analysis in this Department (Mason 1966, Kirkby 1967). Table 5.1 gives details of previously determined parameters for these samples used in this present work. These are growth method, concentration of chromium ions, degree of crystalline imperfection expressed as mean c-axis misorientation determined by analysis of Laue X-ray photographs and values of ε_{xx} and ε_{zz}, the compressive strain components acting in the x and z axes of the lattice (see Kirkby and Thorp 1968 and Section 2.4). The linewidth studies resulting in the values of ε_{xx} and ε_{zz} were performed at 77°K using the Q-band spectrometer described in Chapter 3. The chromium ion concentrations in the samples were determined by optical spectrographic analysis at the Chemical Inspectorate, Woolwich Arsenal, by courtesy of Dr R. A. Mostyn.

5.2 Present Results

The results of the work described in this thesis consist of a series of measurements of the spin-lattice relaxation time (T_1) at 4.2°K for the ruby specimens listed in Table 5.1. T_1 was measured at magnetic fields corresponding to X,J,K,Q and O-band frequencies (9.3, 16, 22, 35.5 and 71 GHz),

Table 5.1

Sample	Growth method	Concentration Cr^{3+}, at. %	Mean c-axis misorientation, min	Strain components ϵ_{xx}	ϵ_{zz}
G2A	Vapour Phase	0.032	74	171	140
312B	Vapour Phase	0.041	71	138	113
L2	Czochralski	0.045		86	80
337C	Vapour Phase	0.052	36	129	106
354	Vapour Phase	0.20	72	190	155

for polar angles of 0° and 90° for the various $\Delta M = 1$ transitions detectable under these conditions. Polar angles of 0° and 90° were selected for the measurements for the following reasons. For a polar angle of 0°, for all values of magnetic field (H), the ground state energy levels of the Cr^{3+} ion in ruby are pure spin states, characterised by quantum numbers $\mp 1/2$ and $\mp 3/2$. In addition, the energy levels of Cr^{3+} constitute a multilevel system and the relaxation behaviour of any pair of levels which is being monitored will be modified by relaxation constants appertaining to the other pairs of levels in the system. This is shown in Equations 1.26 and 1.27, where the C_{ij} are amplitude constants corresponding to the relaxation times T_{ij} for the various pairs of levels, $|i\rangle, |j\rangle$. These amplitude constants have been evaluated by Doncho (1964) and he has shown that at polar angles of 90° and close to 0° one constant C_{ij} is of large magnitude and the others are very small. The relaxation behaviour at these polar angles is therefore predominantly that of a single pair of energy levels and so presents essentially the simplest case for study.

The variation of spin-lattice relaxation time with applied magnetic field for the various transitions in the samples is shown graphically in Figures 5.1 to 5.16. In order to determine the exponent of H to which the relaxation time is proportional the results have been plotted on

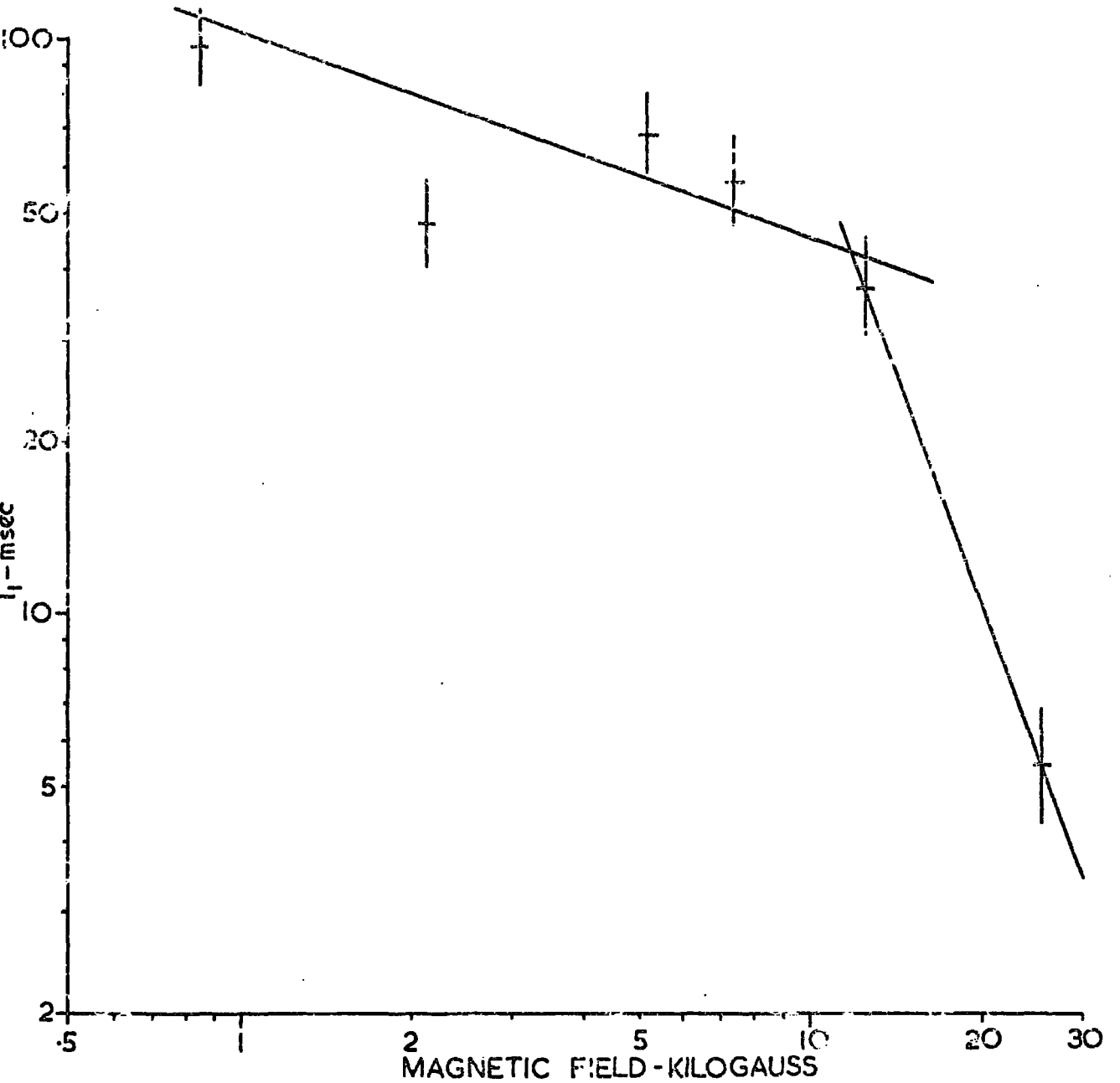

FIGURE 5.1 DEPENDENCE OF T_1 ON MAGNETIC FIELD
RUBY L2, $\vartheta = 90^\circ$, TRANSITION 2↔3, $T = 4.2^\circ K$

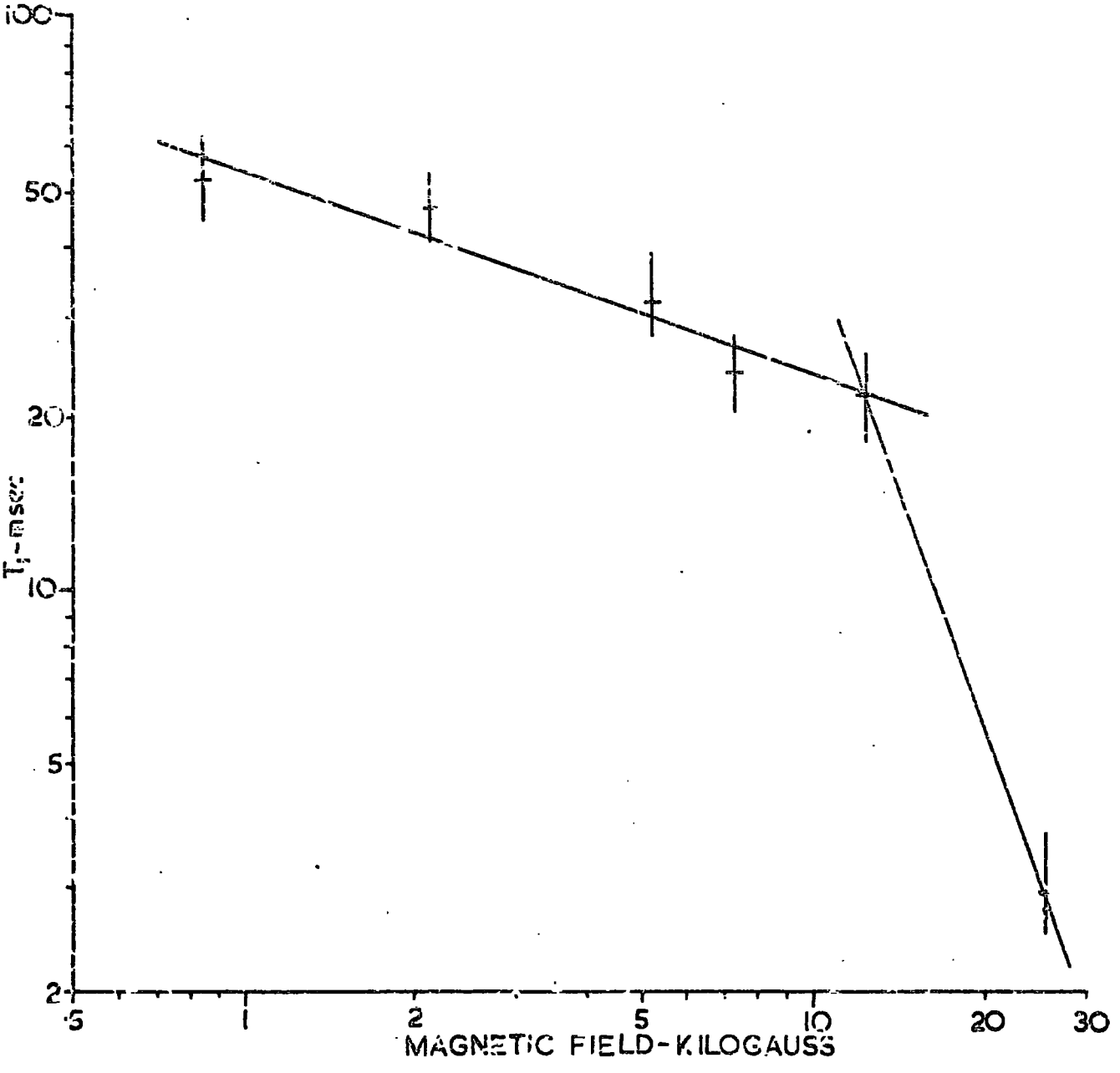

FIGURE 5.2 DEPENDENCE OF T_1 ON MAGNETIC FIELD
RUBY G2A, $\vartheta = 90^\circ$, TRANSITION 2↔3, $T = 4.2^\circ K$

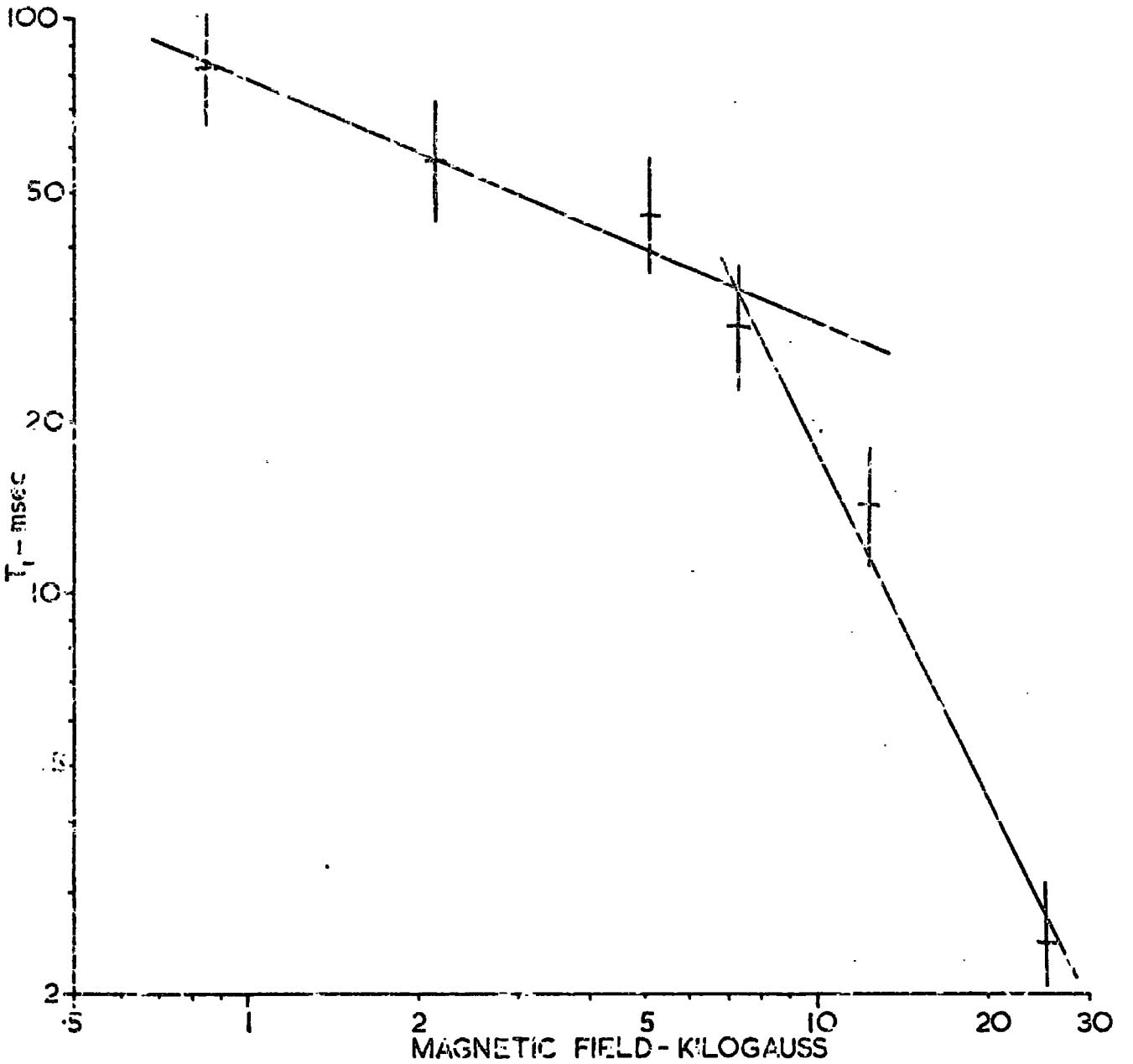

FIGURE 5.3 DEPENDENCE OF T_1 ON MAGNETIC FIELD
RUBY 312B, $\vartheta = 90°$, TRANSITION 2↔3, $T = 4.2°K$

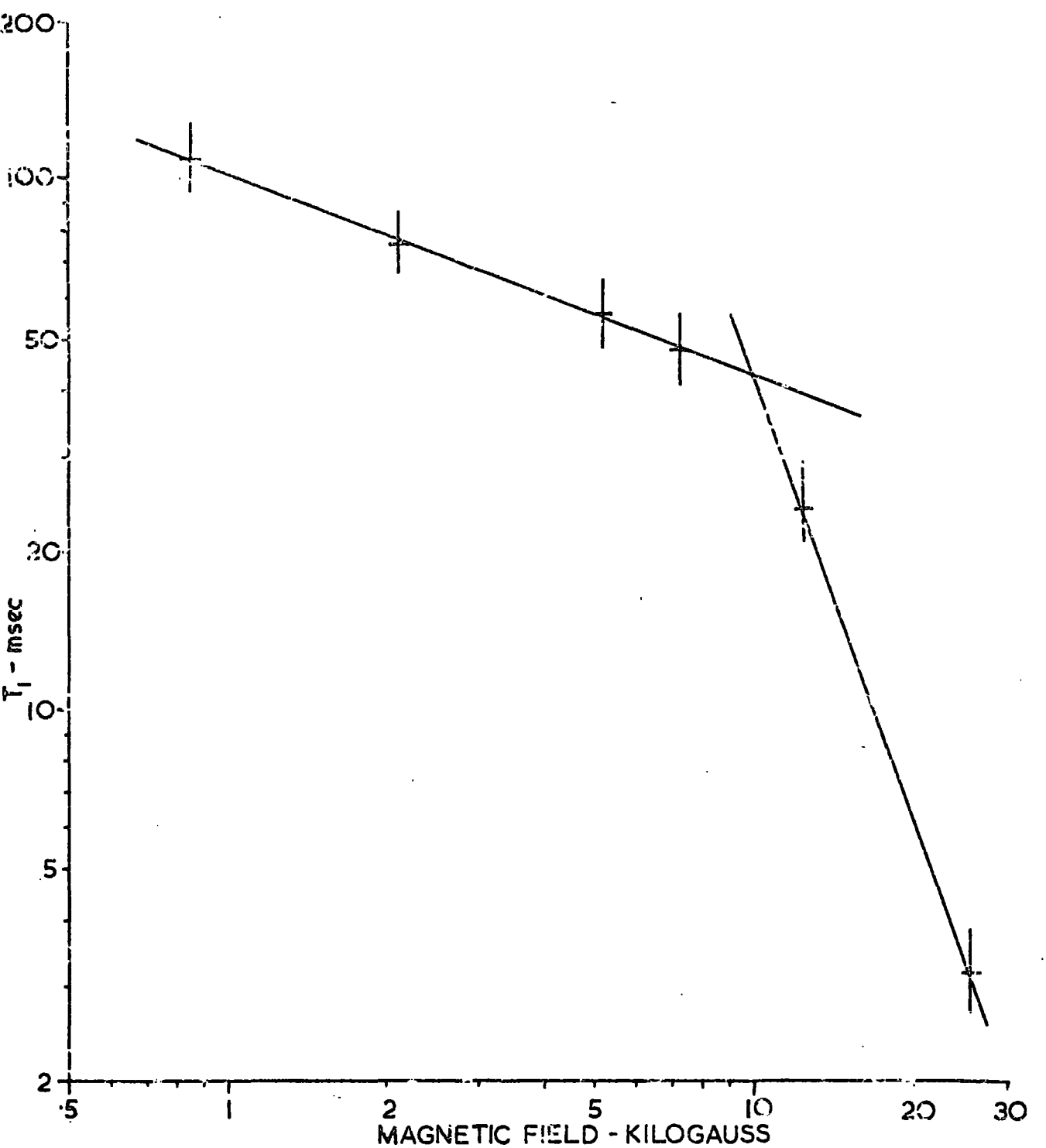

FIGURE 5.4 DEPENDENCE OF T_1 ON MAGNETIC FIELD
RUBY 337A, $\vartheta = 90^\circ$, TRANSITION 2↔3, $T = 4.2^\circ K$

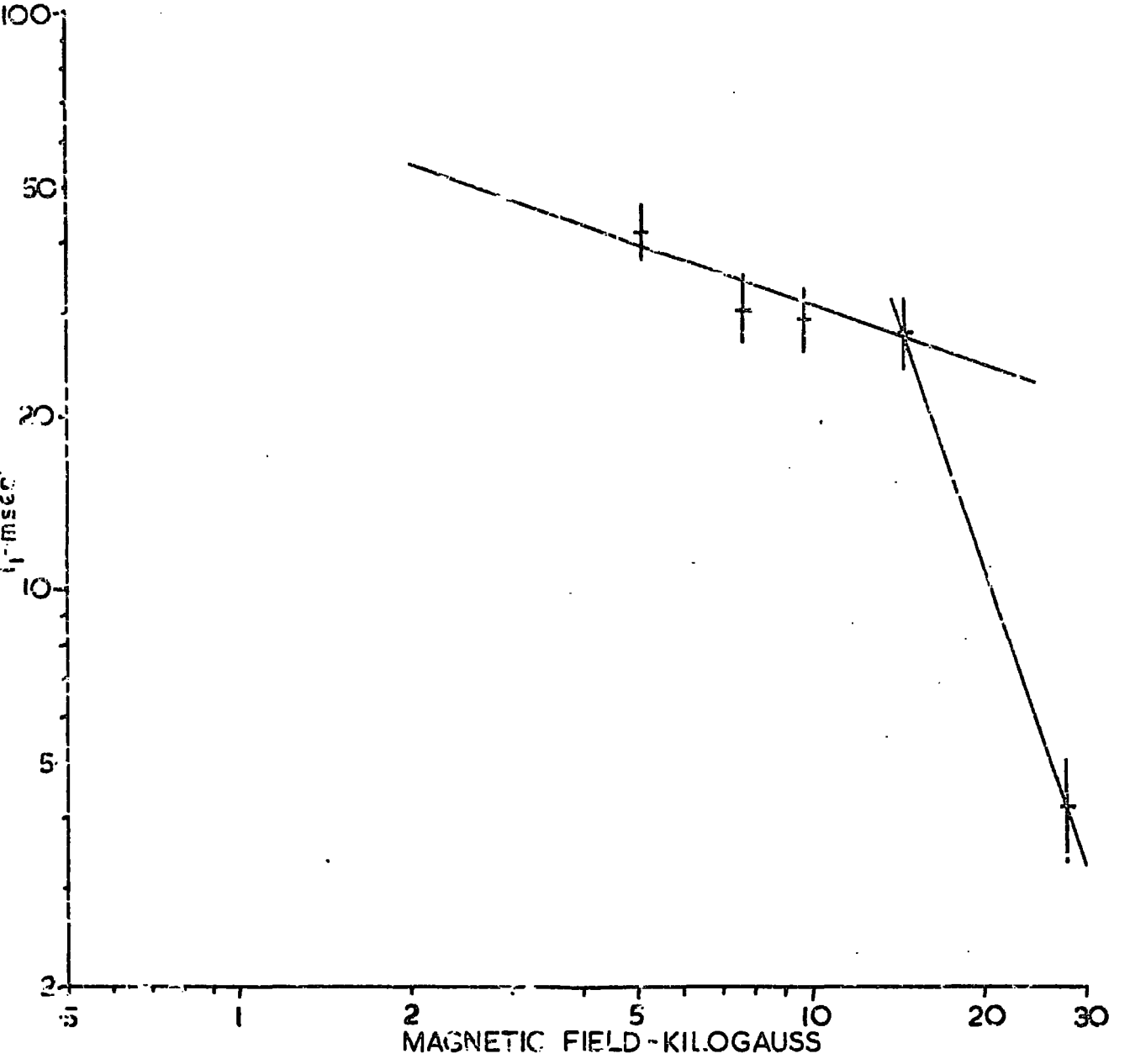

FIGURE 5.5 DEPENDENCE OF T_1 ON MAGNETIC FIELD
RUBY L2, $\vartheta = 90^{\circ}$, TRANSITION 1↔2, $T = 4.2^{\circ}K$

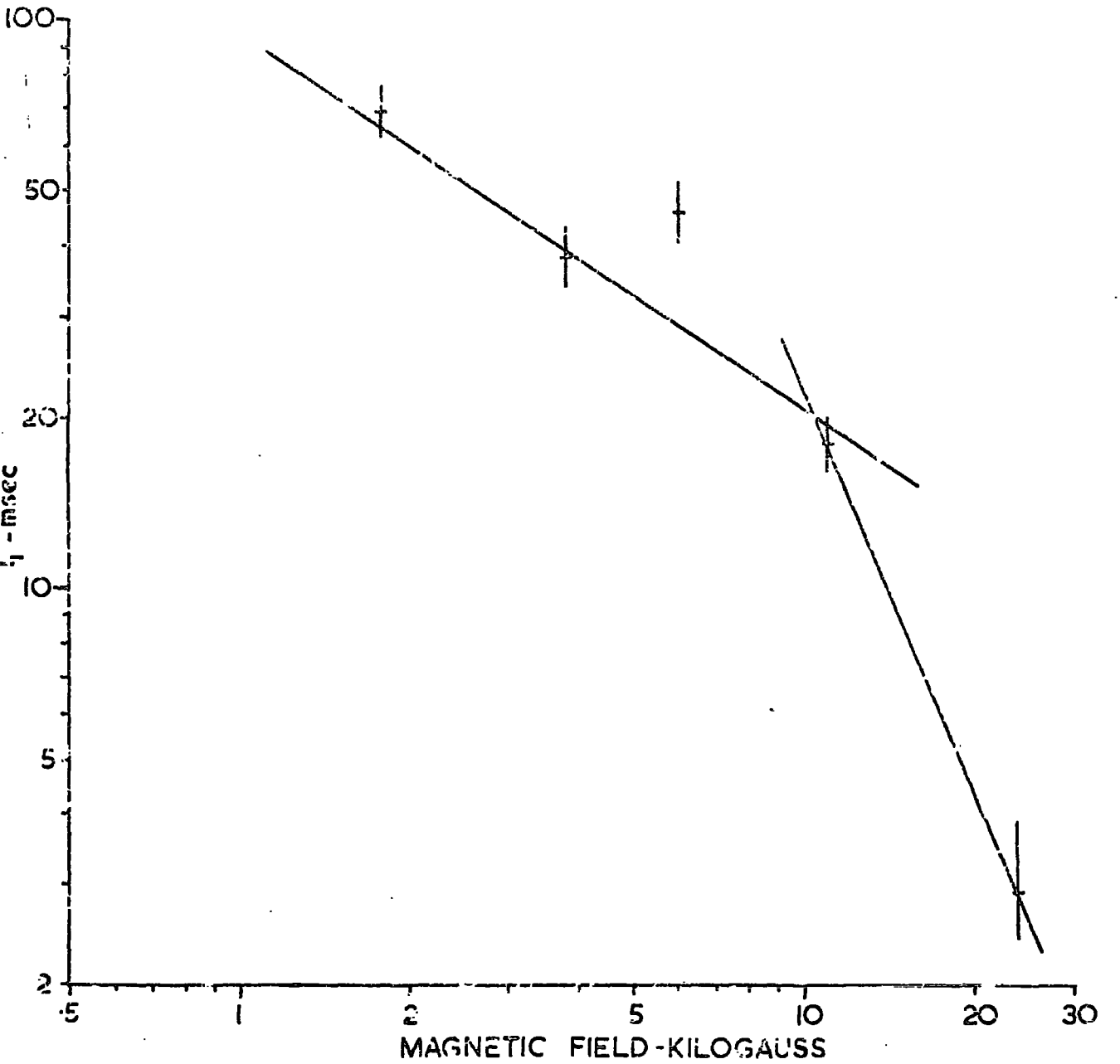

FIGURE 5.6 DEPENDENCE OF T_1 ON MAGNETIC FIELD
RUBY L2, $\vartheta = 90°$, TRANSITION 3↔4, $T = 4.2°K$

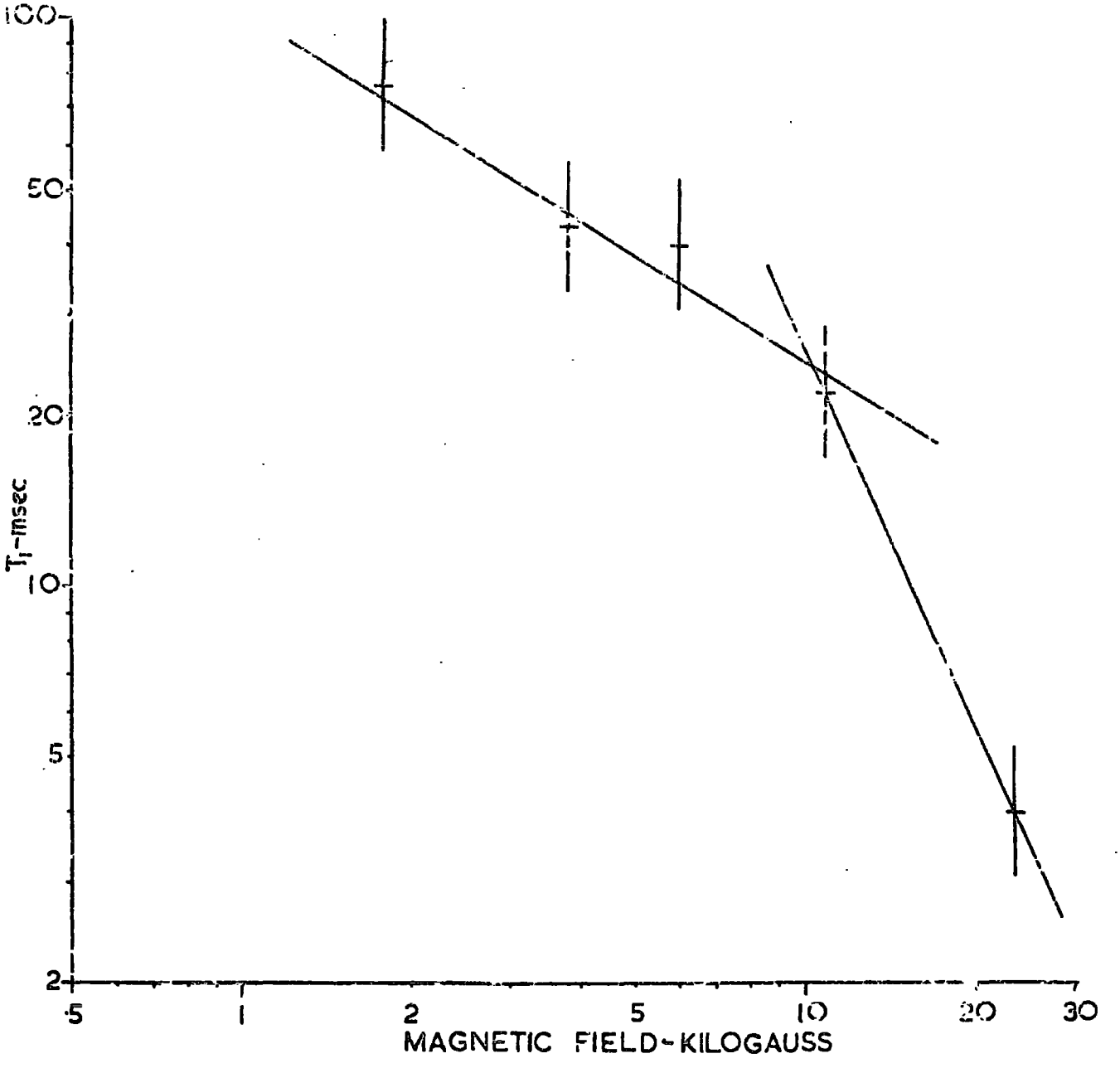

FIGURE 57 DEPENDENCE OF T_1 ON MAGNETIC FIELD
RUBY 337A, $\vartheta = 90^\circ$, TRANSITION 3↔4, $T = 4.2^\circ K$

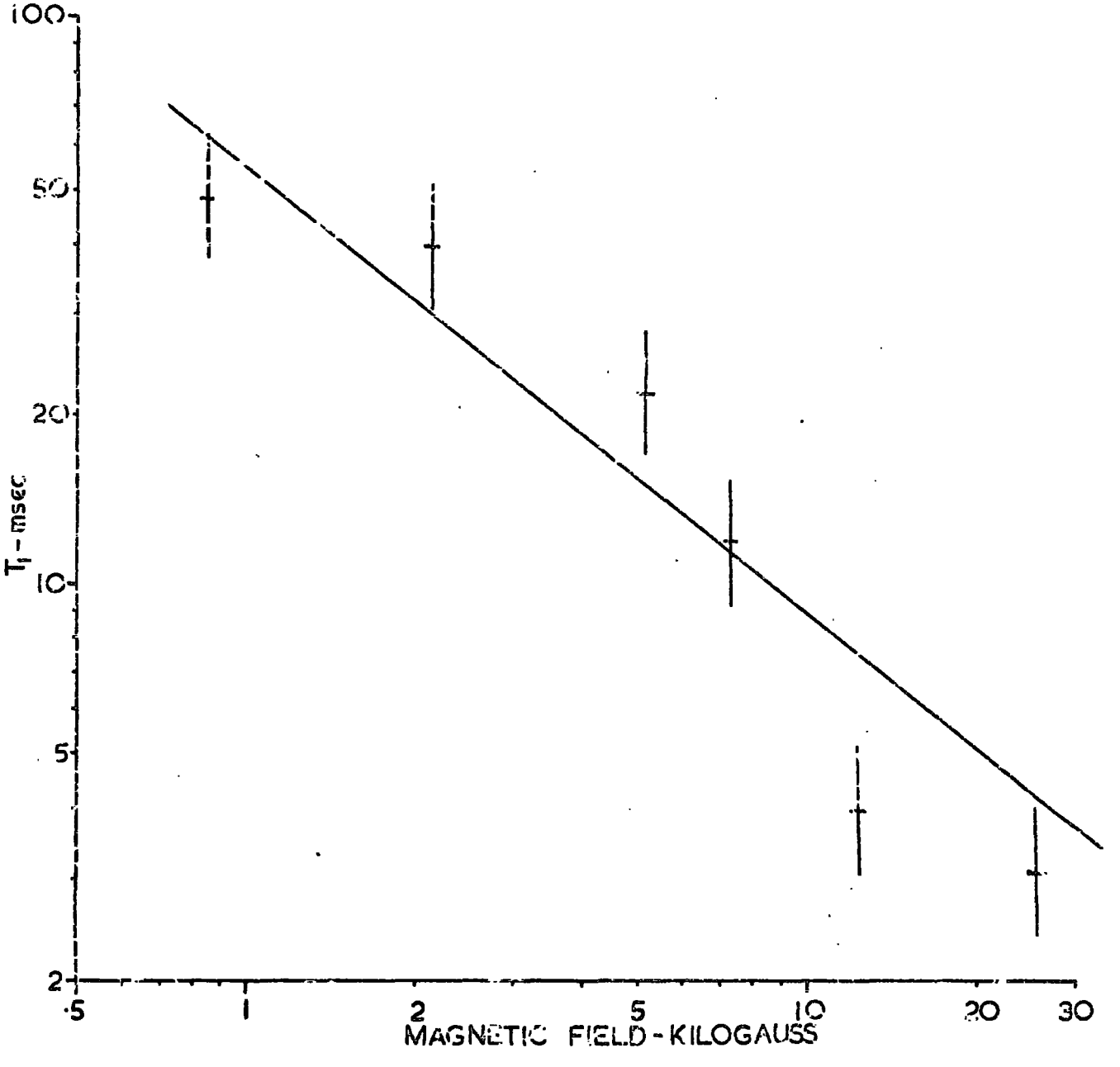

FIGURE 5.8 DEPENDENCE OF T_1 ON MAGNETIC FIELD
RUBY 354 , $\vartheta = 90°$, TRANSITION 2→3 , T = 4.2°K

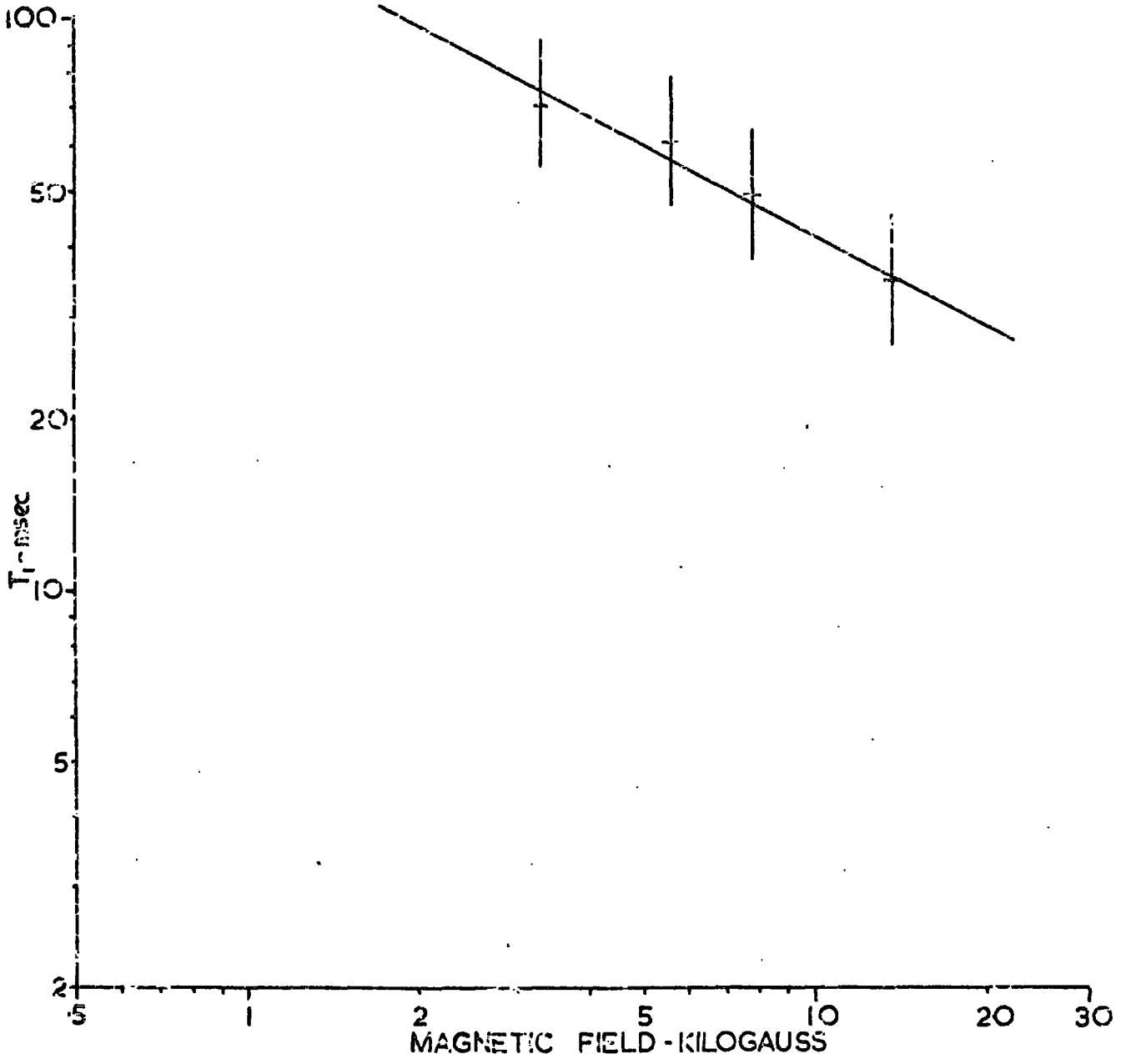

FIGURE 5.9 DEPENDENCE OF T_1 ON MAGNETIC FIELD
RUBY L2, $\vartheta = 0^\circ$, TRANSITION $1/2 \leftrightarrow -1/2$, $T = 4.2^\circ$ K

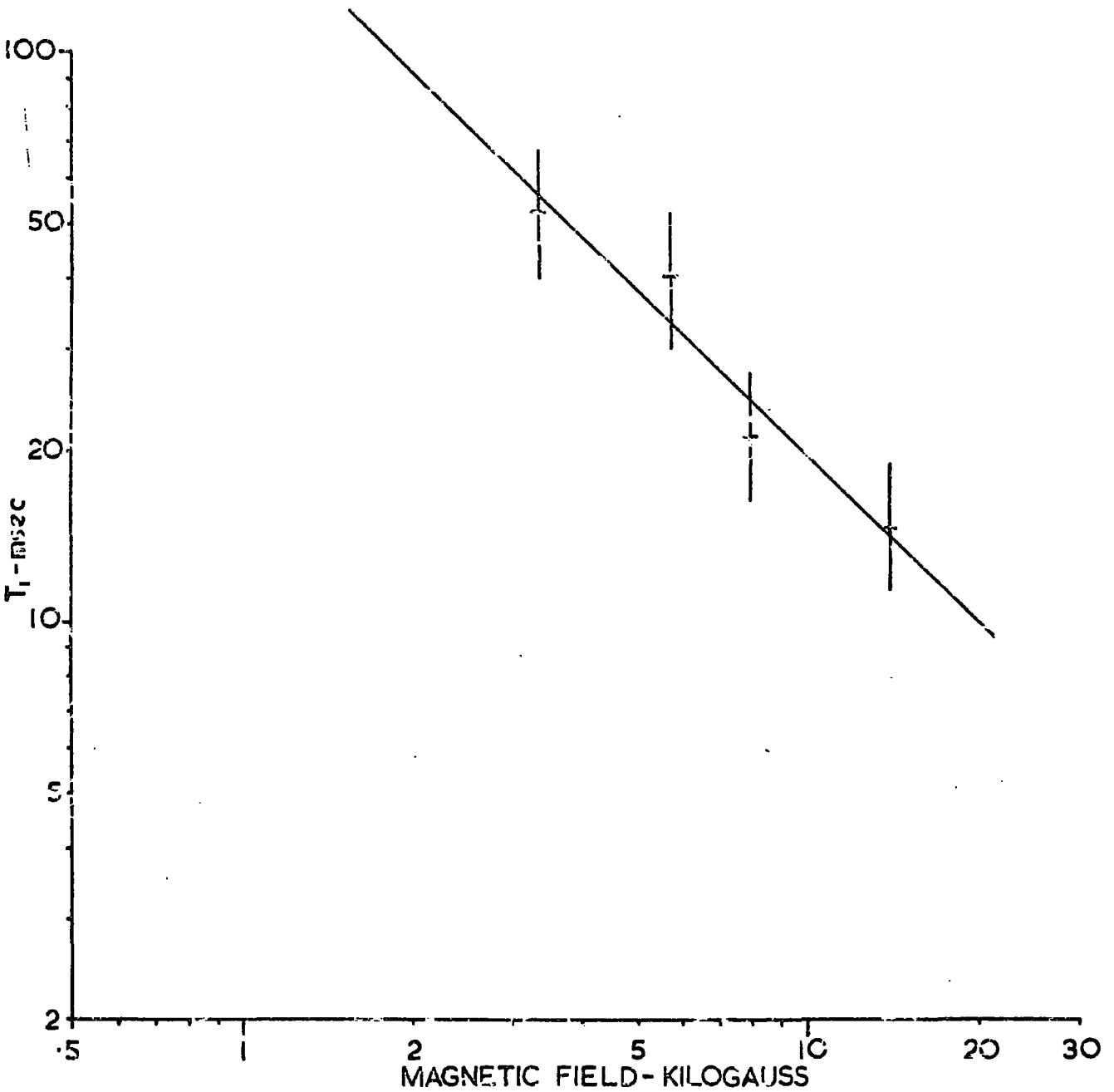

FIGURE 5.10 DEPENDENCE OF T_1 ON MAGNETIC FIELD
RUBY G2A, $\vartheta = 0^\circ$, TRANSITION $1/2 \leftrightarrow -1/2$, $T = 4.2^\circ K$

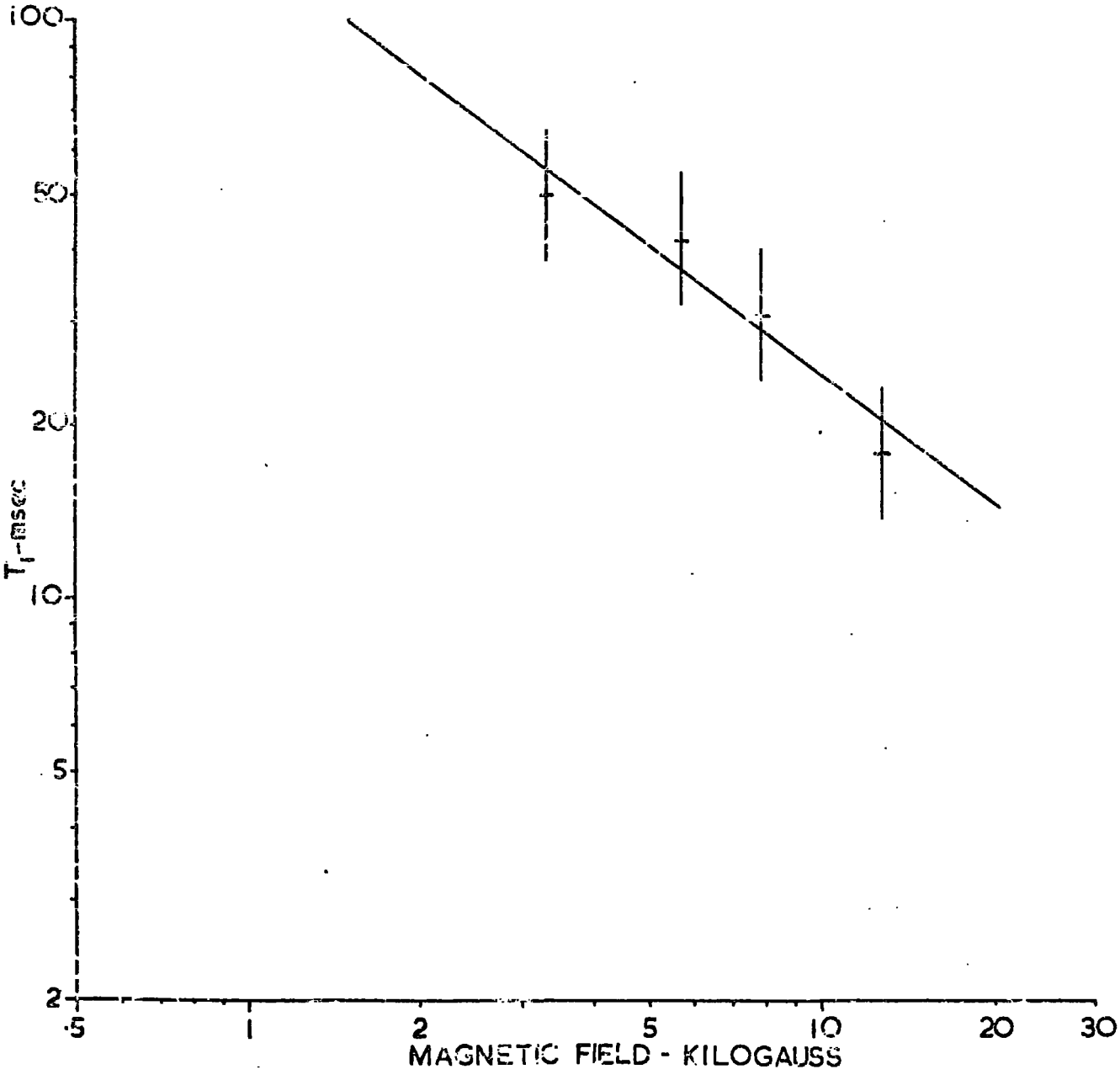

FIGURE 5.II DEPENDENCE OF T_1 ON MAGNETIC FIELD
RUBY 312B, $\vartheta = 0°$, TRANSITION $1/2 \leftrightarrow -1/2$, $T = 4.2°K$

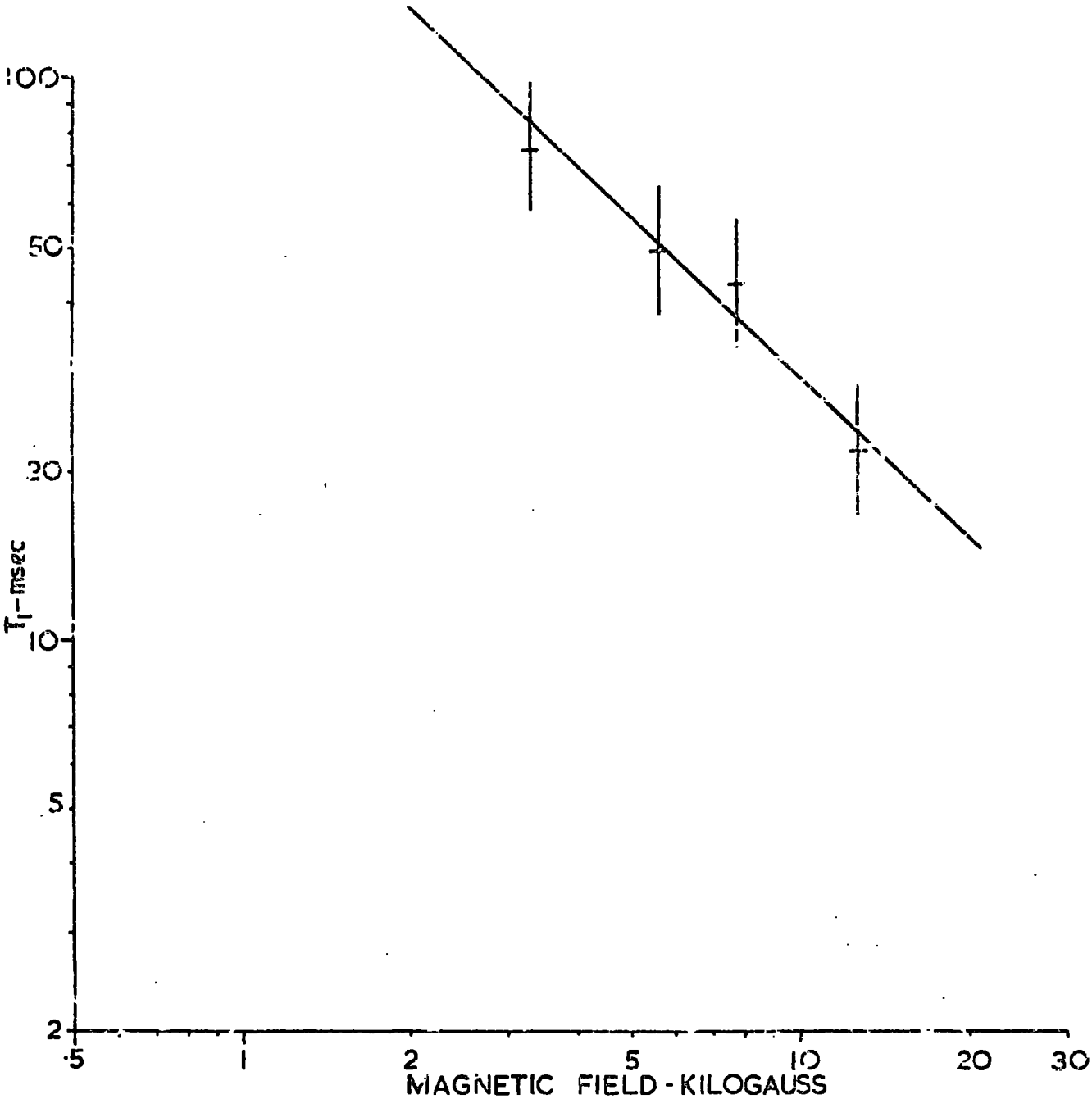

FIGURE 5.12 DEPENDENCE OF T_1 ON MAGNETIC FIELD
RUBY 337A, $\vartheta = 0°$, TRANSITION $1/2 \leftrightarrow -1/2$, $T = 4.2°K$

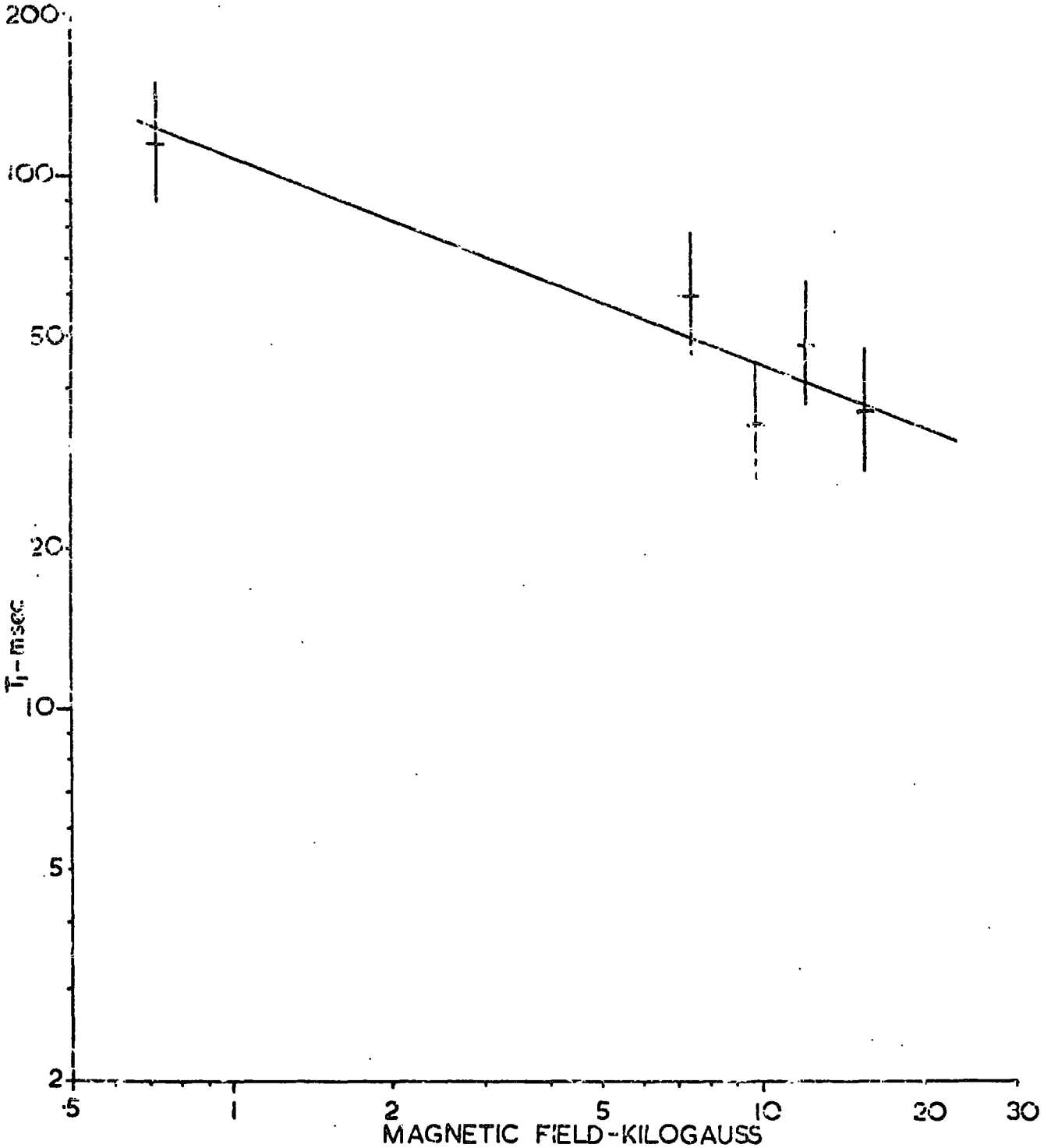

FIGURE 5.13 DEPENDENCE OF T_1 ON MAGNETIC FIELD
RUBY L2, $\vartheta = 0^\circ$, TRANSITION 1/2 → 3/2, T = 4.2°K

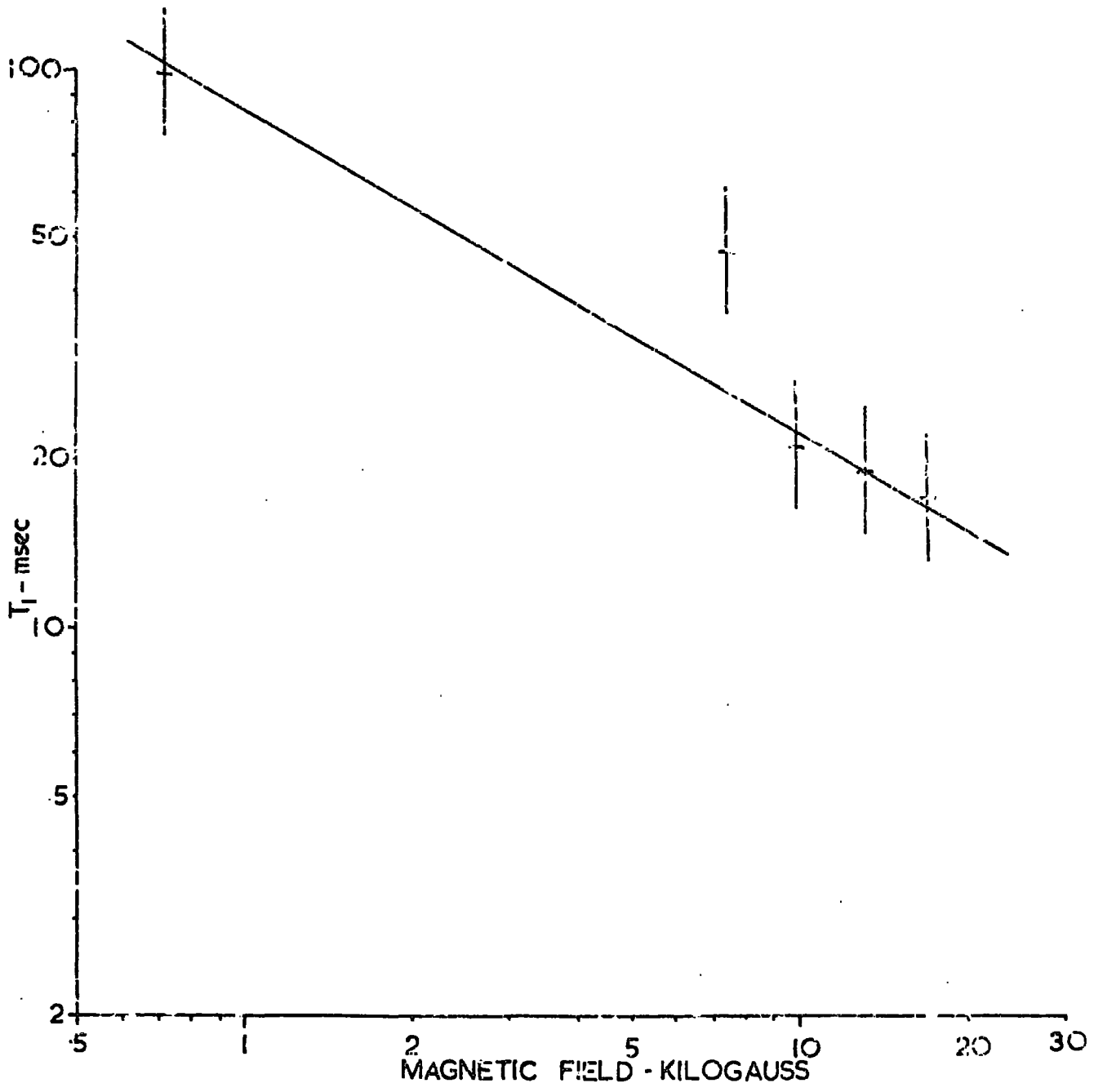

FIGURE 5.14 DEPENDENCE OF T_1 ON MAGNETIC FIELD
RUBY G2A, $\theta = 0^\circ$, TRANSITION 1/2 ↔ 3/2, $T = 4.2^\circ K$

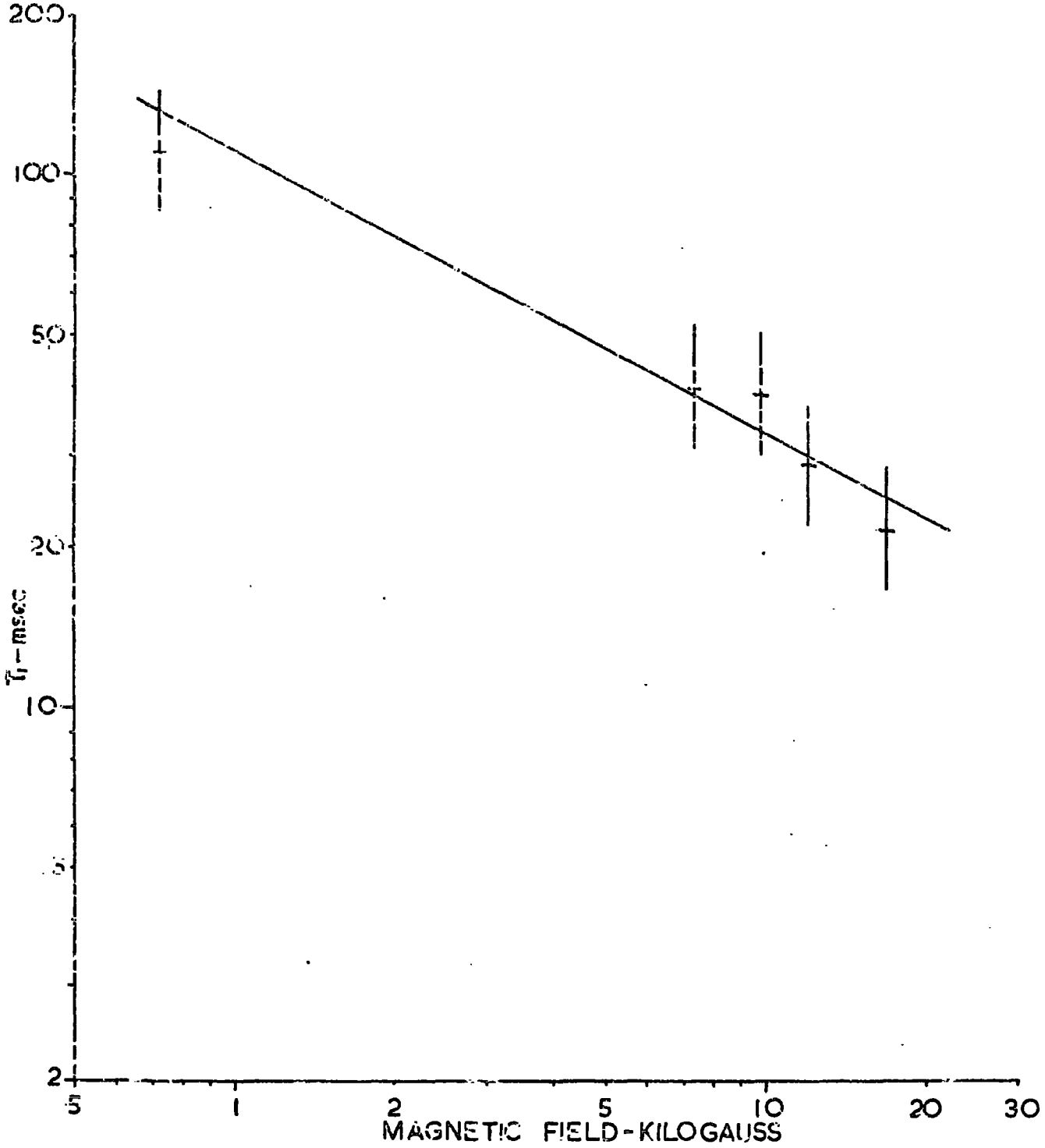

FIGURE 5.15 DEPENDENCE OF T_1 ON MAGNETIC FIELD
RUBY 337A, $\vartheta = 0°$, TRANSITION $1/2 \rightarrow 3/2$, $T = 4.2°K$

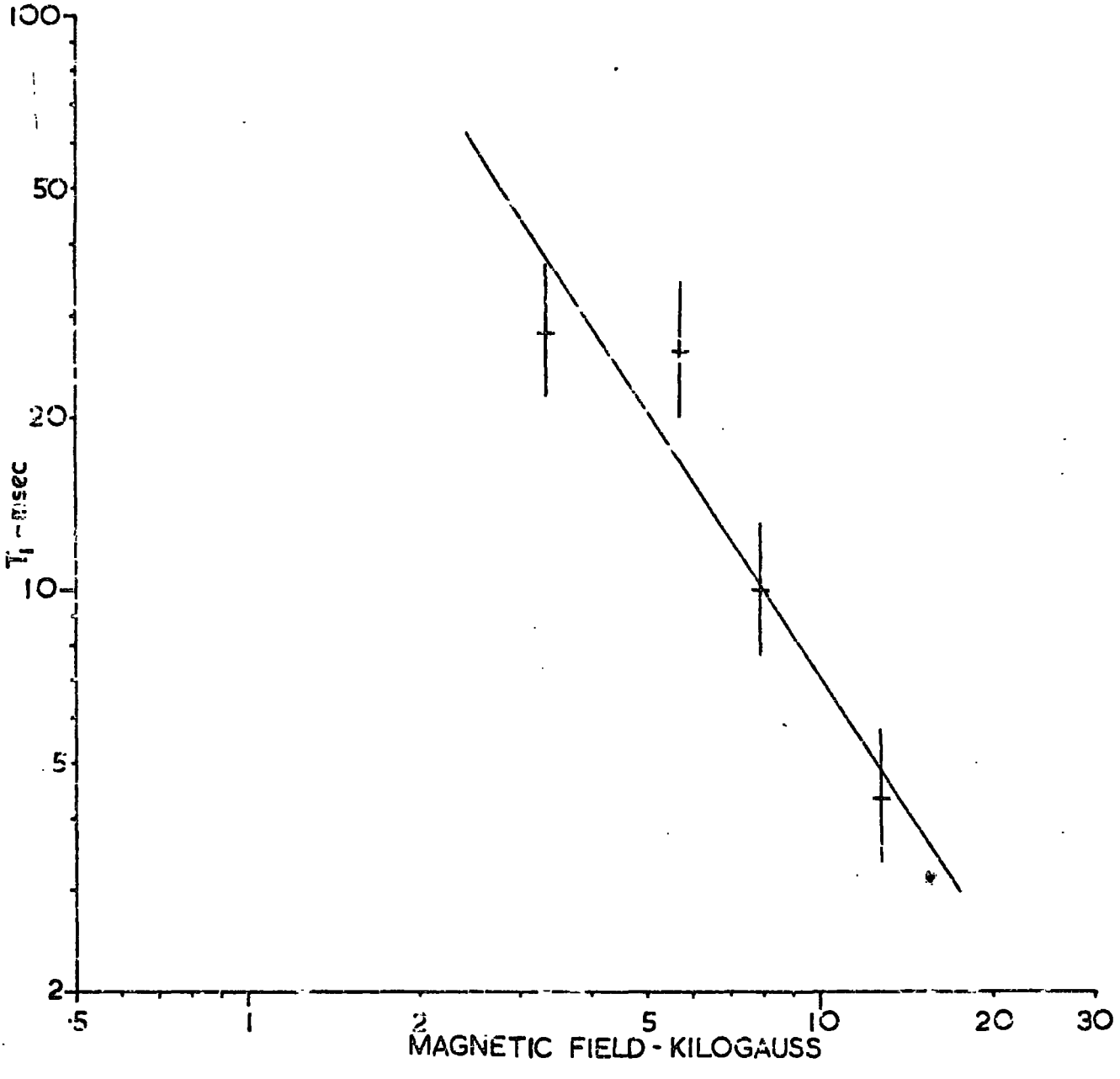

FIGURE 5.16 DEPENDENCE OF T_1 ON MAGNETIC FIELD
RUBY 354, $\vartheta = 0^{\circ}$, TRANSITION 1/2↔-1/2, $T = 4.2^{\circ}K$

log-log scales, the required exponent being the slope of the resulting straight line graph in each case. The graphs for all samples except No 354 show a general similarity, T_1 decreasing with increasing magnetic field. No results are shown for polar angle 0° at O-band due to the shape of the samples used, which could only be fitted into the WG 22 waveguide so as to place the c-axis perpendicular to the axial field of the superconducting solenoid used in this spectrometer (see Section 3.6).

In the graphs of measurements made at a polar angle of 90°, which include relaxation times measured at a very high magnetic field ($\sim$ 25kG) with the O-band spectrometer, these measurements diverge widely from the straight line which can be drawn through the points relating to measurements made at lower magnetic fields with the X, J, K and Q-band equipments. As this wide divergence of the high field T_1 from the lower field values suggests a modification of the relaxation behaviour of the xx Cr^{3+} ions, the exponent of H at high field has been taken in most cases, in the absence of any intermediate or higher field measurements, as the slope of the join of the points corresponding to the Q and O-band measurements of T_1. The straight line drawn through the low field points was fitted by the method of least squares in each case.

The exponents of H to which T_1 is proportional, derived from Figures 5.1 to 5.16 are tabulated in Table 5.2,

the 90° polar angle results being divided into those for high and low magnetic field. No results are shown for the -3/2 to -1/2 transition at 0° polar angle, as this transition cannot be observed at X-band since the zero field splitting of Cr^{3+} in ruby (11.4 GHz in frequency units) is greater than the microwave quantum energy (9.3 GHz in frequency units) and at 0° polar angle the rate of divergence of the energy levels of the $\overline{+}3/2$ doublet is greater than that of the $\overline{+}1/2$ pair. This means that the separation in energy in frequency units of the -3/2 and -1/2 energy levels is never less than 11.4 GHz and absorbtive transitions between these levels cannot take place under these conditions (see Figure 1.2a).

The results shown in Figures 5.1 to 5.16 and Table 5.2 are only for those samples and transitions for which a complete set of T_1 measurements had been made at frequencies from X-band to O-band (at $\theta = 0^{\circ}$ to Q-band only).

5.3 Discussion of Results

The exponents of H associated with each transition show fair consistency from sample to sample, with the exception of Sample 354 which is of high chromium concentration (0.20 at.%) and is included to show the modification of relaxation behaviour due to the effects of spin-spin relaxation and other cooperative relaxation processes, in contrast with the other samples of lower Cr^{3+} concentration.

All of these measurements were made at $4.2^{\circ}K$, at which

Table 5.2

Sample	Polar Angle	90°						0°	
	Transition	3-4		2.3		1-2		-1/2-+1/2	+1/2-+3/2
	Mag.Field Range	low	high	low	high	low	high	low	low
G2A				0.35	2.74			0.97	
312B				0.38	2.16			0.74	
L2		0.66	2.37	0.36	2.66	0.35	2.95	0.53	0.39
337C		0.56	2.24	0.38	2.76			0.94	0.53
354				0.98				1.53	

temperature the predominant relaxation process in ruby is the direct (one phonon) process discussed in Section 2.2.3.a. The temperature dependence of the relaxation time of the samples used has been investigated (Mason and Thorp, 1967) and the transition between direct and Raman relaxation was found to occur at approximately $30^{\circ}K$; as the Raman contribution to relaxation at $4.2^{\circ}K$ is very small it has been disregarded.

The concentration of Cr^{3+} in the samples (except for 354) was up to 0.052 at.%, which is below the concentration at which spin-spin interaction has been observed to affect the direct relaxation process (Standley and Vaughan, 1965). In addition, there was no evidence in the microwave spectra of any of these samples of the presence of absorption lines due to Cr^{3+} ion pairs (Gill, 1962) and the results are therefore regarded as characterising the behaviour of single ions. Schawlow, Wood and Clogston (1959) also found no evidence of lines due to exchange coupled pairs in the optical fluorescence spectra of ruby at a Cr^{3+} concentration of 0.04 at.%.

Under these conditions, the idealised theoretical treatment of spin-lattice relaxation given in Chapter 2 predicts a dependence of T_1 on magnetic field as H^{-2} for a non-Kramer's ion and H^{-4} for an isolated Kramer's doublet. At low magnetic fields, the exponents of H in Table 5.2, with the exception of Sample 354, lie between -0.3 and -1,

whereas at high field the exponent of H is between -2.1 and -3, averaging -2.55 for the $\Delta M = 1$ transitions observed at $\theta = 90^{o}$. These results suggest that the relaxation behaviour is tending towards that expected from theory at high magnetic field and that the energy levels are behaving as isolated Kramer's doublets.

At low magnetic fields, the major contribution to the separation δ_{ij} of the energy levels between the two doublets of the Cr^{3+} ion in ruby is the zero field splitting (Z.F.S.) of 11.46GHz and this tends to dominate any effect on the separation of the energy levels that their divergence under the influence of increasing magnetic field may have. Consequently the Z.F.S. has a masking effect on the influence of the magnetic field on T_1, since T_1 is proportional to δ_{ij}^{-2}, by Equation 2.19, for transitions between the two Kramer's doublets (i.e. at polar angles other than 0^{o}, transitions such as 2-3, 2-4 etc. (see Fig. 1.2b)). For transitions between the two levels of a Kramer's doublet (i.e. 1-2 and 3-4) the matrix elements of the ion are proportional to H^2 and consequently T_1 is theoretically proportional to H^{-4} (Equation 2.20). However, at polar angles other than 0^{o} for the Cr^{3+} ion in ruby, the energy levels are mixtures of the pure spin states which exist at $\theta = 0^{o}$ (Equation 1.02) and where this situation appertains, the theoretical dependence can no longer be expected to apply, as the relaxation process involves all spin states,

and not an isolated Kramer's doublet. The highest degree of mixing of spin states occurs where the energy levels are experiencing the greatest departure from a linear divergence with increasing magnetic field, i.e. where their curvature is greatest. In ruby, at all angles except $\theta = 0^{\circ}$, this is the low field region, up to approximately 9 kG, where the separations of the energy levels for $\theta = 90^{\circ}$ are approximately 30 GHz, which roughly corresponds to Q-band (35.5 GHz) results in Figures 5.1 to 5.16.

Above 9 kG however the divergence of the levels with H is linear and the energy levels become closer approximations to pure spin states as they become more isolated in energy. The 90° high field results in Table 5.2 do not show any significant difference between the exponents of H for transitions 3-4 and 1-2 and those for transition 2-3, probably because the mixing of states is not removed completely, even at 25 kG and also the Z.F.S. still constitutes 16% of the energy separation of levels 2 and 3 at this field.

These factors taken together and in particular the curvature of the energy level diagram at polar angles other than $\theta = 0^{\circ}$, producing a non-linear relationship between δ_{ij} and H, lead to a slower dependence of T_1 on H than the simple theoretical model predicts. It is therefcre to be expected that the exponents of H in this relationship, for ruby, will be less than the -2 and -4 predicted for the

transitions between and within the Kramer's doublets.

When the applied magnetic field is aligned along the z-axis (or c-axis or optic axis) of ruby, the energy levels are pure spin states, with good quantum numbers $|\pm 1/2\rangle$ and $|\pm 3/2\rangle$ for all values of magnetic field. The only strictly allowed transitions are those for which $\Delta M = 1$ and there is no curvature of the energy levels or mixing of the spin states. The Z.F.S. is still present however and is a major contribution to the energy separation of the doublets at low magnetic field. The exponents of H shown in Table 5.2 for $\theta = 0^{\circ}$ do not show any agreement with the theoretical predictions for values of H up to 15 kG (Q-band). The $-1/2 \rightarrow +1/2$ is a transition within the Kramer's doublet and the $+3/2 \rightarrow +1/2$ transition is one between the doublets and, as there is no mixture of the states, these might be expected to show dependencies of T_1 on magnetic field as H^{-4} and H^{-2} respectively. The dependencies in Table 5.2 do show that for the $-1/2 \rightarrow +1/2$ transition to be more rapid (average value -0.8) than that for the $+3/2$ - $+1/2$ (average value -0.5) and both of these are more rapid than the average low field dependency at $\theta = 90^{\circ}$ of -0.4. Equation 2.19 gives the proportionality $T_1 \propto \mathcal{E}_{ab}^{-2}$ and it is only when the two energy levels $|a\rangle$ and $|b\rangle$ are linearly divergent with H from the same energy at zero field that this proportionality becomes $T_1 \propto H^{-2}$. The Z.F.S. of 11.46 GHz separates the $|+3/2\rangle$ and $|+1/2\rangle$ levels however and consequently

invalidates the proportionality. Unfortunately no measurements at $\theta = 0^{o}$ were possible at O-band, where the influence of the Z.F.S. is much smaller and the T_1 value would be expected to be much lower than an extrapolation of the straight lines in Figures 5.13 to 5.15 would suggest.

In contrast to the case of ruby, the clearest experimental demonstration of the validity of the Van Vleck theory of relaxation in the direct region for a simple system was given by Davids and Wagner (1964). They showed the near perfect fourth power dependence of T_1 on magnetic field for the Fe^{3+} ion in $K_3Co(CN)_6$ up to approximately 4 kG. Fe^{3+} in the cyanides has the configuration $3d^5$ and an effective spin, S', of 1/2, due to strong covalent bonding. The energy levels, with H parallel to the z axis, therefore occur at $\pm 1/2 g_z \beta H$, i.e. they are linearly divergent from the same point at H = 0, there being no zero field splitting. This is effectively the theoretical case of an isolated Kramer's doublet (for dilute crystals) and so the predicted H^{-4} dependence of T_1 on H is followed very closely. In addition $K_3Co(CN)_6$ is a 'soft', water soluble, crystal, in which little crystalline imperfection or strain might be expected to occur to disrupt the relaxation process.

Another factor which will affect the relaxation is crystalline imperfection. Table 5.1 gives the mean c-axis misorientations for the samples and in a unidirectional homogeneous magnetic field parts of the sample will not have

their c-axis parallel to the field. In addition due to the method of mounting the samples in the cavity or waveguide, alignment of the magnetic field to the c-axis could only be made in the horizontal plane, by rotation of the electromagnet about a vertical axis coincident with that of the waveguide feeder into the cryostat (Chapters 3 and 4). The alignment of the c-axis into the horizontal plane was entirely determined by (a) the accurate cutting of the sample from the ruby boule after X-ray location of the c-axis, to align the axis parallel to one edge of the rectangular section sample, (b) the accurate alignment of this edge perpendicular to the vertical axis of the waveguide feeder, whilst positioning the sample correctly in the waveguide or cavity and (c) accurately aligning the waveguide feeder so that its axis is both vertical and coincident with, or at least parallel to, the axis of rotation of the electromagnet poles.

The cumulative errors in this alignment procedure probably ensure that the results presented for a polar angle of nominally 0° are for a polar angle close to 0°, but with a possible error of 5°. This consideration does not apply with the same degree of criticality at $\theta = 90^{\circ}$, as the requirement is only for the c-axis to be lying in a vertical plane to enable the magnetic field to be aligned perpendicularly by simple rotation about the vertical axis. In addition, the energy levels are pure spin states only at exactly $\theta = 0^{\circ}$, whereas the differences in the nature of the energy levels

(degree of mixing of pure spin states) within 5^{o} of $\theta = 90^{o}$ are very slight. These factors will contribute to the discrepancy between these measurements and the theoretical relationship between T_1 and H at $\theta = 0^{o}$, as they cause the energy levels being observed at what is nominally 0^{o} to be actually mixed energy levels of a polar angle close to 0^{o}.

5.4 The Effect of Lattice Strain on T_1

Previous authors have determined the frequency (magnetic field) dependence of T_1 in ruby by a collation of results obtained at various frequencies by other workers, using unrelated samples of varying concentration and degrees of crystalline perfection. This has led to the conclusion that T_1 in ruby shows very little, if any, frequency dependence up to Q-band frequencies (Donoho, 1964; Pace, Sampson and Thorp, 1960). This approach ignores other variables which vary from sample to sample and which may have an effect of equal or even greater magnitude on absolute value of relaxation time than the relatively small variation due to the dependence of T_1 on magnetic field. At higher concentrations than those present in the samples discussed, T_1 becomes concentration dependent due to spin-spin coupling. The presence of impurities which may act as fast relaxing centres to which the Cr^{3+} ions can cross relax will also drastically reduce the measured spin relaxation time. These factors are not considered contributory to the variation in relaxation time in the present samples however, as, except

for sample 354 (0.2 at.% Cr^{3+}) the concentrations, as noted earlier, are lower than those at which concentration dependent relaxation has been observed (Section 5.3). Spectrographic analysis of these samples to determine their Cr^{3+} concentration, in addition to their e.s.r. spectra, have failed to show detectable concentrations of other ions which could act as fast relaxing centres.

The degree of crystalline imperfection of the present samples has been investigated, as mentioned in Section 5.1 and Mason and Thorp (1967) established a linear dependence of T_1 on mean c-axis misorientation. Kirkby and Thorp (1968) measured the static strain components ε in these samples by analysis of the broadened linewidths of their e.s.r. spectra. Section 2.4 contains a derived expression (equation 2.41) which links transition probability, w_{ab}, and compressive strain, ε .

Assuming that the coefficients A to C in equation 2.41 depend only on the position vectors $\underline{r}_1$, C will be the largest and to a very rough approximation, using a binominal expansion, $w_{ab}^{s} \propto (1 + 8\varepsilon)$, which, if T_1 is taken, as a simplification, to be proportional to w_{ab}^{-1}, can be expressed as

$$T_1^s = T_1^u (1 + 8\varepsilon) \qquad 5.1$$

for a compressive strain $-\varepsilon$. The strain components measured by Kirkby and Thorp are ε_{xx} and ε_{zz} representing compressive strains in the x and z axes, and ε_{xz}, a shear

strain in the plane of the z axis of the aluminium oxide lattice.

Following equation 5.1, T_1 (T_1^S) has been plotted against total strain (vector sum of ε_{xx} and ε_{zz}), each sample providing one point (T_1^S and ε), at each magnetic field (frequency) of observation. As a complete set of measurements for all samples existed for the 2-3 transition at $\theta = 90^o$, this data was used to plot six graphs, one for each magnetic field value in figures 5.1 to 5.4 and 5.8. Figures 5.17 to 5.22 show these dependencies of T_1 on strain for the various magnetic fields. The straight lines through the points have been fitted by the method of least squares in each case. The T_1 measurement for the 2-3 transition for Sample L2 at the X-band (high-field) point appears to be in error, as it is anomalously low for no apparent reason except experimental error, and it has been ignored (although plotted) in Figure 5.18, as in Figure 5.1. The points fit a straight line (linear) dependence of T_1 on reasonably well at high field, but not so well at low field. The slope in all cases is negative (T_1 decreasing with increasing ε), but it is not constant, decreasing from -4.6 at the lowest field to -0.2 at the highest (Figures 5.17 to 5.22). This variation of slope is in agreement with equation 5.1, which has a slope of ($-8T_1^u$), which will decrease with increasing magnetic field, since T_1^u decreases with increasing field as discussed in Section 5.3. The slopes of the lines in Figures

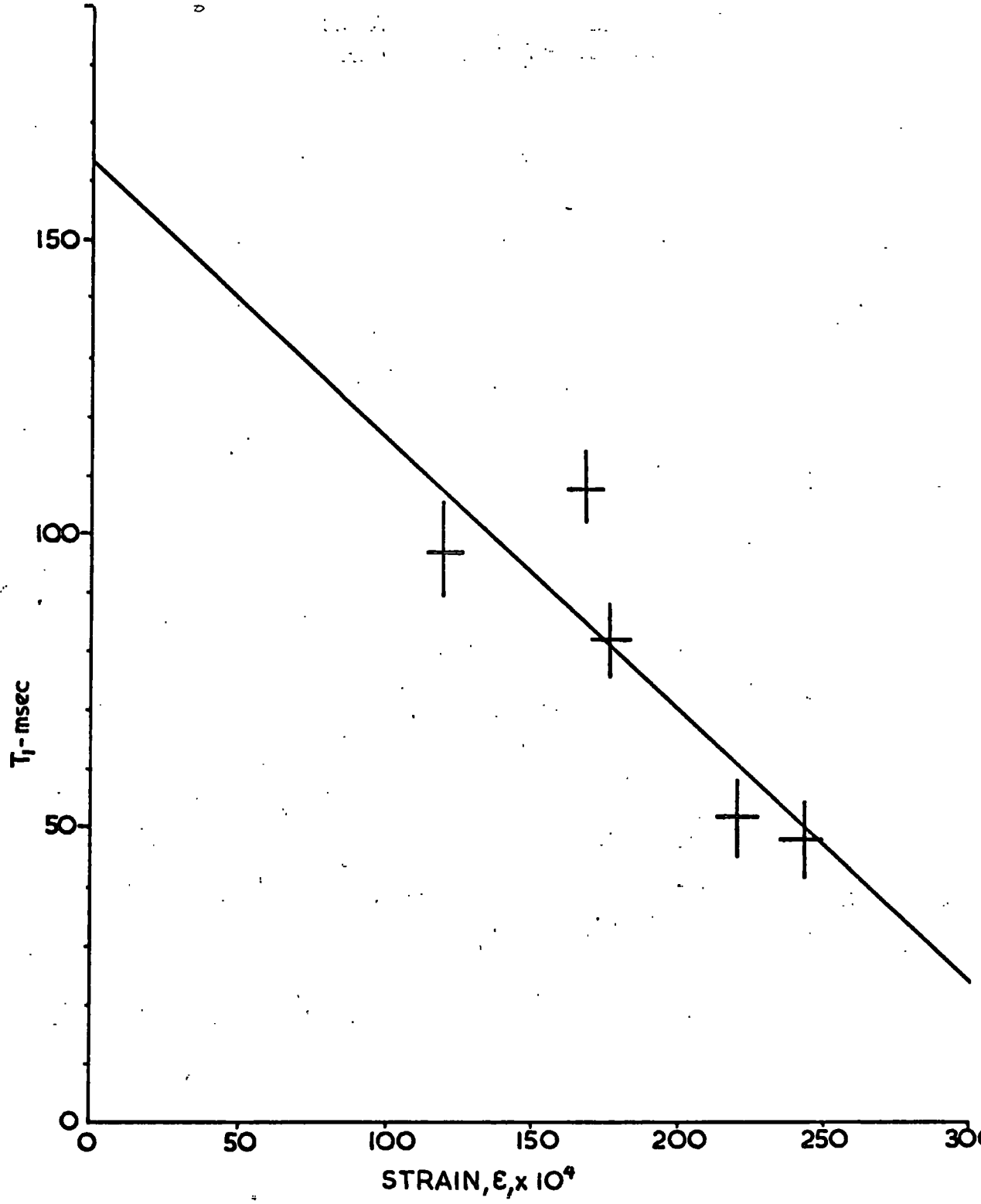

FIGURE 5.17 · VARIATION OF T_1 WITH UNANNEALED STRAIN IN RUBY: $\vartheta = 90°$, TRANSITION 2–3, $T = 4.2°$ K, 9.3 GHz (low field), $T_1^U = 163$ msec, SLOPE = -4.62 .

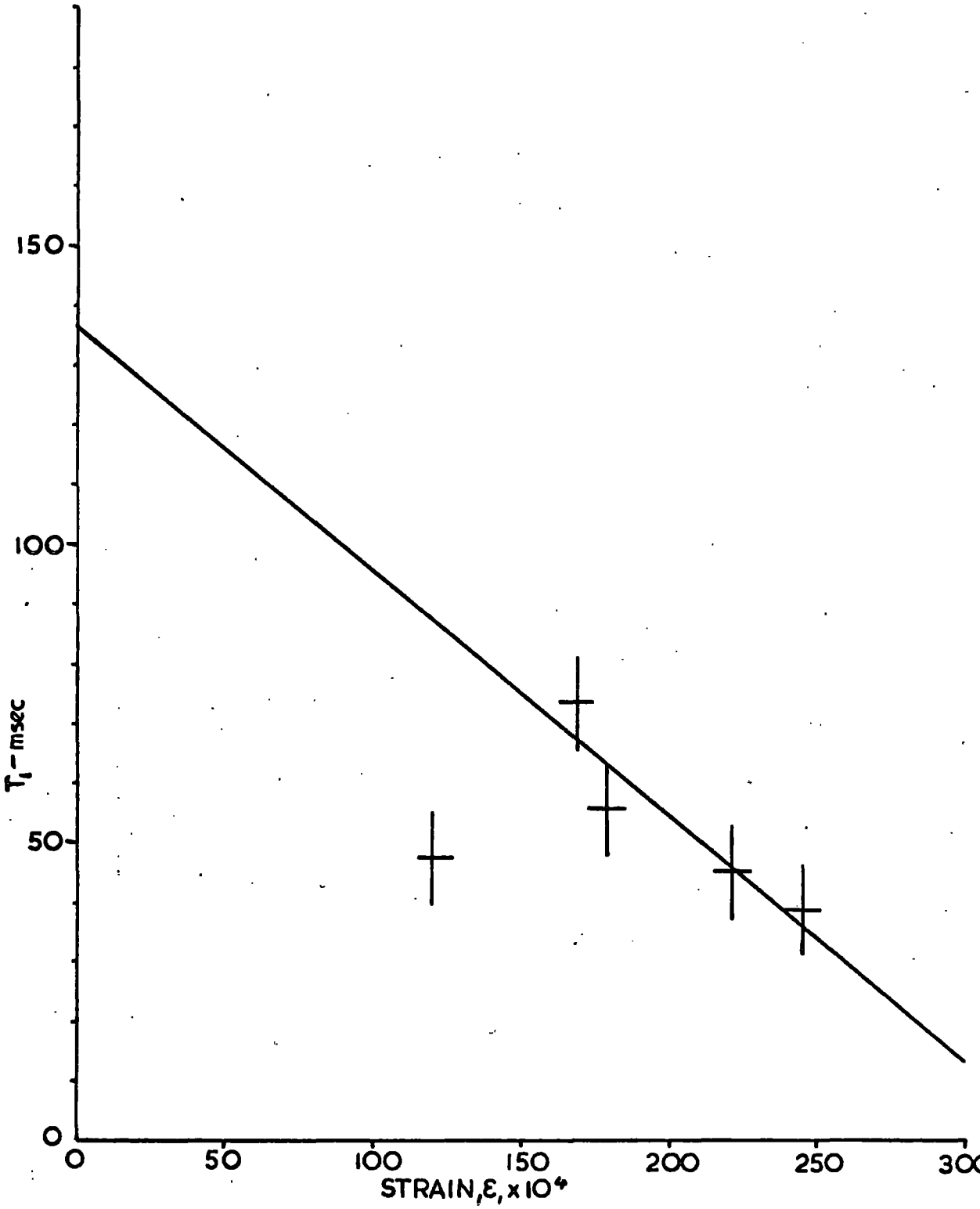

FIGURE 5.18 VARIATION OF T_1 WITH UNANNEALED STRAIN IN RUBY: $\theta = 90^\circ$, TRANSITION 2-3, $T = 4.2^\circ K$, 93 GHz (high field), $T_1^U = 137$ msec, SLOPE = −4.08

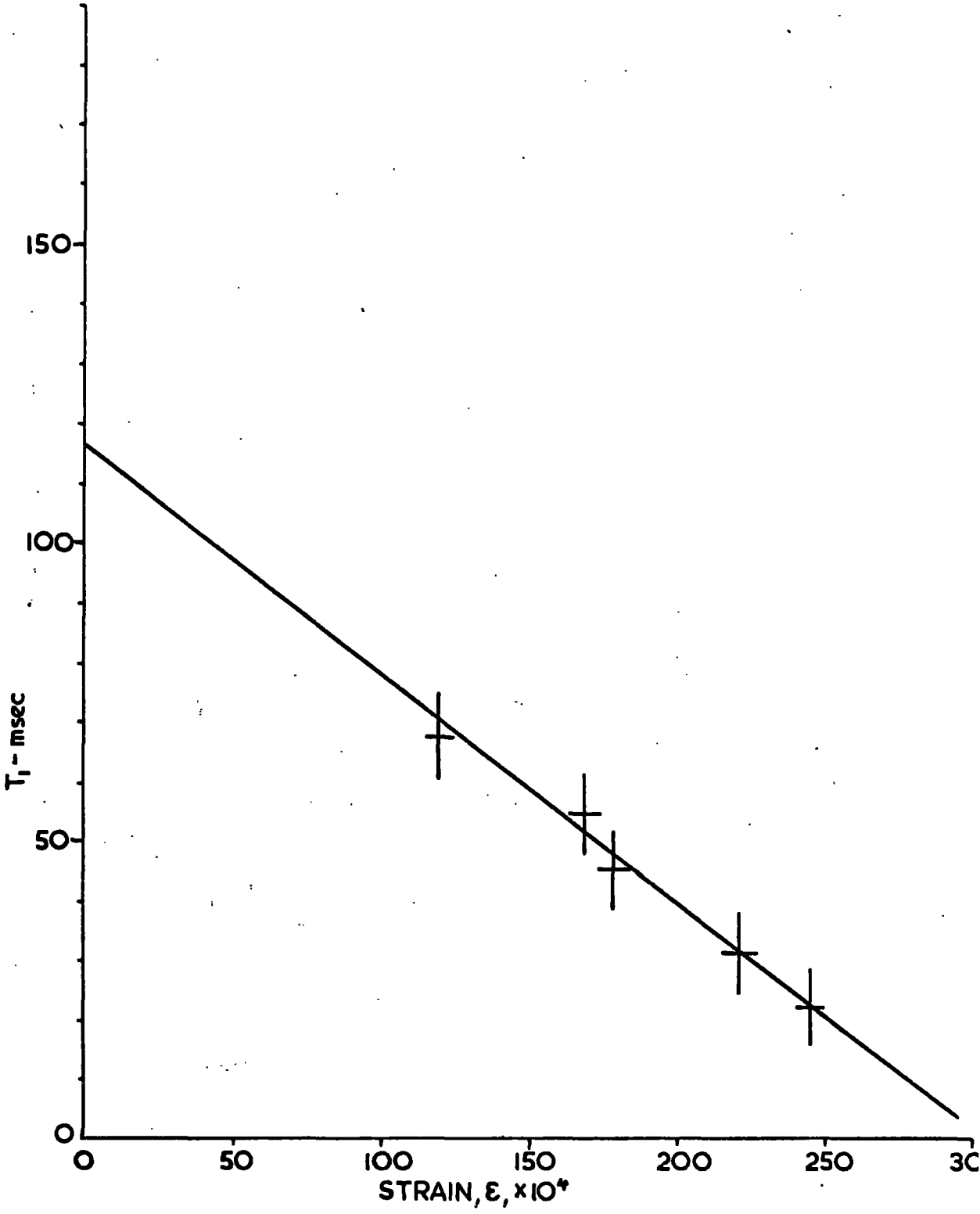

FIGURE 5.19 VARIATION OF T_1 WITH UNANNEALED STRAIN IN RUBY: $\vartheta = 90°$, TRANSITION 2 – 3, T = 4.2° K, 16 GHz, T_1^u = 115 msec, SLOPE = -3.78

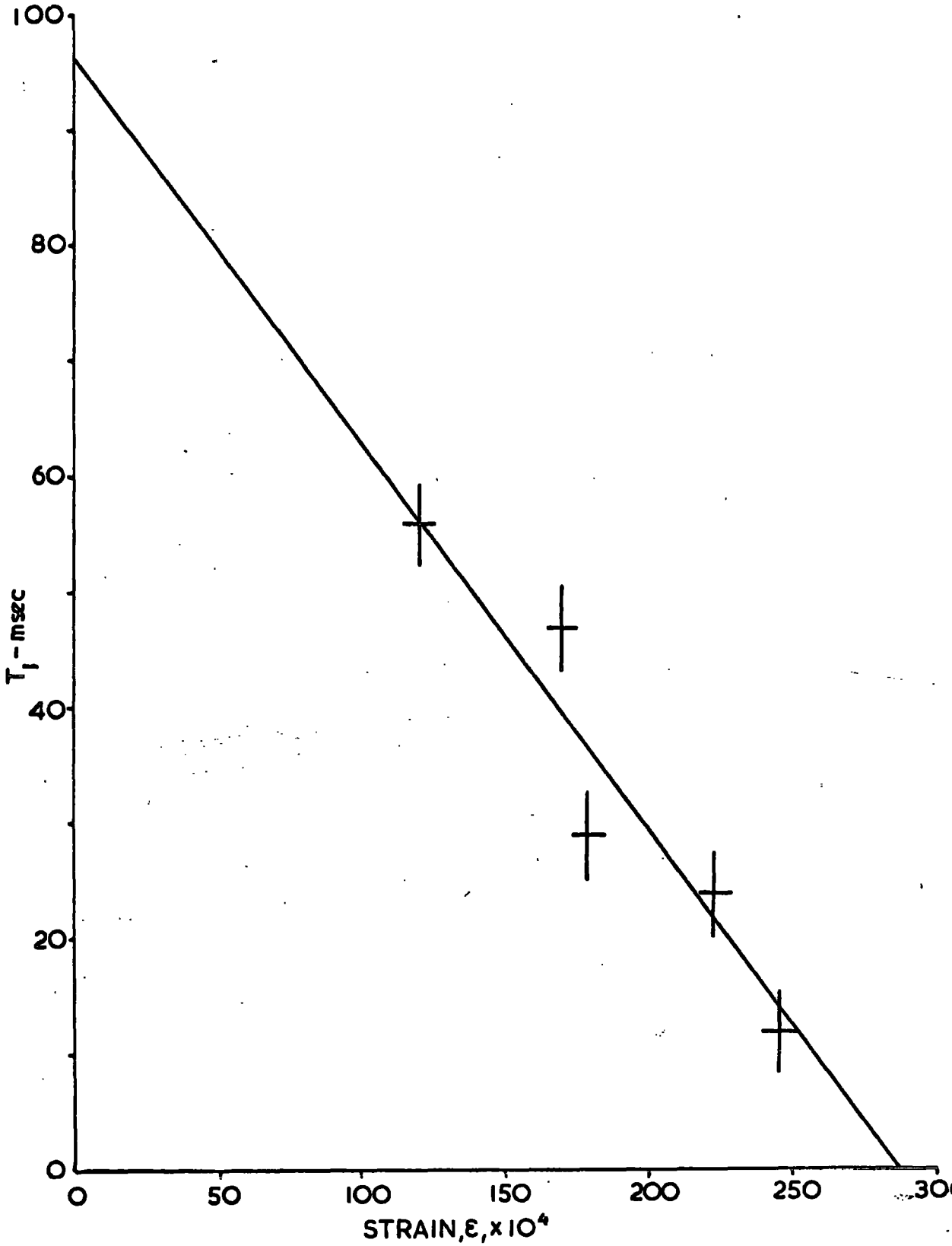

FIGURE 5.20 VARIATION OF T_1 WITH UNANNEALED STRAIN IN RUBY: $\vartheta = 90^\circ$, TRANSITION 2-3, $T = 4.2^\circ K$, 22 GHz, $T_1^U = 96$ msec, SLOPE = -3.36

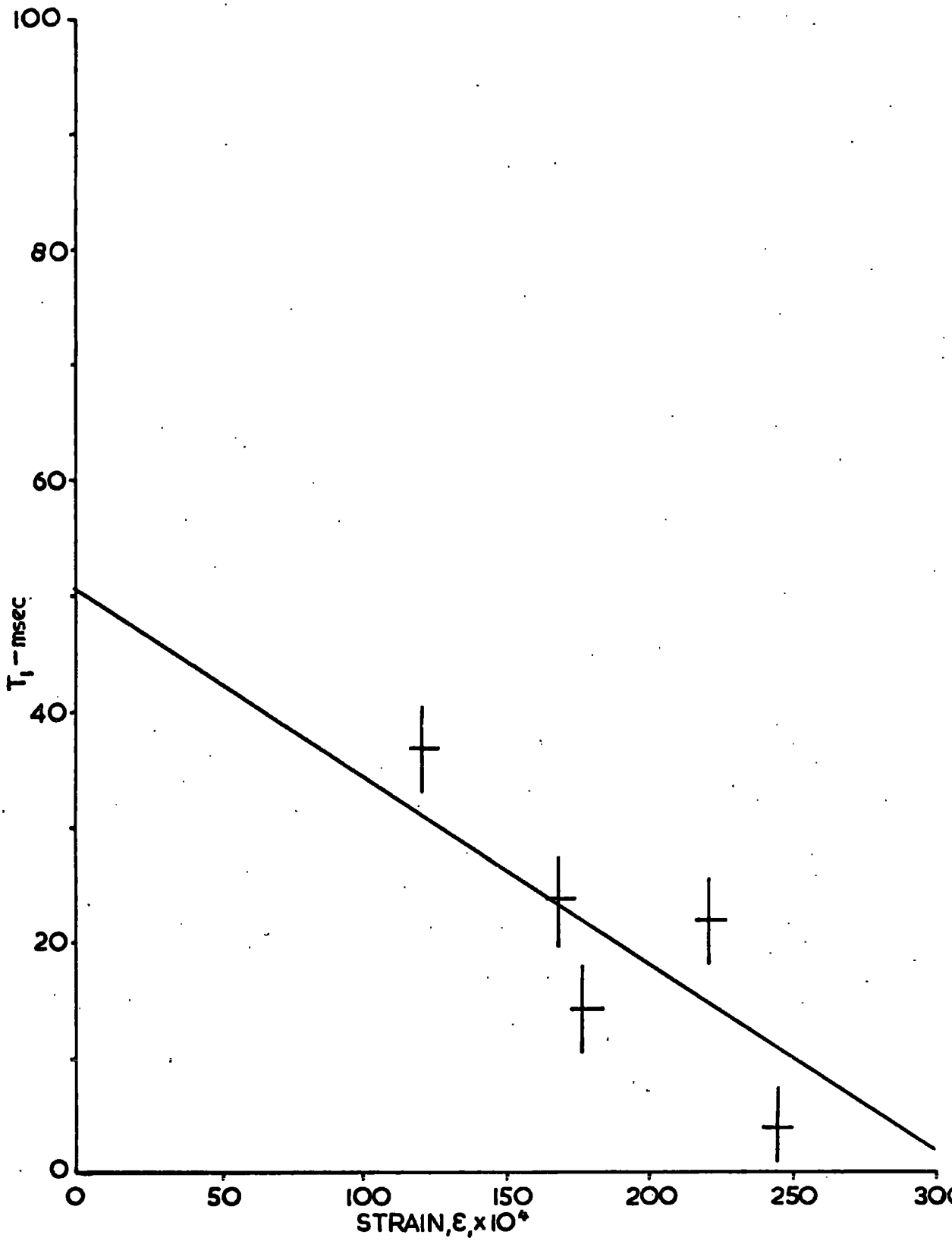

FIGURE 5.21 · VARIATION OF T_1 WITH UNANNEALED STRAIN IN RUBY: $\vartheta = 90^\circ$, TRANSITION 2-3, $T \simeq 4.2^\circ K$, 35.5 GHz, $T_1^u = 50.3$ msec, SLOPE = – 1.61

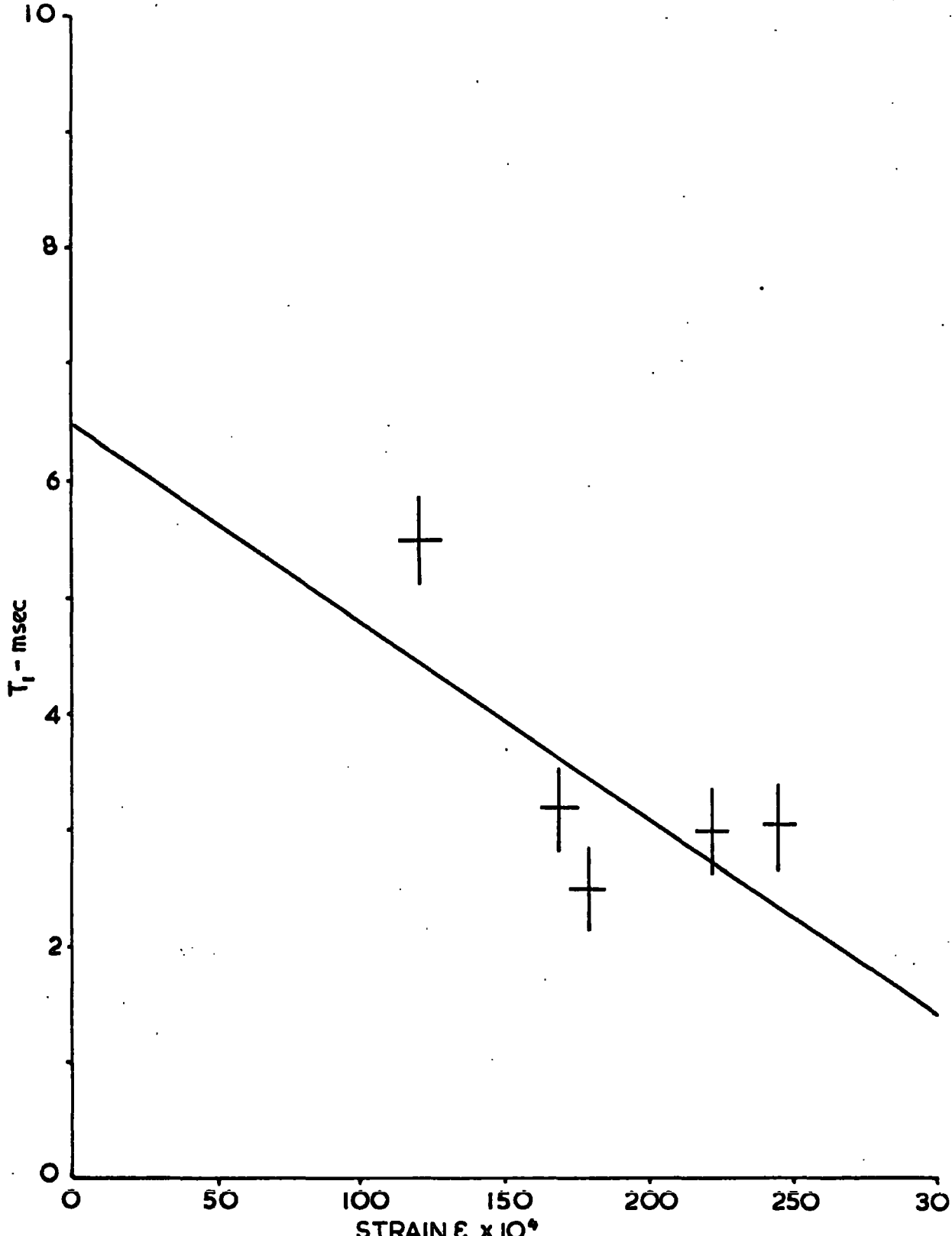

FIGURE 5.22 VARIATION OF T_1 WITH UNANNEALED STRAIN IN RUBY: $\vartheta = 90^\circ$, TRANSITION 2-3, $T = 4.2^\circ K$, 71 GHz, $T_1^u = 6.5$ msec , SLOPE = -0.17

5.17 to 5.21 are all approximately four times steeper than the slopes calculated from equation 5.1 which vary from -1.3 to -0.05, using the intercept on the T_1 axis of the extrapolation of the line in each case as the value of T_1^u for that magnetic field. These derived values of T_1^u are themselves plotted against magnetic field in Figure 5.23, which shows the same form as 5.1 to 5.4 and 5.8, from which it is derived, the low field part of the graph having a slope of -0.42 and the high field part a slope of -2.93.

These results show compressive strain of the host lattice at the paramagnetic ion site to be a variable which materially affects the spin-lattice relaxation time and the behaviour of T_1 with varying strain is described qualitatively, if not quantitatively, by Section 2.4. The major contribution to the increase in the transition probability appears to be the change in gradient of the crystal field due to displacement of the ligand ions. The simple model of Section 2.4 considers only isotropic strain displacing the ligand in the direction of its radius vector $\underline{r}_1$ and disregards angular displacement with respect to the Cr^{3+} ion. The effects of modification of the phonon spectrum appear to be slight and the effects of localised phonon modes discussed at the end of Section 2.4 have been disregarded, as these measurements are all in the direct relaxation region.

It is most unlikely that microscopic strain is the whole explanation for the variation in T_1 from sample to

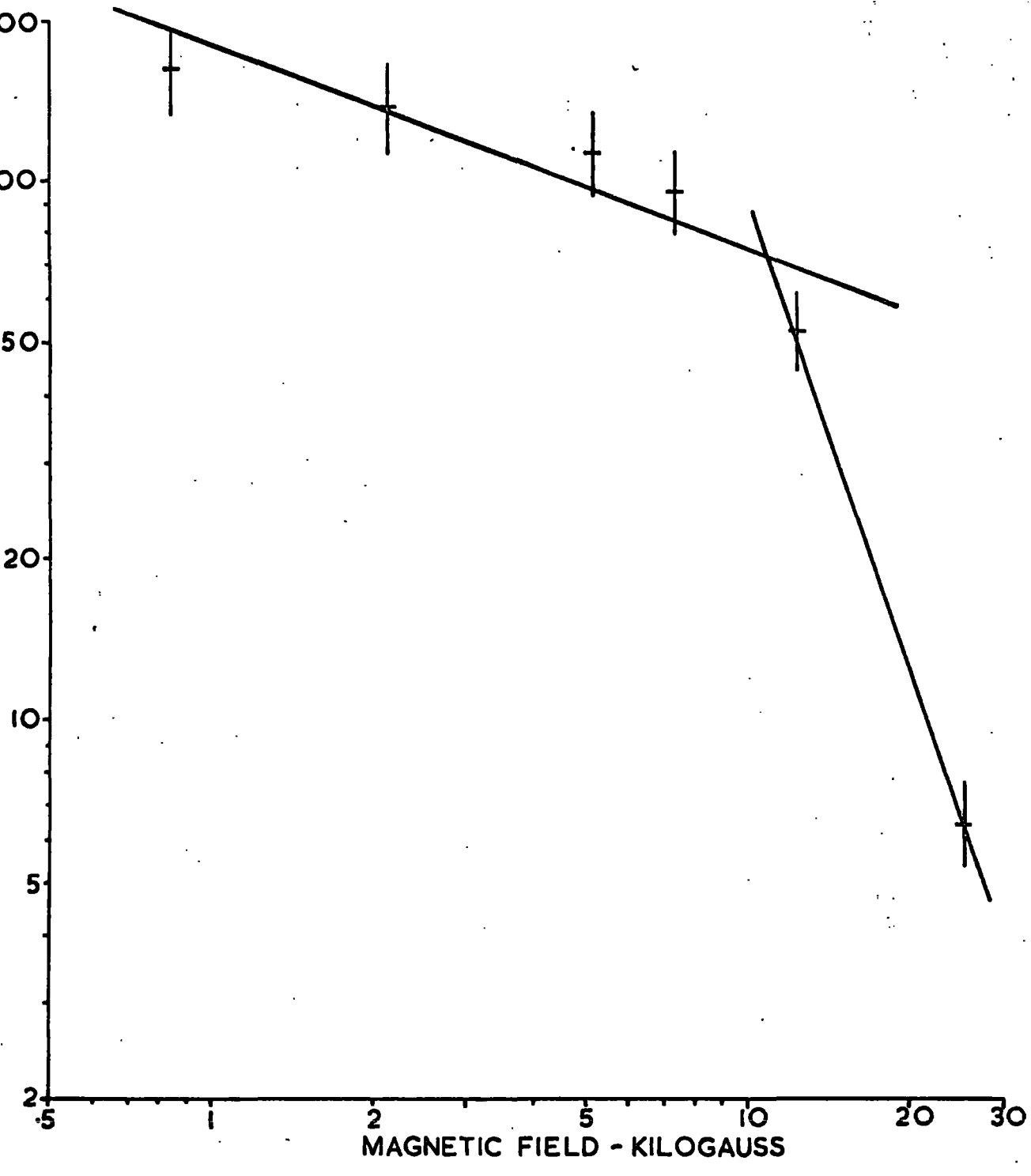

FIGURE 5.23 DEPENDENCE OF T_1^U ON MAGNETIC FIELD
$\vartheta = 90^\circ$, TRANSITION 2-3, $T = 4.2^\circ K$

nominally similar sample under the same experimental conditions. The effects of clustering of Cr^{3+} ions are likely to be a relevant factor and earlier work (Thorp, Curtis and Mason, 1964) showed that Cr^{3+} ions in ruby do tend to accumulate in distorted regions of the material, where their local concentration will rise, introducing the various possible cooperative relaxation mechanisms which are discussed in Section 2.5, all of which tend to reduce the spin-lattice relaxation time.

5.5 Conclusion

The conclusion of earlier authors, that the spin-lattice relaxation time of the Cr^{3+} ion in ruby shows little dependence on applied magnetic field, drawn from comparisons of measurements made by various workers on different samples has been shown to be incorrect, especially at higher magnetic fields; the earlier erroneous conclusion has probably been due to the masking effects on T_1 of other variables than experimental conditions, which are inherent in the sample due to its method of growth.

In samples of low concentration, up to 0.05 at.% Cr^{3+}, at a polar angle of 90° the relaxation time decreases approximately as $H^{-0.4}$ from fields corresponding to X-band to Q-band frequencies, but at very high fields, up to 25 kG (O-band, the limit of observation) the average proportionality for the $\Delta M = 1$ transitions is to $H^{-2.5}$. This approaches the dependence expected from theory of between

H^{-2} and H^{-4} for polar angles other than 0°. The divergence from the predicted dependence at low field is probably due to the large contribution of the zero-field splitting to the energy separations of the levels and the high degree of admixture of pure spin states at polar angles other than 0° in the levels being observed. The reduction of these effects at high fields permits the relaxation behaviour to become a closer approximation to that of the theoretical model.

The results for $\theta = 0^{\circ}$ are for a polar angle close to zero, but due to the lack of precision possible in aligning the samples in the magnetic field, they probably do not represent exactly $\theta = 0^{\circ}$. The low field behaviour of T_1 is similar to that at 90°, but shows a slight tendency towards the theoretical dependence in as much as the average exponent of H for the $-1/2 \rightarrow +1/2$ transition is -0.8, which is significantly larger than the average exponent of -0.5 for the $+3/2 - +1/2$ transition, but the agreement with theory in terms of absolute value of the exponent of H is very poor (-4 and -2 respectively for transitions within and between Kramer's doublets); this is possibly due to a combination of the effects of zero-field splitting, crystalline imperfection and physical misalignment of the samples in the applied magnetic field.

Correlation of T_1 measurements for the range of samples with microscopic strain in their host lattices, measured in earlier work by analysis of linewidth measurements, shows T_1

to be linearly proportional to strain, the linearity of the dependence being better at high magnetic fields. The slopes of the graphs of T_1 against ε are approximately four times greater at each frequency of measurement than a very approximate model would predict, but extrapolated values of T_1^u, the relaxation time in a theoretically unstrained lattice, when plotted against magnetic field, show the same behaviour as the individual samples for the 2-3 transition at $\theta = 90^\circ$.

One of the original motivations for this work, to establish the feasibility of efficient millimetric frequency maser operation, based on the criterion of relaxation time, has been somewhat pre-empted by the development of other types of low noise millimetric amplifiers, notably the parametric amplifier, which are considerably simpler to operate than a maser, although possibly inferior in some aspects of performance. However, the onset of the rapid decrease of T_1, as $H^{-2.5}$, at magnetic fields above those corresponding to Q-band (8 mm wavelength) argues against achieving high inversion ratios and consequently high maser efficiency, at frequencies above this. In addition, at very high fields, the energy levels diverge linearly and the degree of mixing of pure spin states at angles other than 0° decreases, also decreasing the matrix elements and hence the transition probabilities for the $\Delta M = 2$ pump transitions (see Section 1.4). This would lead to a demand for very high pump powers at frequencies necessarily higher

than the signal frequency, where, even now, high power c.w. microwave sources are very expensive and unreliable and are not capable of very high power levels.

REFERENCES

Abragam,A. and Pryce,M.H.L.,Proc.Roy.Soc.,A205,135,1951.

Al'tshuler,S.A.,Sov.Phys.J.E.T.P.,16,1637,1963.

Basov,N.G. and Prokhorov,A.M.,Sov.Phys.J.E.T.P.,1,184,1955.

Bleaney,B. and Stevens,K.W.H.,Rep.Progr.Phys.,16,108,1953.

Bleaney,B.,Loubser,J.H.N. and Penrose,R.P.,Proc.Phys.Soc., 59,185,1947.

Bloch,F.,Phys.Rev.,70,460,1946.

Bloembergen,N.,Phys.Rev.,104, 324,1956.

Bloembergen,N.,Purcell,E.M. and Pound,R.V.,Phys.Rev.,73 679,1948.

Bloembergen,N.,Shapiro,S.,Pershan,P.S.,and Artman,J.O., Phys.Rev.,114,445,1959.

Bloembergen,N. and Wang,S.,Phys.Rev.,93,72,1954.

Bowers,K.D. and Mims,W.B.,Phys.Rev.,115,285,1959.

Brown,G.,Mason,D.R. and Thorp,J.S.,J.Sci.Instr.,42,648,1965.

Brown G. and Thorp,J.S.,Brit.J.Appl.Phys.,18,1423,1967.

Buckmaster,H.A. and Dering,J.C.,J.Sci.Instr.43,404,1966.

Candela,G.A. and Mundy,R.E.,Rev.Sci.Instr.,36,338,1965.

Casimir,H.B.G. and Du Pre,F.K.,Physica,5,507,1938.

Castle,J.G.jr.,Chester,P.F. and Wagner,P.E.,Phys.Rev.,119, 953,1960.

Castle,J.G.jr.,Feldman,D.W. and Klemens,P.G.,Quantum Electronics,Proc.2nd.Conf.Columbia U.P.1961.

Castle,J.G.jr.,Feldman,D.W.,Klemens,P.G. and Weeks,R.A. Phys.Rev.130,577,1963.

Chang,W.S.C.,Quantum Electronics,Columbia U.P.,1960.

Cleeton,G.E. and Williams,N.H.,Phys.Rev.,45,234,1934.

Cummerow,R.L. and Halliday,D.,Phys.Rev.,70,433,1946.

Damon,R.W.,Rev.Mod.Phys.,25,239,1953.

Davids,D.A. and Wagner,P.E.,Phys.Rev.Lett.,12,141,1964.

Davis,C.F.,Strandberg,M.W.P. and Kyhl,R.L.,Phys.Rev.,111, 1268,1958.

Dirac,P.A.M.,Quantum Mechanics,O.U.P.,1947.

Donoho,P.L.,Phys.Rev.,133, A1080,1964.

Einstein,A.,Phys.Z.,18,121,1917.

Eschenfelder,A.H. and Weidner,R.T.,Phys.Rev.,92,869,1953.

Faughan,B.W. and Strandberg,M.W.P.,J.Phys.Chem.Solids.,19 155,1961.

Faulkner,E.A.,J.Sci.Instr.,41,347,1964.

Feher,G.,Bell Syst.Tech.J.,36,449,1957.

Feldman,D.W.,Castle,J.G.jr. and Murphy,J.,Phys.Rev.,138, A1208,1965.

Feng,S. and Bloembergen,N.,Phys.Rev.,130,531,1963.

Fierz,M.,Physica,5,433,1938.

Finn,C.B.P.,Orbach,R. and Wolf,W.P.,Proc.Phys.Soc.,77,261, 1961.

Getsic,J.E.,Phys.Rev.,102,1252,1956.

Gill,J.C.,Proc.Phys.Soc.,79,68,1962.

Giordmaine,J.A.,Alsop,L.E.,Nash,F.R. and Townes,C.H.,Phys. Rev.,109,302,1958.

Gordon,J.P.,Zeiger,H.J. and Townes,C.H.,Phys.Rev.,99,1264, 1954.

Gorter,C.J.,Physica,3,503,1936.

Gorter,C.J.,Paramagnetic Relaxation,Elsevier Pub.Co.,1947.

Grant,W.J.C.,Phys.Rev.,134,A1554,1964.

Heitler,W.,The Quantum Theory of Radiation,Clarendon Press, 1957.

Heitler,W. and Teller,E.,Proc.Roy.Soc.,A155,629,1936.

Herve,J.,Paramagnetic Resonance,Proc.1st.Intl.Conf., Academic Press,1963.

Herve,J. and Pescia,J.,Comp.Rend.Acad.Sci.,251,665,1960.

Hutchings,M.T.,Solid State Phys.,16,287,1964.

Kirkby,C.J.,Ph.D.Thesis,University of Durham,1967, (unpublished).

Kirkby,C.J. and Thorp,J.S.,J.Phys.C.,Ser 2,1,913,1968.

Klemens,P.G.,Phys.Rev.,125,1795,1962.

Klemens,P.G.,Solid State Physics,Academic Press,1958.

Klemens,P.G.,Castle,J.G.jr. and Feldman,D.W.,Proc.8th.Int. Conf.Low Temp.Physics,Butterworth,1963.

Kochelaev,B.I.,Doklady Acad.Nauk,SSR.131,1053,1960.

Kopvillem,U.Kh.,Sov.Phys.SS.,3,865,1960.

Kramers,H.A.,Proc.Acad.Sci.Amsterdam,33,959,1930.

Kronig,R.de L.,Physica,6,33,1939.

Kronig,R.de L. and Bouwkamp,C.J.,Physica,5,521,1938.

Landau,L.D. and Lifshitz,E.M.,Quantum Mechanics,Pergamon, 1958.

Llewellyn,P.M.,Whittlestone,P.R. and Williams,J.M.,J.Sci. Instr.39,586,1962.

Lloyd,J.P. and Pake,G.E.,Phys.Rev.,94,579,1954.

Makhov,G.,Kikuchi,C.,Lambe,J. and Terhune,R.W.,Phys.Rev., 109,1399,1958.

Mason,D.R.,Ph.D.Thesis,University of Durham,1966, (unpublished).

Mason,D.R. and Thorp,J.S.,Phys.Rev.,157,191,1967.

Mattuck,R. and Strandberg,M.W.P.,Phys.Rev.,119,1204,1960.

Mims,W.B. and McGee,J.D.,Phys.Rev.,119,1233,1960.

Misra,H.,Rev.Sci.Instr.,29,590,1958.

Montgomery,C.J.,Dicke,R.H. and Purcell,E.M.,Principles of Microwave Circuits,M.I.T.Rad'n.Lab.Series,McGraw-Hill, 1948.

Montrell,E.W. and Potts,R.B.,Phys.Rev.,100,525,1955.

Nash,F.R.,Phys.Rev.Lett.,7,59,1961.

Nice,E.G.,private communication,1969.

Orbach,R.,Proc.Roy.Soc.,A264,458,1961(a).

Orbach,R.,Proc.Roy.Soc.,A264,485,1961(b).

Orbach,R.,Proc.Phys.Soc.,77,821,1961(c).

Orbach,R. and Blume,M.,Phys.Rev.Lett.,8,478,1962.

Pace,J.H.,Sampson,D.F. and Thorp,J.S.,Proc.Phys.Soc.,76,697, 1960.

Pershan,P.S.,Phys.Rev.,117,109,1960.

Portis,A.M.,Phys.Rev.,91,1071,1953.

Pound,R.V.,Rev.Sci.Instr.,17,490,1946.

Ruby,R.H.,Benoit,H. and Jeffries,C.D.,Phys.Rev.,127,52,1962.

Schawlow,A.L.,Wood,D.C. and Clogston,A.M., Phys.Rev.Lett.,3,271,1959.

Schulz-du Bois,E.O.,Bell Syst.Tech.J.,38,271,1959.

Scott,P.L. and Jeffries,C.D.,Phys.Rev.,127,32,1962.

Scovil,H.E.D.,Feher,G. and Seidel,H.,Phys.Rev.,105,762,1957.

Standley,K.J. and Vaughan,R.A.,Phys.Rev.,139,A1275,1965.

Strum,P.D.,Proc.I.R.E.,41,875,1953.

Thorp,J.S.,Curtis,D.A. and Mason,D.R.,Brit.J.Appl.Phys., 15,775,1964.

Thorp,J.S.,Pace,J.H. and Sampson,D.F.,J.Elect.& Control,10, 13,1961.

Van Vleck,J.H.,J.Chem.Phys.,7,72,1939.

Van Vleck,J.H.,Phys.Rev.,57,426,1940.

Van Vleck,J.H.,Phys.Rev.,59,724,1941(1).

Van Vleck,J.H.,Phys.Rev.,59,730,1941(b).

Van Vleck,J.H.,Quantum Electronics,Proc.1st.Intl.Conf.,
Columbia U.P.1960.

Waller,I.,Z.Phys.,79,370,1932.

Waring,R.K.,Rev.Sci.Instr.,34,1228,1963.

Weber,J.,Trans.I.R.E.,ED-3,1,1953.

Zavoisky,E.,J.Phys.USSR.,9,211,1945.

Ziman,J.M.,Electrons and Phonons,Clarendon Press,1960.